

**Functional characterization of human CRN2 (coronin-1C)
in normal and disease conditions**

INAUGURAL-DISSERTATION

zur

Erlangung des Doktorgrades
der Mathematisch-Naturwissenschaftlichen Fakultät
der Universität zu Köln



vorgelegt von

Charles-Peter Xavier

aus Bangalore, Indien

2008

Vorsitzender: Frau Universitätsprofessorin Dr. rer. nat. Karin Schnetz

1. Berichterstatter: Frau Universitätsprofessorin Dr. rer. nat. Angelika A. Noegel

2. Berichterstatter: Herr Universitätsprofessor Dr. rer. nat. Siegfried Roth

Tag der mündlichen Prüfung: 16.02.2009

Erklärung

Ich erkläre hiermit, dass ich die vorliegende Arbeit ohne unzulässige Hilfe Dritter und ohne Benutzung anderer als der angegebenen Hilfsmittel angefertigt habe; die aus fremden Quellen direkt oder indirekt übernommenen Gedanken sind als solche kenntlich gemacht.

Die in dieser Arbeit beschriebenen Experimente sind von mir selbst durchgeführt worden. Anleitungen oder Anregungen zu Experimenten habe ich von Frau Prof. Dr. Noegel, Herrn PD Dr. Clemen und den Mitarbeitern des Institutes für Biochemie I erhalten. Bei verschiedenen Experimenten wurde ich bei der Versuchsdurchführung von technischem Personal unterstützt.

Des Weiteren habe ich nicht die Hilfe eines Promotionsberaters in Anspruch genommen. Dritte haben weder unmittelbar noch mittelbar geldwerte Leistungen für Arbeiten erhalten, die im Zusammenhang mit dem Inhalt der vorliegenden Dissertation stehen.

Die Arbeit wurde von mir bisher weder im Inland noch im Ausland in gleicher oder ähnlicher Form einer anderen Prüfungsbehörde vorgelegt und ist auch noch nicht veröffentlicht.

Köln, den 05.12.2008

(Charles-Peter Xavier)

Acknowledgement

First and foremost I would like to express my heartiest gratitude to Prof. Angelika Noegel for giving me an opportunity to work in her supervision. Her positive attitude, constant encouragement, promptness and sustained interest in my project proved essential for successful completion of my PhD thesis.

I convey my sincere heartfelt gratitude to PD Dr. Christoph Clemen, our group leader, for providing valuable guidance, excellent advice with my work. His constant encouragement, immense optimism and friendly nature are highly acknowledged. It was a privilege to work with him.

Very special thanks to Ms. Maria Stumpf who helped me a lot with my experiments throughout the course of my Ph.D and also for creating a friendly environment with more fun.

I take this opportunity to thank all investigators who extended their support in form of collaborative work. I thank Prof. Dietmar Thal, PD Dr. Stefan Linder, Prof. Andreas Hofmann, Prof. Rolf Schröder and Prof. Micheal Schleicher for successful collaborative efforts. I also thank Dr. André Rosentreter (with whom I shared part of my work), Prof. Reginald O. Morgan, Prof. Maria-Pilar Fernandez and PD Dr. Ludwig Eichinger for their help.

I thank Mr. Rolf Müller for his good technical support in gel filtration assays and cloning. I also thank Mr. Berthold Gassen especially for yummy cakes, antibodies and cell culture work.

I thank Vivek, Subhanjan, Deen, Vel, Sabari, Palani, Sharada, Yogikala, Sam and Channa for their help and good company. I like to sincerely thank Pastor David, Annie, Bro. Samy, Pastor Nathan, Bro. Robert, Dr. Pradheep and Andrew.

I also thank all members of the lab, Raphael, Mary, Karthik, Kalle, Christian, Surayya, Rashmi Rosi, Hua, Sudhir, Tanya, Anne, Margit, Georgia, Eva, Sascha, Ria, Budi, Francisco and Akis for their good company, help and support. I also thank Ms. Dörte Püsche for her help and co-operation with the administrative work that made my life easy. I take this opportunity to thank Gudrun for her prompt help anytime needed. I could also like to thank my friends Veena (special thanks), Fareed, Sam, Deepak, Selva, Vinayaga, Ram, Vinod and Raja for their wonderful company.

I express my heartfelt gratitude to my brother Vincent, parents and family members for their patience, tolerance, sacrifice and encouragement throughout my life. I also thank Dr. Betty Daniel and Dr. Viloo Patel for their support and encouragement.

My heartfelt sincere gratitude to Suja for her company, patience and encouragement.

I also thank the Deutsche Forschungsgemeinschaft for financial assistance during my Ph.D.

Cologne, 5th Dec 2008

Charles-Peter Xavier

Contents

I. INTRODUCTION	1
1.1 Coronins	1
1.2 Coronin Structure	4
1.2.1 N-terminal domain (β-propeller structure)	4
1.2.2 Unique region	4
1.2.3 Coiled coil domain	5
1.3 Oligomerisation	5
1.4 Interactions with Arp2/3 complex	6
1.5 Coronin regulation by phosphorylation	6
1.6 Coronins in disease	8
1.7 CRN2 (coronin-1C, coronin-3)	8
1.8 Aim of the work	10
1.9 Preliminary publications	11
II. RESULTS	12
2.0 Role of CRN2 in cellular processes	12
2.1 CRN2 interacts with the F-actin cytoskeleton in vivo	12
2.2 Absence of CRN2 or lack of single domains inhibits fibroblast migration	13
2.3 Expression of the WD-repeat domain of CRN2 inhibits cell proliferation	15
2.4 CRN2 participates in the formation of cellular protrusions	16
2.5 Full-length CRN2 is essential for the process of fluid phase pinocytosis	17
2.6 CRN2 forms a complex with the Arp2/3-complex and with cofilin	18
2.7 Structural properties of CRN2 deduced from the CRN4 crystal structure	19
3.0 Expression of CRN2 in diffuse gliomas is related to malignancy	21
3.1 CRN2 is expressed in a subset of human brain tumours and in reactive astrocytes	21
3.2 CRN2 expression correlates with the grade of malignancy in diffuse gliomas	25
	IV

3.3 CRN2 knockdown inhibits cellular functions related to tumour malignancy	27
4.0 Structural and functional diversity of novel CRN2 isoforms.	32
4.1 Identification of three CRN2 proteins encoded by two mRNA species	32
4.2 Evolutionary insight into CRN2 regulation	34
4.3 CRN2i3 is part of the myogenic differentiation program	36
4.4 Different oligomerization state of the CRN2 isoforms	37
4.5 Structural models of CRN2 isoforms	38
4.6 GFP-fusion proteins of CRN2 isoforms localize to F-actin structures	40
4.7 CRN2 is a novel component of podosomes	41
4.8 CRN2i3 is a structural component of neuromuscular junctions and myofibrils	43
5.0 Influence of phosphorylation on structure and function of CRN2	46
5.1 Posttranslational modifications of CRN2	46
5.2 CRN2 interacts with actin cytoskeleton regulator CK2 α kinase	46
5.3 In vivo phosphorylation of CRN2	47
5.4 In vitro phosphorylation of CRN2 by CK2 α kinase	48
5.5 Phosphorylation of Ser463 regulates oligomerisation of CRN2	49
5.6 Phosphomimetic S463D mutant CRN2 inhibits actin polymerisation	50
5.7 Phosphomimetic S463D mutant of CRN2 suppresses migration	51
5.8 Phosphomimetic S463D mutant CRN2 hinders formation of cellular protrusions	52
III. DISCUSSION	53
6.0 Role of CRN2 in cellular processes	53
6.1 Structural properties of CRN2	53
6.2 CRN2 regulates F-actin processes	53
6.3 Influence of phosphorylation on structure and function of CRN2	55
6.4 Structural and functional diversity of novel CRN2 isoforms	56
7.0 Expression of CRN2 in diffuse gliomas is related to malignancy	59
IV. MATERIALS AND METHODS	61
1.0 Kits and Reagents	61
1.2 Enzymes, antibodies, radioactive probes, antibiotics, inhibitors	61
1.2.1 Enzymes for molecular biology	61

1.2.2 Inhibitors	62
1.2.3 Antibodies	62
1.2.4 Antibiotics	62
1.2.5 Radiolabelled nucleotide	63
1.3 Reagents	63
1.4 Plasmids	64
1.4.1 Oligonucleotides	65
1.5 Bacterial host strains	65
1.6 Insect cell lines	65
1.7 Mammalian cell lines	65
1.8 Media and buffers	65
1.8.1 Media for <i>E. coli</i> culture	66
1.8.2 Media for Mammalian cell culture	66
1.8.3 Media for Insect Cell Culture	66
1.9 Instruments and Equipments	66
1.10 Immunoblotting and antibodies	66
1.11 Mammalian cell culture	66
1.12 2D-gel electrophoresis	67
1.13 Statistical methods	67
2.0 Role of CRN2 in cellular processes	67
2.1 Generation of EGFP–fusion constructs of CRN2 domains	67
2.2 Subcellular fractionation	68
2.3 RNAi silencing	68
2.4 Immunofluorescence, confocal microscopy, and live cell imaging	68
2.5 In vitro wound healing, proliferation, cytokinesis, and cell activity assays	68
2.6 Co-immunoprecipitation	69
3.0. Expression of CRN2 in diffuse gliomas is related to malignancy	70
3.1 Neuropathology	70
3.2 Visualization of invadopodia	70
3.3 Lentiviral transduction of shRNA vectors	70

3.4 Determinations of cell based assays.	71
4.0 Structural and functional diversity of novel CRN2 isoforms	71
4.1 Immunofluorescence and immunohistochemistry	71
4.2 Mammalian cell culture	71
4.3 RNA purification, northern blotting, 5'-RACE, 5'-RLM-RACE, and RT-PCR	72
4.4 Differential centrifugation, subcellular fractionation, and gel filtration	72
4.5 Plasmids for expression of CRN2 isoforms	73
4.6 Bioinformatic analysis	73
5.0 Influence of Phosphorylation on Structure and function of CRN2	73
5.1 Expression of wild-type and mutant CRN2 coiled coil peptides.	73
5.2 In vitro wound healing and single protrusion assay	74
5.3 In vitro phosphorylation assay	74
5.4 Actin polymerization assays	74
5.5 Co-immunoprecipitation	75
5.6 CRN2 pull down experiments	75
IV. BIBLIOGRAPHY	77
VI. APPENDIX	85
1. Abbreviations	85

I. Introduction

Dynamic remodelling of the actin cytoskeleton is indispensable for many physiological processes, which comprise cell migration, intracellular trafficking of vesicles and organelles, cell polarity, and signal transduction. Cell motility defines critical role in various disease states like cancer and autoimmunity. Cell motility is a highly coordinated process involving dynamic re-organization of the actin cytoskeleton. Actin dynamics comprising polymerization and depolymerisation of actin filaments is a tightly regulated process engaging various actin binding proteins. The precise molecular mechanism underlying this regulation has been one of the domains of intense study for decades in actin biology (Uetrecht and Bear, 2006). At the heart of this process of actin regulation is the evolutionarily conserved seven-subunit containing Arp2/3 complex, which brings about actin nucleation and branching. Arp2/3 by itself is relatively inactive and requires necessary interaction and activation by the WA/VCA domain of a nucleation-promoting factor (NPF), such as the SCAR/WASp family of proteins (Rodal et al., 2005). The Arp2/3 mediated formation of the F-actin network is a crucial process and demands a tight regulation of Arp2/3 complex. One of the protein family that seems to contribute to this regulation is the coronin family of proteins (Uetrecht and Bear, 2006).

1.1 Coronins

The coronin family of proteins is prominent amongst the WD-repeat-actin binding proteins (Fig.1). They are evolutionarily conserved across different organisms, with origin from simple eukaryotes to higher vertebrates. Coronin was first discovered from actin-myosin preparations in *Dictyostelium discoideum*. The term coronin was coined, due to its co localization with the actin rich crown-shaped cellular projections (de Hostos et al., 1991). Even though coronin protein involvement in actin-dependent processes appears primordial, the individual members of the coronin protein family contribute to largely different cellular functions like like signal transduction, transcriptional regulation, remodelling of the cytoskeleton, and regulation of vesicular trafficking (for an extensive review on coronin proteins see (Clemen et al., 2008)).

Phylogenetic analyses revealed twelve subfamilies of coronin proteins, comprising seven vertebrate paralogs and five subfamilies in nonvertebrate metazoa, fungi and protozoa, some of them unclassified so far. Delineation of these twelve subfamily clades has been used to propose a comprehensive revision of the coronin protein nomenclature (Fig. 2) (Morgan and Fernandez, 2008). Currently, two nomenclature systems are used for coronin proteins. Both do not cover all coronin subfamilies and moreover, do not allow unambiguous labelling of

gene duplications and isoforms. These disadvantages will be overcome using the revised coronin protein nomenclature which is based on evolutionary history, structural change and functional adaptation. The coronin subfamilies were united and re-numerated, and 'CRN' has been proposed as the new symbol for coronin proteins.

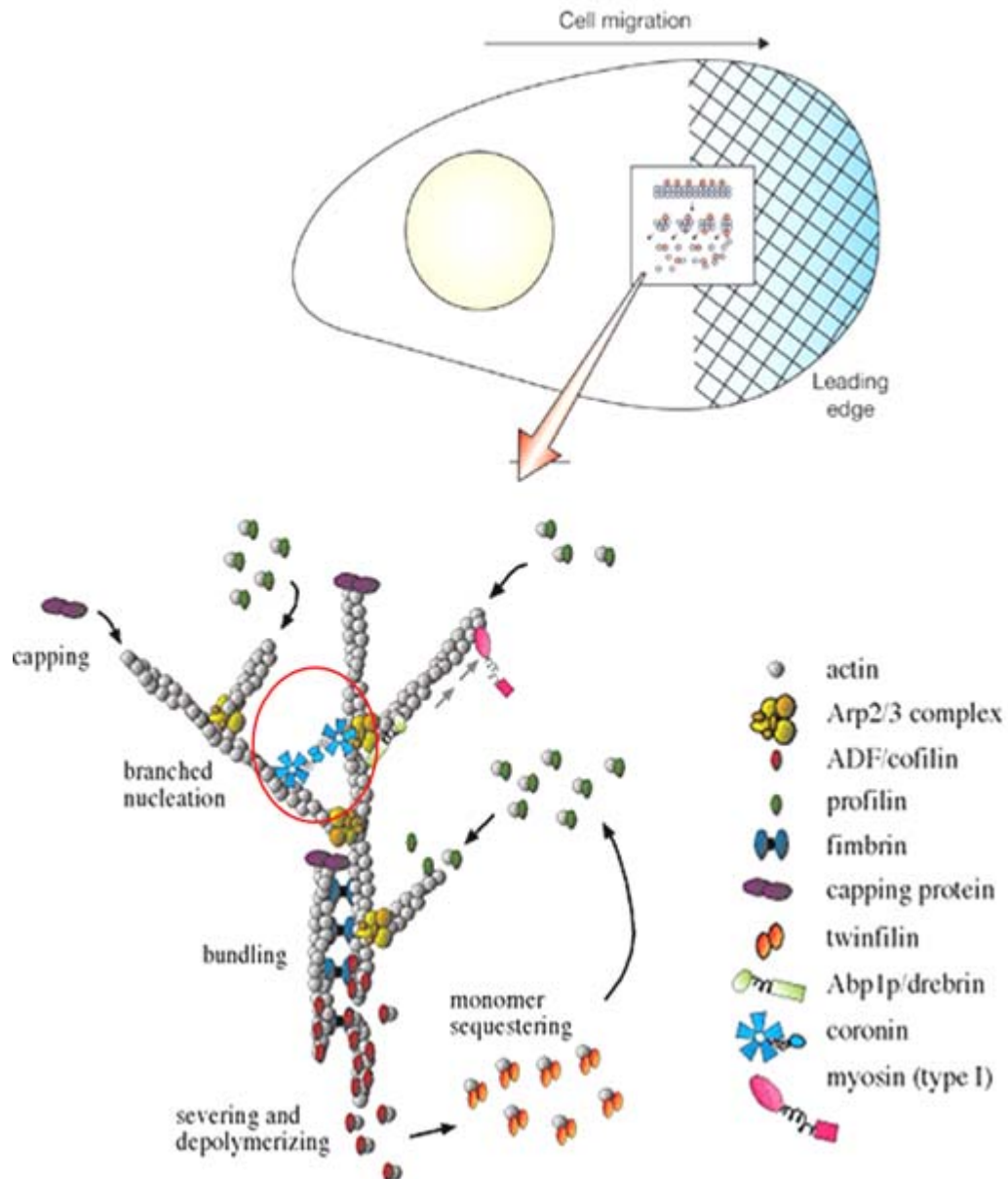


Figure 1. Coronin proteins involved in cytoskeletal F-actin binding and cross-linking, the red circle indicates dimerized coronin cross-linking two F-actin filaments. Taken from www.bio.brandeis.edu/faculty.

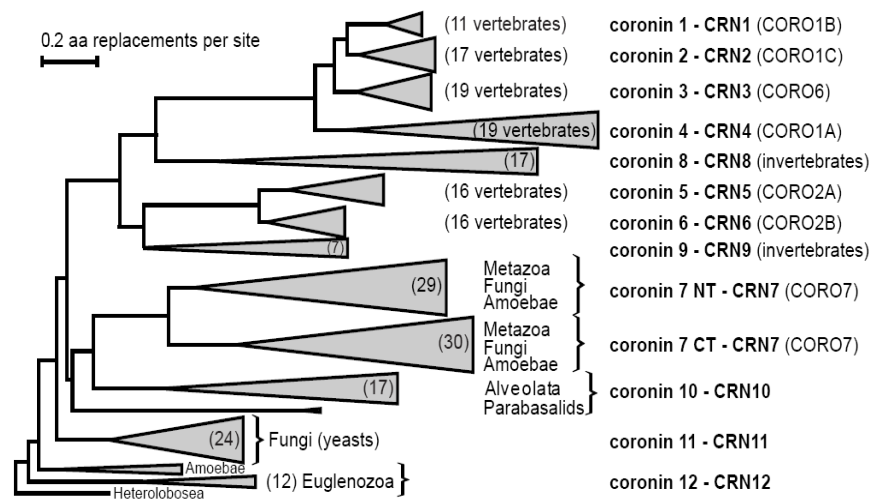


Figure 2. Molecular phylogeny of the coronin family of proteins across different organisms using the proposed new nomenclature: current official symbols in brackets. According to (Morgan and Fernandez, 2008), taken from (Clemen et al., 2008)

On the basis of amino acid content, mammalian coronins can be distinguished into two subfamilies (Rybakin and Clemen, 2005). Short coronins CRN1-6 display three different structural domains. The long coronin CRN7 contains the short coronin topology in duplicate. Table. 1 illustrates the seven coronins present in mammals (Xavier et al., 2008).

Coronin	AA/MW/%I	Expression/Localization	Function
Human CRN1 (CORO1B)	489aa, 54kDa, 38%	Ubiquitously expressed and localizes to the leading edge of the cell	F-actin turnover by Arp2/3 complex and by cofilin in lamellipodial protrusions
CRN2 (CORO1C)	474aa, 57kDa, 46%	Cortex, cytosol, leading edge	Actin-binding protein
CRN3 (CORO6)	472aa, 52kDa, 40%	Expressed in brain	N.A.
CRN4 (CORO1A)	461aa, 51kDa, 35%	Cell cortex, cytoplasm, phagosomes of thymocytes, T-cells, macrophages, neutrophils	Activation of Ca ²⁺ -dependent signalling reactions, Actin-binding protein
CRN5 (CORO2A)	525aa, 59kDa, 31%	Expressed in brain, epidermis	N.A.
CRN6 (CORO2B)	475aa, 54kDa, 44%	Focal adhesions, neurite tips, cell body and stress fibers	Actin and vinculin binding protein
CRN7 (CORO7)	925aa, 104kDa, 29%	Expressed in Cytosol, Golgi	Vesicular trafficking with Dd CRN7

Table.1 Summary of all mammalian coronin proteins with their corresponding molecular weight, amino acid content, percentage identity with *Dictyostelium* short coronin CRN12, expression and function.

1.2 Coronin Structure

Short coronins exhibit a characteristic three-domain organisation, consisting of an N-terminal domain containing a WD repeat- β -propeller structure, an unique C-terminal extension and a C-terminal coiled coil domain. (Fig 3).

1.2.1 N-terminal domain (β -propeller structure)

The WD40 repeat region is the signature domain of coronin family of proteins (de Hostos, 1999). The crystal structure of murine CRN4 (synonyms: coronin-1A, coronin-1) lacking its coiled coil domain, disclosed a seven-bladed β -propeller structure assembled from five canonical WD repeats and two non-canonical repeats (Appleton et al., 2006). The secondary structure motif of WD repeat sequence forms four consecutive β -strands connected by loops and turns, together defined as β -propeller. Within the propeller, each blade is built up of four anti-parallel β -strands extending from the centre to the periphery and the blades are arranged in a circular fashion around a central axis. Structurally the innermost β -strands A, B, and C of a blade and the outermost strand D are contributed by the second, third and fourth strands of one and the first strand of the next WD sequence repeat, respectively. results in stability Additionally, two tandem stretches of conserved residues located in the C-terminal extension tightly pack against the bottom side of the propeller, which possibly provides further structural integrity (McArdle and Hofmann, 2008). Even though β -propeller structures are in principle thought to serve as a stable platform for protein-protein interaction, so far only F-actin has been identified as a potent binding partner of this region in *Dictyostelium*, yeast and mouse CRN1. Therefore, thorough evaluation of this domain may reveal new binding partners (Gandhi and Goode, 2008).

1.2.2 Unique region

A region in the coronin structure that remains poorly understood is the unique C-terminal region. It highly varies in length, sequence and functions (Gandhi and Goode, 2008a). Notably this region in *S. cerevisiae* CRN11 (synonym: Crn1p) and *D.melanogaster* CRN7 (synonym: Dpod1) showed sequence homology with the microtubule-binding region of mammalian MAP1B. Correspondingly, purified coronin protein of these organisms was shown to crosslink microtubules and actin filaments in vitro. In *Drosophila*, CRN7 is required for proper axonal guidance. (Goode et al., 1999; Rothenberg et al., 2003)

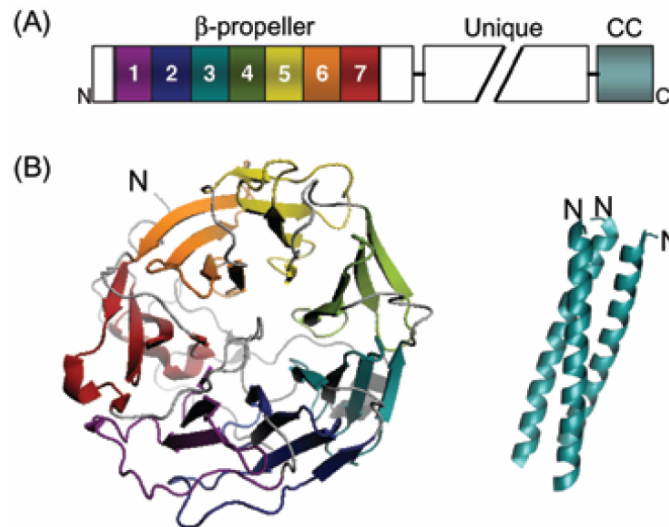


Figure 3. Coronin domain organisation and protein structure. A. Schematic of coronin domain architecture B. Crystal structure of mouse CRN4 β -propeller domain (Appleton et al., 2006) and coiled-coil domain (Kammerer et al., 2005). Taken from (Gandhi and Goode, 2008).

1.2.3 Coiled coil domain

The very C-terminus of short coronin proteins is composed of a moderately conserved coiled coil domain (~35-50 residues, 4-7 heptad repeats) which in CRN4 is identified to possess a leucine zipper motif. Eventhough, it is the smallest functional domain of coronin structure, it mediates at least three crucial functions like homo-oligomerisation and interaction with F-actin and Arp2/3 complex (Gandhi and Goode, 2008a). Coiled coil motifs are found to display a characteristic hepta-peptide repeat $(abcdefg)_n$, where positions a and b are predominately hydrophobic residues and positions e and g are charged residues (McArdle and Hofmann, 2008). In case of CRN4 threefold repeat of such a characteristic hepta-peptide sequence is determined and the motif R-L/I/V-X-X-L/V-E (450-455 in CRN4) has been recognised as a mediator of trimerisation in coiled coil (Kammerer et al., 2005).

1.3 Oligomerisation

All mammalian short coronins reported so far exhibit a coiled coil domain that has been implicated in oligomerisation (Utrecht and Bear, 2006). A number of studies have shown that oligomerization of coronins is exclusively homotypic (Cai et al., 2005; Gatfield et al., 2005; Oku et al., 2005). A functional significance of coronin oligomerisation is to execute actin filament bundling (Goode et al., 1999). Therefore this observation leads to one possible model in which multimerization of the coronin β -propeller would establish actin bundling. Deletion of the coiled-coil domain weakened the actin binding affinity of coronin (Cai et al., 2005). Another study reports, that the ability of the coiled-coil domain is to increase the actin binding

affinity through multimerization of the β -propeller domain (Cai et al., 2007). This gives rise to the second possibility, in which individual (non-oligomerised) coronin molecules might cross-link actin filaments using two separate actin binding sites, one in the β -propeller and another in coiled-coil domain (Gandhi and Goode, 2008).

1.4 Interactions with Arp2/3 complex

The diversity of F-actin structures and associated cellular functions depends on many actin-binding proteins (Cvrckova et al., 2004; Sutherland and Witke, 1999). The submembranous area of a cell is enriched in branched F-actin filaments and the Arp2/3 complex (Goley and Welch, 2006). Prime examples of a cellular function involving branched F-actin are the formation of lamellipodia and cellular motility. The Arp2/3 complex is enriched in the periphery of lamellipodia and plays a key role in forming a short-branched F-actin network that generates the protruding force depending on a locally well-organized assembly and disassembly of F-actin (Fig. 4) (Nabi, 1999; Pantaloni et al., 2001; Ponti et al., 2005; Rybakin and Clemen, 2005). The Arp2/3 complex consists of seven subunits. p34 (Arc35, ARPC2) together with ARPC4 forms the center of the Arp2/3 complex which initiates site-directed branching and elongation of actin filaments and nucleates new actin filaments (Cooper et al., 2001; Gournier et al., 2001; Pollard and Beltzner, 2002; Stradal and Scita, 2006).

In addition to F-actin binding the unique C-terminal region and the coiled-coil domain of yeast CRN11 was shown to bind with Arp2/3 complex (Humphries et al., 2002; Machesky et al., 1997). Further, purified yeast CRN11 was demonstrated to execute inhibitory effect on Arp2/3 driven F-actin polymerisation. The inhibitory influence is due to maintenance of Arp2/3 complex in an inactive or open confirmation which becomes unavailable for WASp activation which results in Arp2/3 mediated actin polymerisation. CRN11 constructs lacking the coiled-coil domain were inefficient to interact with Arp2/3 complex (Rodal et al., 2005). Colocalization studies of CRN1 (synonyms: coronin-1B, coronin-2) with Arp2/3 complex was also reported in a variety of cells. In addition, mouse CRN4 was shown to control steady-state F-actin levels via an Arp2/3 complex driven mechanism in T-lymphocytes (Foger et al., 2006).

1.5 Coronin regulation by phosphorylation

A number of evidence demonstrates mammalian coronins to be regulated by phosphorylation (Utrecht and Bear, 2006). CRN4 was shown to be phosphorylated in vitro by purified PKC, which is stimulated in vivo by PMA treatment (Itoh et al., 2002). In addition, PKC inhibitor celerythrine was shown to block both phosphorylation and dissociation of CRN4 from

phagosomes (Gatfield et al., 2005). Similar studies pertaining to PKC stimulation with phorbol ester PMA and down regulation using PKC inhibitors were shown to be responsible for phosphorylation of CRN1 (Cai et al., 2005). Further, CRN7 was shown to get phosphorylated on tyrosine residues (Rybakin et al., 2004).

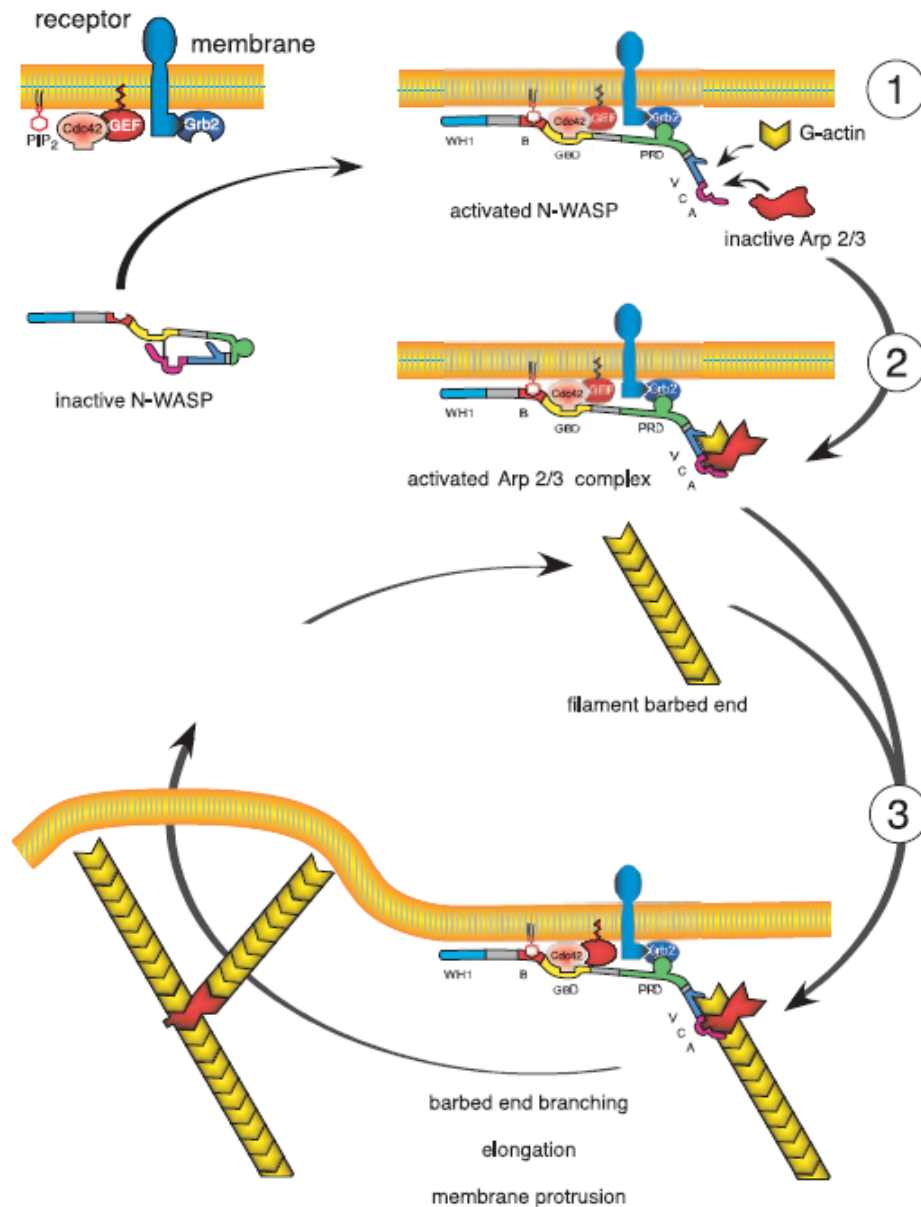


Figure 4. Arp2/3 mediated actin polymerisation at the leading edge. N-WASP is activated and targeted to the membrane by signaling molecules (circled 1). G-actin and the Arp2/3 complex together bind to N-WASP (VCA), forming a branching complex (circled 2), binding of the branching complex with a filament leads to the formation of a branch (circled 3). Both the branches grow at equal rates. N-WASP catalyzes several consecutive cycles of branching. Taken from (Pantaloni et al., 2001).

1.6 Coronins in disease

Since regulation of actin dynamics is an essential part of many disease states, actin binding coronin proteins could play a role in diseases. A role of CRN4 in pathogenic bacterial infection can be considered as one of the best-characterized examples (Ferrari et al., 1999). A well established mechanism to destroy engulfed bacteria by macrophages are through controlled membrane fusion of phagosomes with lysosomes, wherein delivery of lytic enzymes acidify phagolysosomes resulting in effective destruction of bacteria (Anes et al., 2003; Vergne et al., 2004). Actin polymerisation around nascent phagosomes plays a potential role in driving these critical vesicle fusion events, emphasizing importance of actin dependent process in immune response to combat bacterial infections (Anes et al., 2003). Recent studies reveal that pathogenic *Mycobacterium tuberculosis* are able to circumvent the normal immune response by macrophages through retaining CRN4 function to alter the actin dynamics on the phagosome, thereby preventing the maturation of phagosomes and permitting bacterial propagation within the macrophage (Ferrari et al., 1999). Further CRN1 was linked with neurite formation and axon regeneration with subsequent spinal cord injury (Di Giovanni et al., 2005).

1.7 CRN2 (coronin-1C, coronin-3)

CRN2 (current official symbol: CORO1C, current official name: coronin-1C, most common synonym: coronin-3) is a short coronin protein (Rybakin and Clemen, 2005) of 474 amino acids with a calculated molecular mass of 53 kDa in human and murine cells; the apparent molecular mass from SDS-PAGE analysis is approximately 57 kDa (Fig.5). Based on the crystal structure of CRN4 a structural homology model of CRN2 was proposed (Fig.6) (McArdle and Hofmann, 2008). At the subcellular level CRN2 exists in two different pools, an actin cytoskeleton associated non-phosphorylated pool and a diffusely distributed phosphorylated cytosolic pool and represented as multiple spots on 2D gels (Spoerl et al., 2002). CRN2 has been identified as an actin filament-crosslinking and bundling protein (Hasse et al., 2005; Spoerl et al., 2002) involved in distinct cellular functions like proliferation, migration, formation of cellular protrusions, endocytosis and secretion (Rosentreter et al., 2007). Recent studies indicate CRN2 as an important factor in the development of the murine brain (Hasse et al., 2005) as well as a potential marker for melanoma progression (Roadcap et al., 2008).

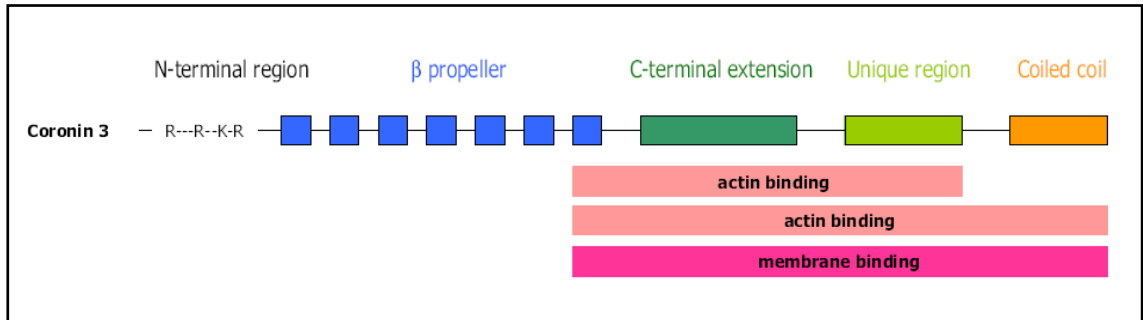


Figure 5. Human CRN2 domain organisation. Mapped membrane and actin binding sites are indicated. Taken from (McArdle and Hofmann, 2008).

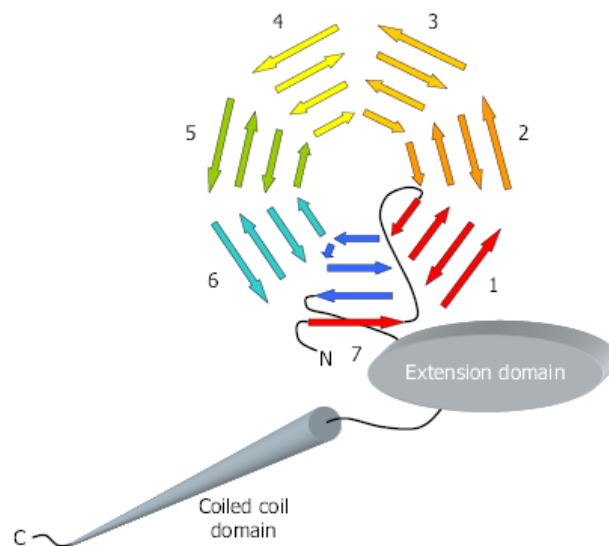


Figure 6. Putative topology of CRN2 based on structural information of CRN4 showing the N-terminal 7-blades of the β propeller structure and the C-terminal extension and coiled coil domain. Taken from (McArdle and Hofmann, 2008).

1.8 Aim of the work

Coronins are one of the most versatile family of proteins evolutionarily well conserved amongst eukaryotes and mammals including *Dictyostelium*, *Drosophila*, mouse and humans. With its origin as a single gene in simple eukaryotes, the mammalian coronin gene family has shown expansion to include seven members. Human CRN2 is one of the ubiquitously expressed short coronin proteins with F-actin binding and cross-linking properties. In this thesis work we attempt to characterize human CRN2 with respect to its biochemical and cellular functions.

- We investigate the role of CRN2 in cellular processes in association with actin cytoskeleton through over expression of coronin domains, down-regulation of CRN2 levels using the RNAi technique and co-immunoprecipitation studies.
- We analyse the expression of CRN2 in normal as well as various types of malignant and benign human brain tumours. Further we pursue *in vitro* functional studies using CRN2 knockdown in glioblastoma cells and investigate the role of CRN2 in regulating cell proliferation, migration and invasion.
- We study functional and structural diversity of three human CRN2 isoforms, designated as CRN2i1, CRN2i2 and CRN2i3.
- We investigate the regulation of the cellular activity of CRN2.

Note: In some of the figures CRN2 is specified as coronin-3 or coronin-1C which are synonyms of CRN2.

1.9 Preliminary publications

Significant parts of this work have been published as research articles:

- **Xavier C-P**, Rosentreter A, Reimann J, Cornfine S, Linder S, Hofmann A, Morgan RO, Fernandez MP, Stumpf M, Müller R, Jungbauer T, Schröder R, Noegel AA, Clemen CS. Coronin-1C isoforms are novel components of podosomes and sarcomeres. *Submitted for publication*.
- **Xavier C-P**, Eichinger L, Fernandez MP, Morgan RO, Clemen CS. Evolutionary and Functional Diversity of Coronin Proteins. In: The Coronin Family of Proteins. Vol. 48. Eds.: Clemen CS, Eichinger L, Rybakin V. *Landes Bioscience & Springer. 2008*. ISBN 978-0-387-09594-3. Open access at <http://www.eurekah.com/chapter/3808>.
- **Thal DR, Xavier C-P**, Rosentreter A, Waha A, Pietsch T, Stumpf M, Noegel AA, Clemen CS. Expression of coronin-3 (coronin-1C) in diffuse gliomas is related to malignancy. *J Pathol 2008* 214:415-24. *Equal contributors*.
- Rosentreter A, Hofmann A, **Xavier C-P**, Stumpf M, Noegel AA, Clemen CS. Coronin 3 involvement in F-actin dependent processes at the cell cortex. *Exp Cell Res 2007* 313:878-95.

II. Results

2.0 Role of CRN2 in cellular processes

2.1 CRN2 interacts with the F-actin cytoskeleton in vivo

In HaCaT cells endogenous CRN2 shows a characteristic however not continuous localization to the submembranous area. This localization is particularly obvious in cells, which exhibit a strong accumulation of actin filaments underneath the plasmamembrane. CRN2 additionally was detected at punctate structures in the cytoplasm, with a perinuclear accumulation of these spots (Fig. 7A, upper panel). To confirm the subcortical enrichment of CRN2, HaCaT cells were retrovirally transduced to express GFP-CRN2. The distribution of GFP-CRN2 (Fig. 7B, left panel) and endogenous CRN2 (Fig. 7B, right panel; this is a higher magnification of the upper left image of Fig. 7A) are congruent, however, the GFP-signal of CRN2 more clearly shows the protein's cortical localization.

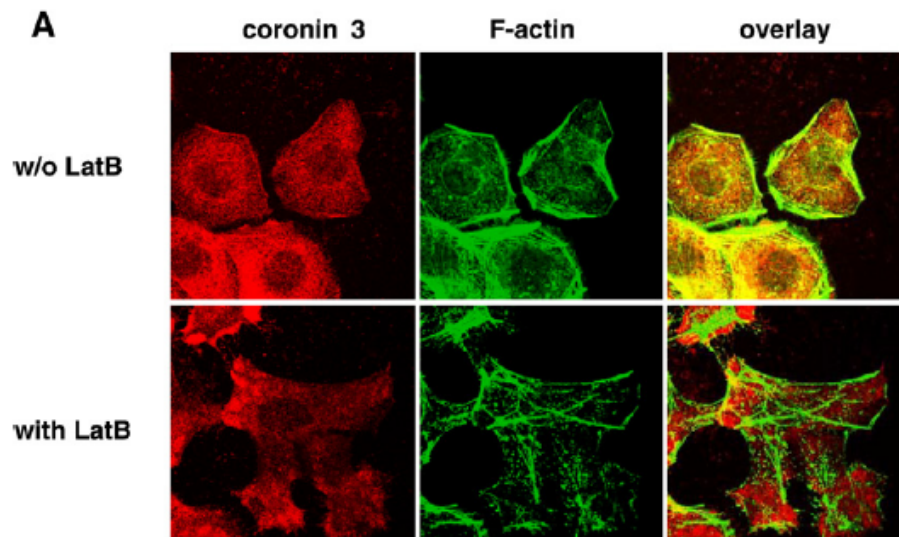


Figure 7. CRN2 shows an F-actin-dependent distribution in HaCaT cells. A. HaCaT cells treated with or without latrunculin B were first fixed with 4% paraformaldehyde and then permeabilized with 0.2% Triton X-100 (data shown). CRN2 was detected using mAb K6-444 and goat anti-mouse Cy3 as secondary antibody; F-actin was visualized using FITC-phalloidin.

This cortical localization of endogenous CRN2 is maintained after Triton X-100 permeabilization prior to fixation (data not shown), indicating a stable association of coronin3 and F-actin in vivo. By contrast, HaCaT cells treated with latrunculin B prior to fixation never showed any accumulation of CRN2 underneath the plasmamembrane, but CRN2 appears in spots clearly distinguishable from the remaining F-actin staining (Fig. 7A, lower panel). The

latter F-actin structures represent a pool that is resistant to the treatment with latrunculin B (Ammar et al., 2001). HaCaT cells treated with latrunculin B and Triton X-100 prior to fixation neither showed a structured staining of CRN2 nor of F-actin (data not shown); most of both proteins disappeared and only a diffuse residual staining remained.

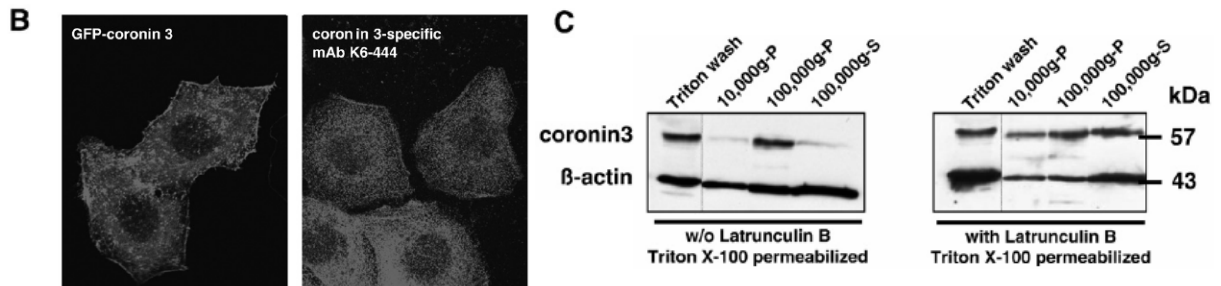


Figure 7, continued. B Higher magnifications of HaCaT cells expressing GFP–CRN2 (left; same expression vector is used in HEK293 cells, Fig. 7B) and of antibody-stained endogenous CRN2 (right; higher magnification of the upper left image from A) demonstrate a submembranous localization of CRN2. **C.** Corresponding to A, cells were incubated with or without latrunculin B, washed with Triton X-100, and lysed cells were separated by differential centrifugation. Samples of the Triton X-100 soluble fraction (Triton wash) and the centrifugation steps were analyzed by SDS–PAGE followed by Western blotting using antibodies against CRN2 (mAb K6-444) and β -actin. S, supernatant, P, pellet fractions.

These observations were confirmed by differential centrifugation and immunoblotting (Fig. 7C). The relative distribution of CRN2 within different fractions of each experiment can be compared. In untreated HaCaT cells CRN2 is most abundant in the 100,000 g pellet; minor amounts are detectable in the 10,000 g pellet and in the 100,000 g supernatant. CRN2 as well is detected in the Triton X-100 soluble fraction (Triton X-100 wash). Note that the 10,000 g pellet contains the crude cytoskeletal fraction (highly crosslinked actin filaments) and the pellet of 100,000 g includes cytoskeletal elements associated with membranes (free or loosely crosslinked actin filaments) (Fox, 1985; Lehtonen et al., 2002; Tohyama et al., 1994). After treatment with latrunculin B the amount of CRN2 in the 100,000 g pellet is markedly reduced and instead appears in the 100,000 g supernatant. The data from immunofluorescence analysis and differential centrifugation confirmed a binding of CRN2 to F-actin as previously described (Spoerl et al., 2002) and clearly demonstrate a localization of CRN2 that depended strongly on F-actin *in vitro* as well as *in vivo*.

2.2 Absence of CRN2 or lack of single domains inhibits fibroblast migration

To determine the contribution of CRN2 in cellular processes, we investigated wound healing of confluent layers of HEK293 cells stably expressing CRN2 proteins. Wound healing was

monitored over 10 h (Figs.8A, B). We observed a statistically significantly reduced velocity of wound closure in case of all CRN2 polypeptides compared to WT cells, which exhibited the fastest wound closure with an average velocity of 23 $\mu\text{m}/\text{h}$. Comparing CRN2-NWDC (20 $\mu\text{m}/\text{h}$) with the other CRN2 polypeptides demonstrated that except for CRN2- ΔCC (21 $\mu\text{m}/\text{h}$; F-actin binding regions are present in this fusion protein) all proteins led to statistically significantly slower wound closure velocities. Cells, which express CRN2-NC and CRN2-NGC, lacking the central WD40 repeats or carrying a glycine loop instead, showed reduced velocities of 14 $\mu\text{m}/\text{h}$ and 15 $\mu\text{m}/\text{h}$ respectively. The strongest impairment in wound healing was noted for CRN2- ΔNC (11 $\mu\text{m}/\text{h}$) and CRN2-WD (11 $\mu\text{m}/\text{h}$).

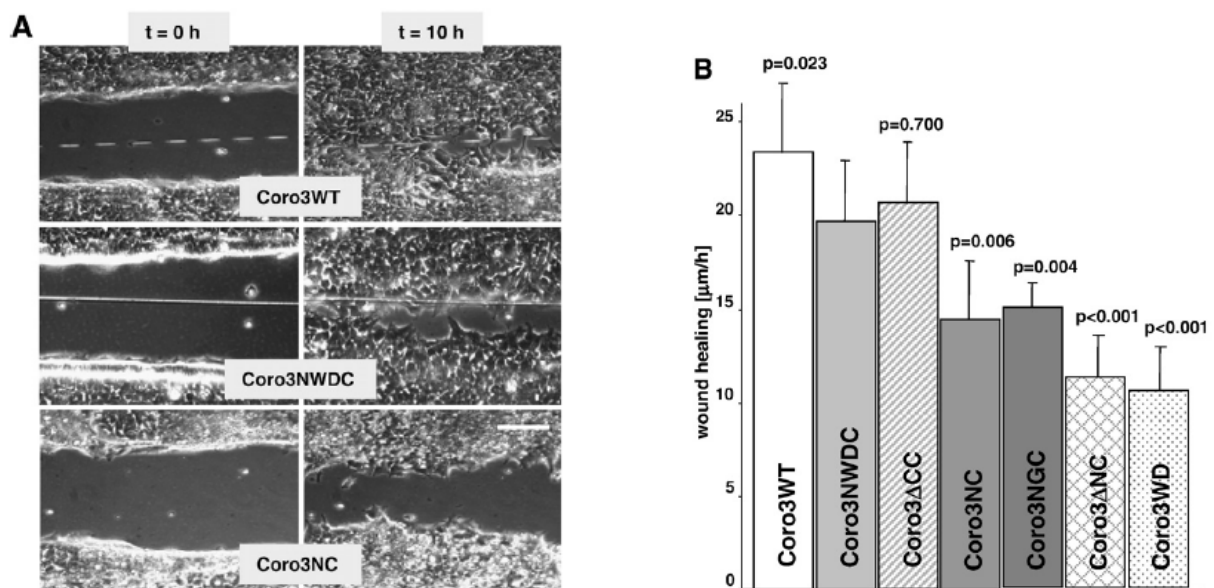


Figure 8. CRN2 knockdown using siRNA as well as expression of EGFP-CRN2 fusion proteins affect wound healing. **A.** Column on the left presents the wounds immediately after wounding a confluent HEK293 cell layer with a needle, the column on the right presents the wounds after 10 h. Cells expressing CRN2-WT (endogenous CRN2), CRN2-NWDC, and CRN2-NC are shown. Scale bar: 100 μm . **B.** Effect of coronin fusion proteins on wound healing. Error bars indicate the standard deviation from three independent experiments, each with three determinations of the width of the wound. p-values refer to the population expressing CRN2-NWDC and were calculated by Student's t-test; $p < 0.05$ is significant. CRN2- ΔCC displayed least effect in wound closure velocity with $p=0.700$ in comparison to CRN2-NC ($p=0.006$), CRN2-NGC ($p=0.004$). Both CRN2- ΔNC and CRN2-WD ($p < 0.001$) exhibited highest inhibitory effect in wound closure.

To further support the involvement of CRN2 in wound healing we performed wound healing assays with NIH3T3 fibroblasts in which the level of CRN2 was significantly decreased by RNAi silencing. 48 h after two treatments with a mixture of four different siRNA duplexes, confluent monolayers of wild-type NIH3T3 and siRNA transfected NIH3T3 cells were wounded. RNAi-treated cells showed a significantly delayed wound closure with an averaged

velocity of 25 $\mu\text{m}/\text{h}$ compared to untransfected wild-type cells (33 $\mu\text{m}/\text{h}$). Control cells treated only with luciferase-specific siRNA or with transfection reagent showed no impairment. Immunofluorescence images of CRN2 siRNA-treated cells did not reveal any obvious change and behaved like wild-type in the F-actin staining, although the CRN2-specific signal intensity was reduced in virtually all cells. The reduction in CRN2 expression calculated from Western blotting was approximately 90% (Fig. 8C).

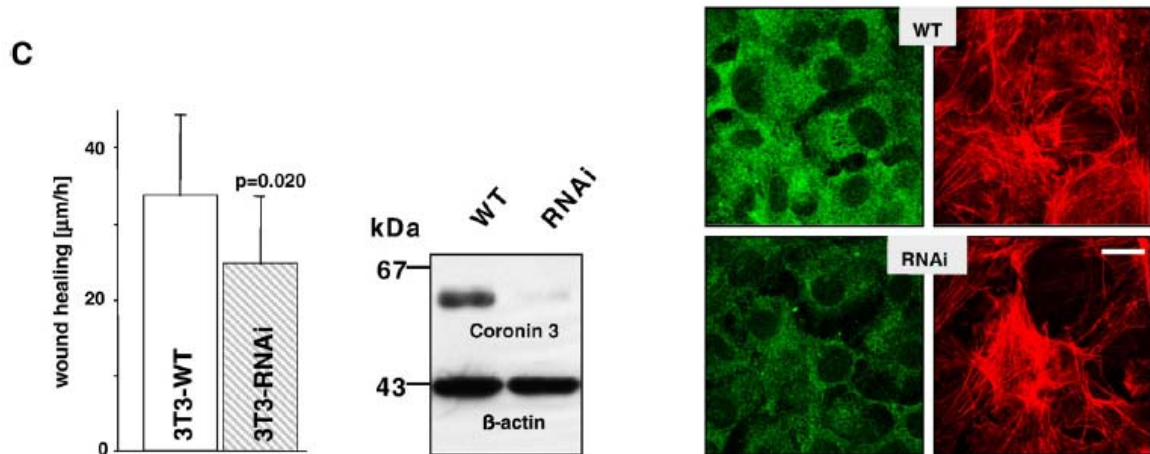


Figure 8, continued. C. Representation of the wound healing behaviour of wt and siRNA-treated NIH3T3 cells. Error bars indicate the standard deviation from three independent experiments, each with five determinations of the width of the wound. Western blot shows a \sim 90% reduction of the CRN2 expression, immunofluorescence imaging as well indicate a decreased expression level of CRN2, but no obvious change in the F-actin cytoskeleton. The p-value was calculated with single factor ANOVA; $p < 0.05$ is significant.

2.3 Expression of the WD-repeat domain of CRN2 inhibits cell proliferation

We addressed the effects of CRN2 on cell proliferation and cytokinesis. Wild-type HEK293 and the stably transfected cell populations, which exhibited differences compared to CRN2-NWDC in the wound healing assay, were seeded in low concentrations and counted again after 3 days to calculate cell proliferation. CRN2-NWDC, CRN2-NC, CRN2-NGC, and wild-type cells showed only slight and insignificant differences in cell proliferation. A statistically significant inhibition of proliferation was detected for cells expressing CRN2- Δ NC and CRN2-WD (Fig.9A).

To verify that the reduced cell proliferation rate is not due to defects in cytokinesis, we repeated the experiment and determined the number of multinucleated cells after 3 days of cultivation (Fig. 9B). Here, only CRN2-NWDC and wild-type HEK293 cells showed similar low levels of multinucleated cells, but cells transfected with any of the CRN2 domain constructs showed approximately five-fold increased levels of multinuclear cells. An

evaluation of the number of cells harboring two, three, or four and more nuclei detected no further differences. Note that CRN2-NC and CRN2-NGC induce defects in cytokinesis though no change in proliferation rate is detected. Only CRN2- Δ NC and CRN2-WD exhibit both, a reduced cell proliferation rate and an increased number in multinucleated cells. Cell proliferation and cytokinesis independently are changed by the presence of CRN2 peptides.

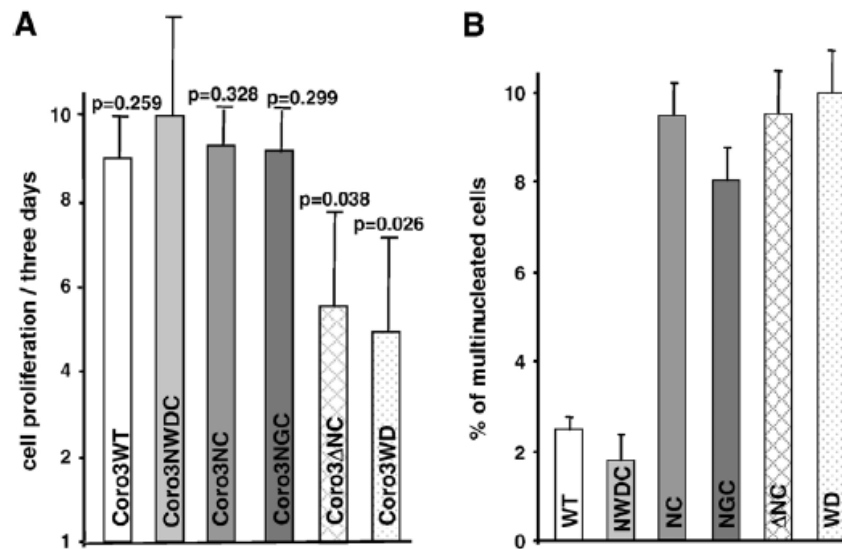


Figure 9. EGFP-CRN2 fusion proteins affect cell proliferation and cytokinesis. **A.** Proliferation rates of HEK293 cells expressing the indicated fusion proteins after 3 days of cultivation. The error bars represent the standard deviation of three independent experiments. p-values refer to the CRN2-NWDC cell population and were calculated by Student's t-test; $p < 0.05$ is significant. **B.** Bars indicate the number of cells having more than one nucleus per cell for different HEK293 cell populations. The values are from two independent experiments with approximately 185 cells analyzed per cell line. A significantly high percentage of multinucleated cells were seen in CRN2-WD, Δ NC, NC, and CRN2-NGC in comparison to CRN2-WT (endogenous coronin) and CRN2-NWDC, where lowest percentage was measured.

2.4 CRN2 participates in the formation of cellular protrusions

One major aspect of cell migration is the formation of cellular protrusions. Therefore, the activity of single wild-type HEK293 cells or cells expressing CRN2 domains were recorded over 30 min (Fig.10A). Figure 10 is representative of several experiments. Wild-type HEK293 cells could not be distinguished from the CRN2- Δ CC, CRN2-NC, and CRN2-NGC populations with respect to the number of protrusions formed. CRN2-NWDC cells exhibit a slightly increased number of protrusions, which was also detected by immunofluorescence images of fixed cells. A markedly reduced number of lamellipodia as well as filopodia were detected in HEK293 cell populations expressing CRN2- Δ NC and CRN2-WD. Further they showed the lowest frequencies of changes in the number of forming or retracting protrusions

(2.5 and 1.0, respectively). Although HEK293 populations expressing CRN2-NC do not exhibit a change in the number of protrusions, the frequency of their formation is reduced (Fig.10B). The presence of the glycine loop between the N- and C-terminus (CRN2-NGC) ameliorates the defect.

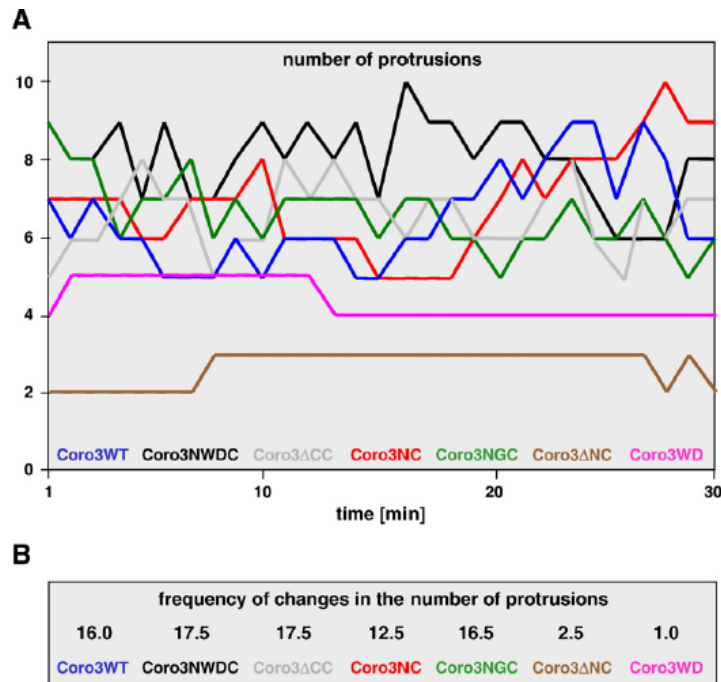


Figure 10. CRN2 fusion proteins alter the activity of HEK293 cells. The changes in the number of cellular protrusions including lamellipodia and filopodia followed over 30 min for the wt and cell populations expressing the CRN2 polypeptides indicated are given. **A.** Graph is representative for several independent experiments.

B. Mean frequency of changes in the number of protrusions of each cell population over the time. A significantly reduced number of lamellipodia or filopodia was demonstrated by CRN2 Δ NC and CRN2-WD. Unlike CRN2-WD, all other constructs (CRN2-WT, NWDC, Δ CC, NC, NGC) displayed almost similar number of cellular protrusions without notable difference.

2.5 Full-length CRN2 is essential for the process of fluid phase pinocytosis

To investigate further possible roles of CRN2 at the submembranous cytoskeleton, the uptake of material was investigated. Phagocytosis is restricted to specialized mammalian cells and was not studied. Fluorescent transferring uptake was used to quantify the receptor-mediated and clathrin-associated endocytosis. This process was found to be unchanged in all HEK293 cell populations compared to the wild-type (data not shown). In contrast, pinocytosis of the fluid phase marker HRP was significantly affected (Fig.11). CRN2- Δ NC and CRN2-WD caused a distinctly reduced pinocytotic activity, while CRN2-NC and CRN2-NGC exhibited an intermediate decrease of pinocytosis.

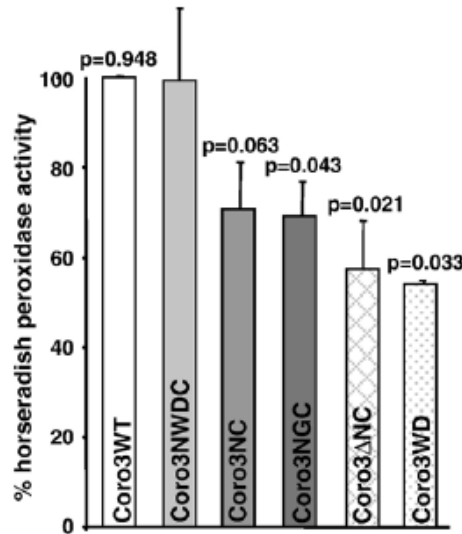


Figure 11. CRN2 proteins influence fluid phase pinocytosis. HEK293 cells expressing CRN2 fusion proteins were harvested and lysed after exposing them for 60 min to HRP-containing medium (2 mg/ml). The experiments were carried out three times in duplicate. The results were normalized to the total protein amount. p-values calculated by single-factor ANOVA refer to the population of CRN2-NWDC; $p < 0.05$ is significant. A statistically considerable reduction in pinocytotic activity was measured in case of CRN2- Δ NC ($p=0.021$) and CRN2-WD ($p=0.033$). Intermediate pinocytotic activity was displayed by CRN2-NGC ($p=0.043$) and CRN2-NC ($p=0.063$) with no difference in case of CRN2-NWDC and CRN2-WT ($p=0.948$).

2.6 CRN2 forms a complex with the Arp2/3-complex and with cofilin

Previous studies had reported an interaction between yeast CRN11 and mammalian CRN1 and the Arp2/3 complex (Humphries et al., 2002) (Cai et al., 2005; Rodal et al., 2005). Here we tested complex formation with CRN2. HEK293 cells expressing CRN2-NWDC were used for several independent co-immunoprecipitation assays employing a monoclonal GFP-antibody (Fig.12). Prior to harvest, the cells were treated with latrunculin B to prevent unspecific co-precipitation of proteins bound to and tied together by F-actin. Precipitated proteins were analyzed by mAb K6-444 detecting the endogenous CRN2 as well as the EGFP-fusion protein. As expected, the endogenous CRN2 binds to and co-precipitates with EGFP-CRN2, most likely in a heterotrimeric complex (Spoerl et al., 2002). Using antibodies specifically recognizing cofilin and the p34 (arc35) subunit of the Arp2/3 complex, we detected these proteins in the immunoprecipitate. For control we used BiP/GRP78- and β -actin-specific antibodies excluding unspecific binding of the cell lysate or actin to the protein G sepharose beads.

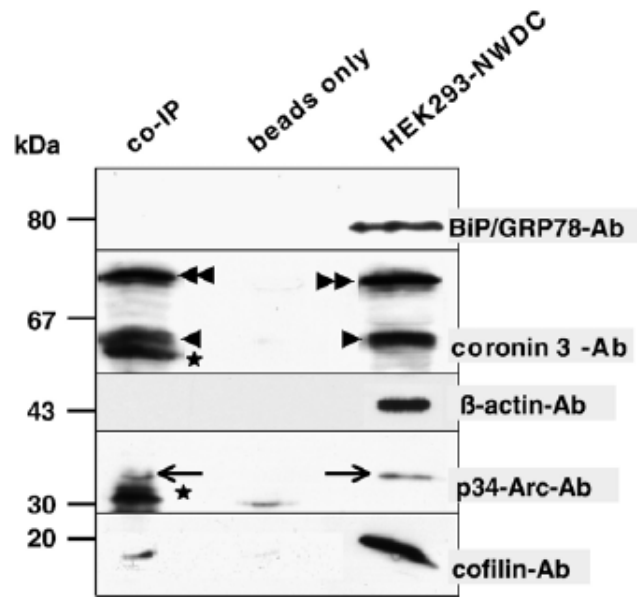


Figure 12. Endogenous CRN2, p34-Arc, and cofilin co-immunoprecipitate with EGFP-CRN2. HEK293 cells expressing EGFP-CRN2 were treated with latrunculin B and used for co-immunoprecipitations with an anti-GFPmAb. Samples were analyzed by immunoblotting using antibodies specifically recognizing CRN2, p34-Arc, and cofilin (co-IP). For control the experiment was carried out with cell lysate (beads only) or with anti-GFP mAb only, and the blot was probed with antibodies directed against BiP/GRP78 and β -actin. Arrowhead, endogenous CRN2; double-arrowhead, EGFP-CRN2; arrow, p34 (arc35); asterisk, unspecific bands of the GFP-antibody solution. The signals for BiP/GRP78, CRN2, and p34-Arc are from the same membrane probed serially; signals for β -actin and cofilin are from parallel Western blots.

2.7 Structural properties of CRN2 deduced from the CRN4 crystal structure

Originally, CRN2, like all short coronin proteins, was thought to consist of an N-terminal domain (aa 1–71), a core region containing five WD40-repeats (aa 72–299), and a C-terminal domain (aa 300–474) (de Hostos, 1999; Rybakin and Clemen, 2005). Based on a manual amino acid alignment, we have proposed a CRN2 structure similar to the seven-bladed propellers known from other WD40 proteins [Hofmann and Clemen, unpublished]. The two additional WD40-repeats of CRN2 are located in the N-terminal domain (aa 1–71) and the conserved part of the C-terminus (aa 300–404) (Fig.13); aa 1–11, the coronin-specific signature motif, and 348–404 do not contribute to the respective WD40-repeats. This hypothesis was confirmed by the crystal structure of truncated CRN4 (aa 10–aa 400) which revealed the presence of seven WD40-repeat domains (Appleton et al., 2006) which had also been predicted by (Gatfield et al., 2005). Based on these data of CRN4, we investigated the overall structure as well as intramolecular interactions of CRN2. It seems highly likely that CRN2 adopts a similar N-terminal fold as CRN4 sharing the characteristic feature of the first N-terminal beta strand completing the last propeller blade of the WD40-repeat domain

constituted by amino acids 13–348 (Fig.13). As identified in CRN4 intramolecular interactions might stabilize the C-terminal extension by anchoring it to the WD40 beta-propeller. The main contributors to these interactions are hydrogen bonds of Tyr362 to the backbone carbonyl groups of Val327 and Glu331, and the side chain interactions of the N-terminal Lys9 with Arg352 and Asp360. There is also a hydrophobic interface being formed between residues His139, Ile157, Trp182 and Ile189 from the WD40-repeat domain and Trp377 and Phe378 from the C-terminal extension. Since there is a high degree of conservation between CRN4 and CRN2 in these regions, the significance of these interactions concluded from the CRN2 homology model seems quite likely. Analyses of structure and electrostatic potential of the surface of CRN4 resulted in the identification of potential F-actin binding sites. They comprise a region on the top of propellers 1, 6, 7, and a second region on the bottom side of propellers 6 and 7 (Appleton et al., 2006). Similar regions can be assigned to CRN2. The F-actin binding site in CRN4 also includes a stretch of positively charged amino acids (400–416 (Gatfield et al., 2005) in the C-terminal extension, which is mirrored in CRN2 (aa 398–aa 419; KNRDLKVVVKNILDSKPTANKK).

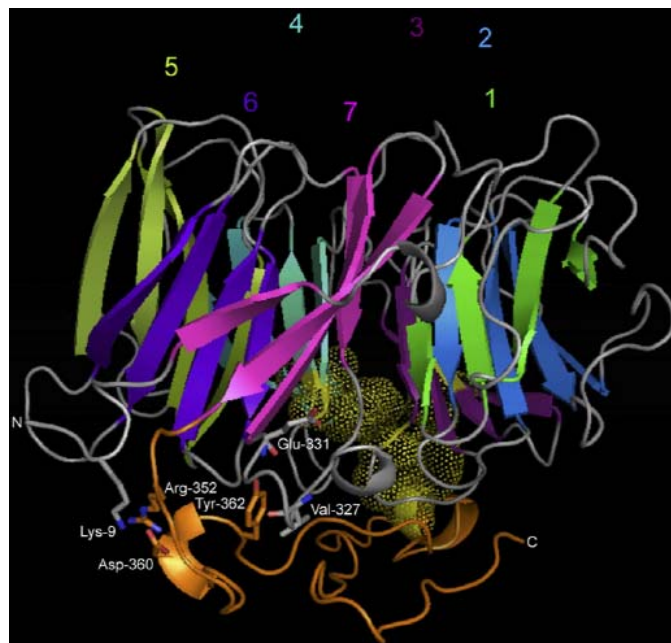


Figure 13. Homology model of CRN2 (aa 7–400). The model has been generated with the CRN4 crystal structure (Appleton et al., 2006) [PDB accession number 2aq5] as template using MODELLER (Sali and Blundell, 1993) and a manual alignment of amino acid sequences. The seven-blade propellers of the N-terminal WD40-repeat domain are colored individually and annotated by their sequential order. The C-terminal extension is shown in brown and polar interactions stabilizing its fold are drawn explicitly. The yellow dot surface maps a hydrophobic interface formed by residues His139, Ile157, Trp182, Ile189, Pro203, Trp377, and Phe378. Figure prepared with PyMOL (W.L. DeLano, 2002). Taken from (Rosentreter et al., 2007).

3.0 Expression of CRN2 in diffuse gliomas is related to malignancy

3.1 CRN2 is expressed in a subset of human brain tumours and in reactive astrocytes

The expression of CRN2 in normal human brain and in brain tumours was determined by histopathological analysis and immunoblotting. Normal human brain tissue in general exhibited virtually no CRN2 protein (data not shown). The white matter did not show CRN2 immunoreactive cells. Cortical neurons, on the other hand, were faintly labelled. Other groups of neuronal cells in the hippocampus (CA1-4, dentate gyrus), the neocortex and the cerebellum (Purkinje cells), as well as subpial astrocytes in neocortical layer I were also faintly labelled (Table 2).

Brain region/lesion/tumour	Substructures/layers/tumour comp.	coronin 3	n (IHC)	n (WB)
Neocortex	Subpial astrocytes in layer I	+	3*	2
	Layer I	-		
	Cortical layers II-VI	+		
	White matter	-		
Hippocampus	Subiculum	+	3*	0
	CA1	+		
	CA2	+		
	CA3	+		
	CA4	+		
	Dentate gyrus granule cells	+		
	White matter	-		
Cerebellum	Molecular layer	-	2*	0
	Purkinje cell layer	+		
	Granule cell layer	-		
	White matter	-		
Reactive gliosis after brain lesion	Astrocytes and microglial cells	+	5	0
Unspecific gliosis	Astrocytes and microglial cells	(+)	3	0
Pilocytic astrocytoma (WHO Grade I)	Astroglial pilocytic tumour cells	+	9	4
Diffuse astrocytoma (WHO Grade II)	Gemistocytic and protoplasmatic cells	+	5	2
	Fibrillar astrocytes	(+)		
Anaplastic astrocytoma (WHO Grade III)		+	5	8
Glioblastoma multiforme (WHO Grade IV)		+	13	2
Oligodendroglioma (WHO Grade II)	Tumour cells	- or (+)	3	2
	Minigemistocytes	- or +		
Anaplastic oligodendroglioma (WHO Grade III)	Tumour cells	+	6	1
	Minigemistocytes	- or (+)		
Oligoastrocytoma (WHO Grade II)	Oligodendroglial component	- or (+)	4	3
	Astroglial component	(+) or +		
Anaplastic oligoastrocytoma (WHO Grade III)	Oligodendroglial component	+	6	0
	Astroglial component	+		
Desmoplastic medulloblastoma (WHO Grade IV)		-	2	0
Neuroblastoma		-	1	0
Meningioma (WHO Grade I)		+	3	0

Table 2. Expression of CRN2 in the human brain and in different types of human brain tumours. +, expression of CRN2; (+), weak expression of CRN2; -, no expression of CRN2; n, number of cases; IHC, immunohistochemistry; WB, western blotting; □, autopsy cases from which different brain regions, i.e. cerebral cortex, hippocampal formation and cerebellum, were observed.

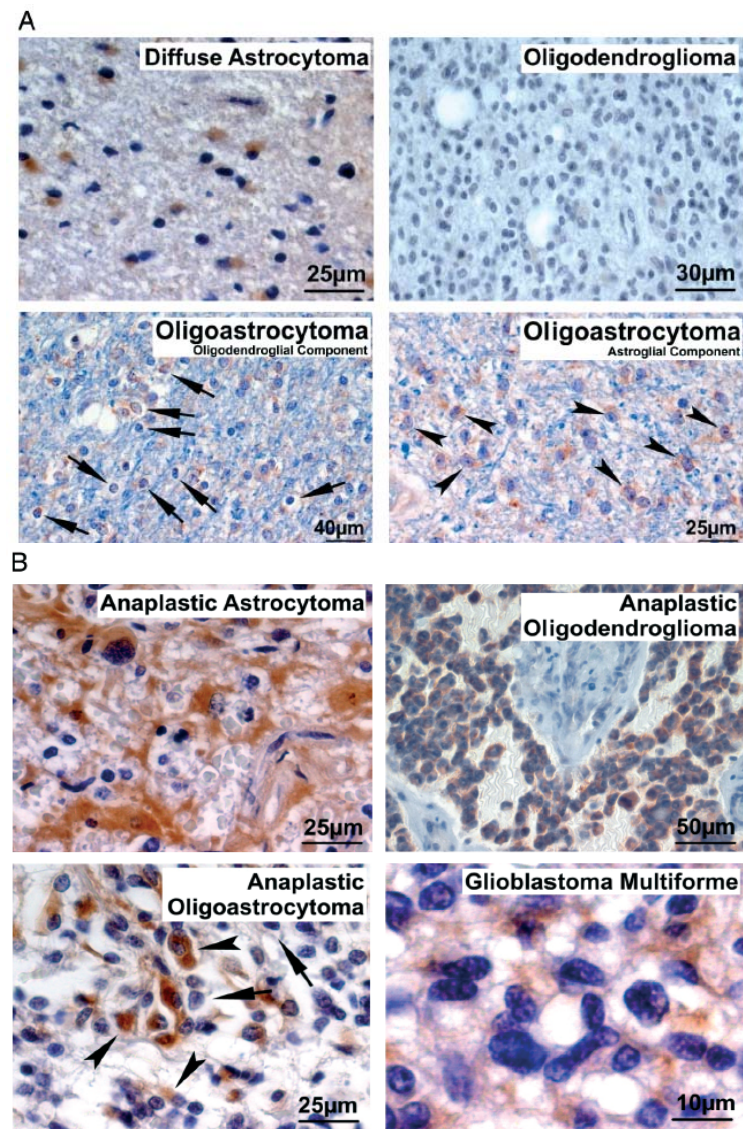


Figure 14. Expression of CRN2 in diffuse gliomas. **A.** Low-grade diffuse gliomas exhibited less prominent expression of CRN2 than high-grade gliomas. The diffuse astrocytoma showed CRN2 expression in no more than 50% of the tumour cells. Oligodendrogliomas often failed to express CRN2 (shown here) or were only weakly stained (refer to Table 2). In benign oligoastrocytomas CRN2 was mainly expressed in the astroglial component (arrowheads), while the oligodendroglial component was either not or only weakly stained (arrows). **B.** In contrast, expression of CRN2 in an increased number of tumour cells was noted in high-grade diffuse gliomas. Anaplastic astrocytomas and anaplastic oligodendrogliomas exhibited CRN2 immunoreactivity in >50% of the tumour cells. In anaplastic oligoastrocytomas, CRN2 was expressed in the malignant tumour component. In the presented case, CRN2 expression was mainly found in the astroglial component (arrowheads), whereas the oligodendroglial component appeared well differentiated and did not stain for CRN2 (arrows). In anaplastic oligoastrocytomas with a malignant transformation of the oligodendroglial component, this component also started to express CRN2. In glioblastomas, nearly all tumour cells showed CRN2 expression.

The expression of CRN2 in tumours varied among different types of brain tumour. No expression of CRN2 was detectable in tumours of neuronal origin, viz in the desmoplastic

medulloblastomas and a neuroblastoma (Table 2). On the other hand, two benign tumour entities, benign meningiomas and pilocytic astrocytomas, exhibited a high number of tumour cells expressing CRN2 (Table 2). Low-grade diffuse astrocytomas, oligodendrogliomas and oligoastrocytomas, however, showed a limited number of CRN2-positive tumour cells (Fig.14A and Table 2; note that oligodendrogliomas showed either no or a small number of tumour cells expressing CRN2), while highgrade anaplastic astrocytomas, anaplastic oligodendrogliomas, anaplastic oligoastrocytomas and glioblastomas exhibited high numbers of CRN2-positive tumour cells (Fig. 14B and Table 2).

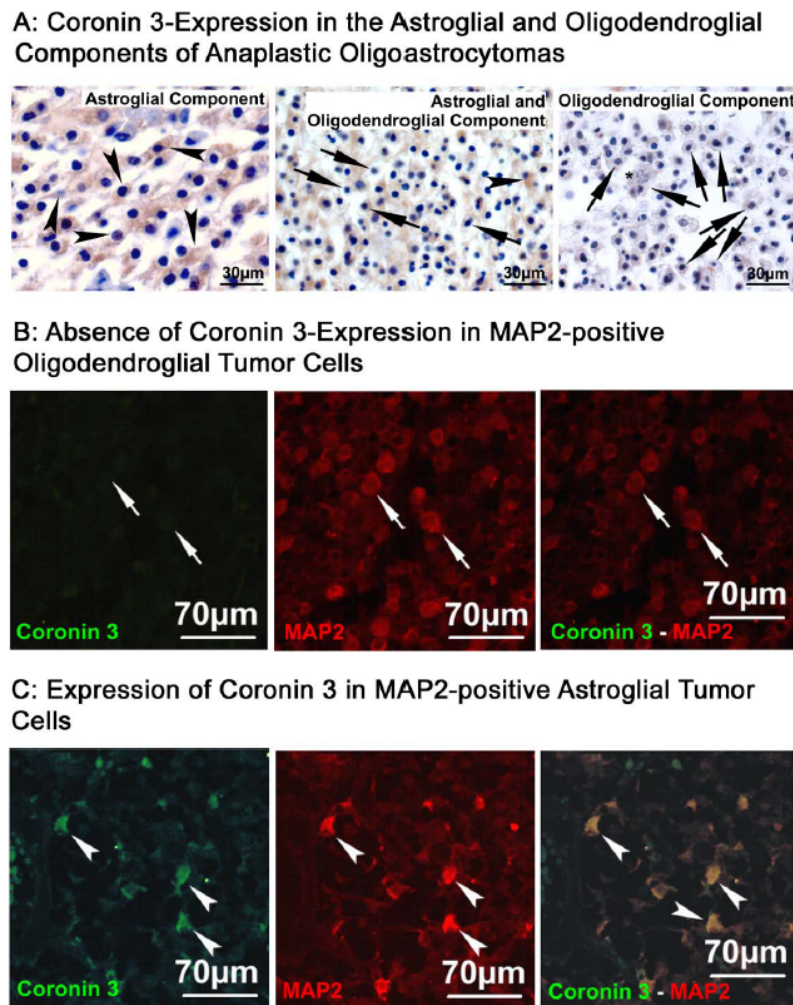


Figure 15. Expression of CRN2 in the astroglial and oligodendroglial component of anaplastic oligoastrocytomas. **A:** Most of the astroglial tumour cells expressed CRN2 (arrowheads). The oligodendroglial component with anaplastic features such as mitoses (asterisk) showed mild to moderate levels of CRN2 (arrows). **B:** Double label immunofluorescence of another anaplastic oligoastrocytoma showed no expression of CRN2 in the oligodendroglial component. This component is characterized by a perinuclear staining pattern of the tumour cells with anti-MAP2. **C:** The astroglial tumour component of this tumour exhibited a co-localization of CRN2 with MAP2. This expression of MAP2 in a pattern showing cell processes indicated the astroglial tumour cell nature of these cells.

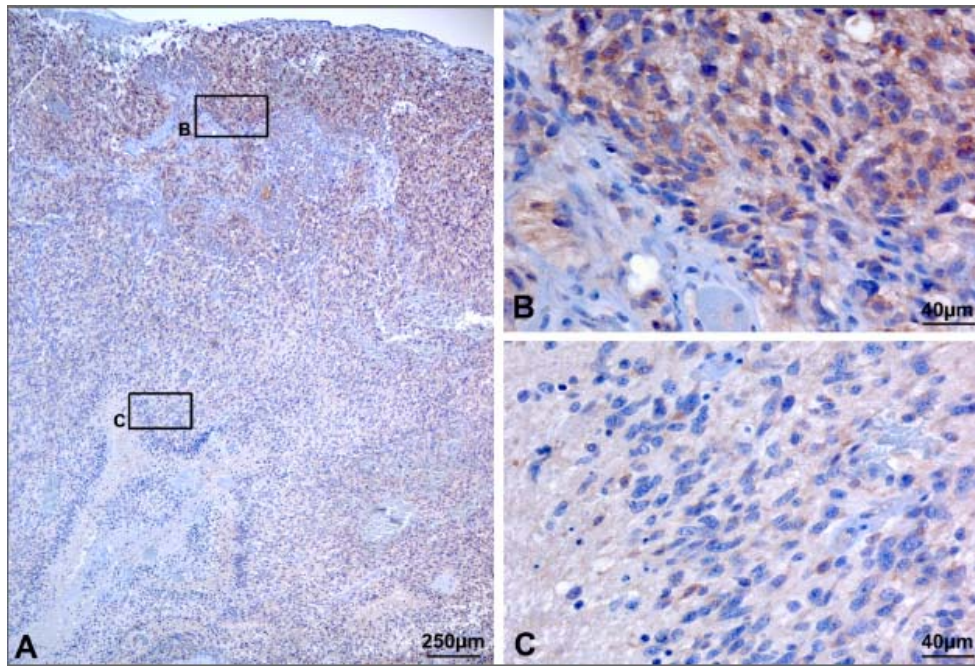


Figure 16. Expression of CRN2 in different regions of a glioblastoma multiforme. A: In a glioblastoma multiforme nearly all tumour cells expressed CRN2. B: The most prominent expression, however, was detected in areas of vital tumour with microvascular proliferation. C: Surviving tumour cells near areas of palisading necroses were only weakly labeled with anti-CRN2. The boxes in A indicate the areas enlarged in B and C.

Within mixed gliomas, i.e. oligoastrocytomas and anaplastic oligoastrocytomas, different expression patterns of CRN2 within both tumour components were detected: the astroglial tumour cells more often expressed CRN2 than those of the oligodendroglial component (Fig.15). Double-label immunofluorescence of CRN2 and MAP2 confirmed the tumour cell nature of the CRN2-positive astroglial cells in oligoastrocytomas. However, in some cases the oligodendroglial compartment also showed a prominent CRN2 expression, mostly occurring in anaplastic oligoastrocytomas with features of malignancy of the oligodendroglial component, such as mitotic figures.

Moreover, particularly in glioblastomas that expressed CRN2 in nearly all tumour cells, a variation in the expression of CRN2 within the tumour was seen (Fig.16). Tumour cells adjacent to proliferating microvessels in the tumour periphery (Fig. 16B) exhibited a stronger CRN2 staining than those adjacent to areas of necrosis (Fig.16C).

The matrix of brain tumours contains a varying number of reactive astrocytes, non-malignant but activated and migrating cells that also expressed CRN2 (Fig.17F-H). These CRN2-positive reactive astrocytes, however, are not restricted to tumours. In the vicinity of other brain lesions, ie infarcts and traumatic lesions, expression of CRN2 was also detectable within reactive astrocytes (Fig.17A). In contrast, non-specific astroglial activation in the absence of a

circumscribed lesion, e.g. in the course of epilepsy, showed only a faint expression of CRN2 in astrocytes (Fig. 17C-E).

Coronin 3 expression in reactive astrocytes and microglial cells

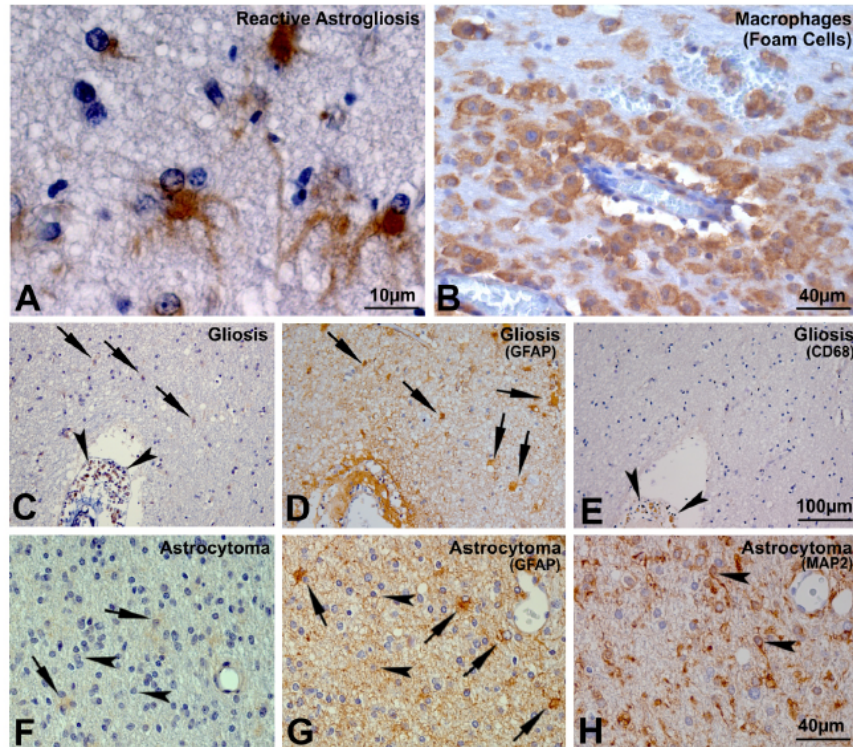


Figure 17. Expression of CRN2 in reactive astrocytes and microglial cells. **A:** Activated astrocytes highly exhibiting CRN2 were present in the brain close to an infarct lesion at the stage at which gliosis was beginning. **B:** In an infarct lesion in the stage of resorption macrophages showing foam cell morphology were labelled by anti-CRN2. **C-E:** Gliosis in a case of chronic epilepsy showed weak CRN2 expression in reactive astrocytes (C, arrows), which also exhibited glial fibrillary acidic protein (GFAP) (D, arrows), and in perivascular macrophages (C, arrowheads) identified by their CD-68 expression (E, arrowheads). **F-H:** CRN2 was detected in tumour-associated reactive astrocytes. Reactive astrocytes were identified comparing the staining of CRN2, GFAP, and MAP2. The latter specifically marked tumour cells (Rosentreter et al., 2007) (arrowheads), whereas GFAP stained both tumour cells (arrowheads) and reactive astrocytes (arrows). Based on the different morphology of tumour cells and reactive astrocytes, CRN2-positive cells in this low-grade astrocytoma were predominantly classified as reactive astrocytes (arrows), while most tumour cells failed to stain for CRN2 (arrowheads).

3.2 CRN2 expression correlates with the grade of malignancy in diffuse gliomas

As our data showed that diffuse gliomas, i.e. astrocytomas, oligodendrogliomas and oligoastrocytomas, exhibited increasing numbers of tumour cells expressing CRN2 with increasing WHO grade, which indicates the malignant potential of a tumour, we focused on these tumours (Fig.18A). A semiquantitative analysis of vital tumour expressing CRN2 demonstrated that oligodendrogliomas, diffuse astrocytomas and oligoastrocytomas contained

only a small number of tumour cells positive for CRN2 (Fig.18A). In contrast, usually more than 50% of the tumour cells were stained by mAb K6-444 anti-CRN2 antibodies in malignant gliomas (Fig.18A; $p < 0.01$). Accordingly, western blots of gliomas showed increased levels of CRN2 compared to normal tissue of grey and white matter (Fig.18B,C; $p < 0.05$). Although Western blotting in general confirmed the increased expression of CRN2 in diffuse gliomas with their grade of malignancy, the analysis of tissue homogenates showed varying expression levels. This was particularly visible in low- and high-grade astrocytomas (Fig.18B, C). The reason behind this is that the area of tumour tissue used for immunoblotting is not exactly defined. Therefore, two factors will interfere with the determination of the CRN2 expression by immunoblotting, but not by immunostaining. First, the expression levels of CRN2 vary in tumour cells within different regions of a certain tumour (Fig.19); and second, the tumour matrix contains a varying number of reactive astrocytes that also express CRN2 (Figs.18A; 17F-H).

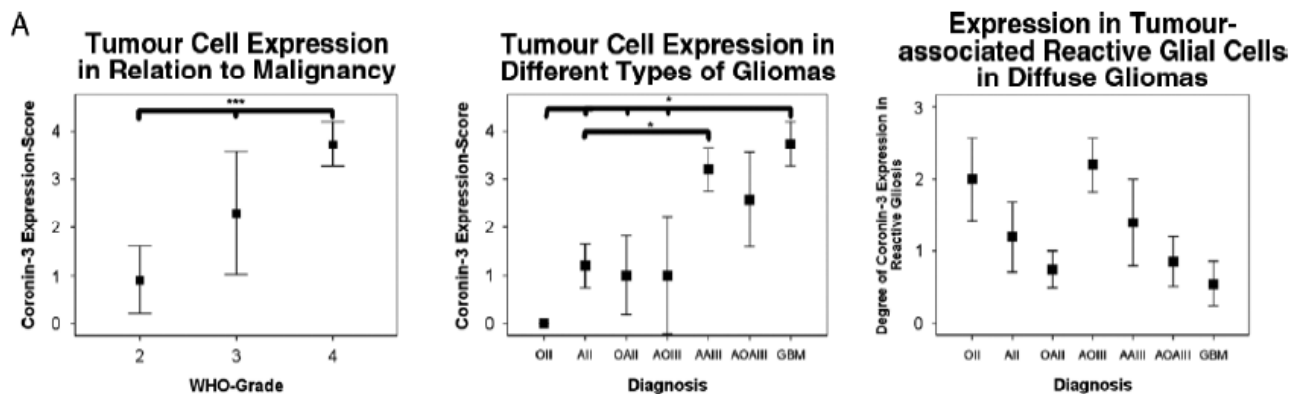


Figure 18 Quantification of the expression of CRN2 in tumour cells and tumour tissues. A. *Tumour cell expression in relation to malignancy* was determined by quantification of the immunohistochemical expression of CRN2 in diffuse gliomas. With increasing malignancy, as indicated by the WHO grade, the number of tumour cells expressing CRN2 increased. Mean and standard deviation are presented; *** indicates $p < 0.01$, as calculated by the Kruskal–Wallis H-test and the trend-test. *Tumourcell expression in different types of gliomas* was analysed by quantification of the immunohistochemical staining pattern of CRN2 within the different types of gliomas. The highest numbers of tumour cells expressing CRN2 were present in anaplastic astrocytomas, anaplastic oligoastrocytomas and in glioblastomas. * Indicates $p < 0.05$, as determined by the Mann–Whitney U-test to compare the different types of tumours. p values were corrected for multiple testing. *Expression in tumour-associated reactive glial cells in diffuse gliomas* was observed by the semiquantitative assessment of the number of reactive astrocytes expressing CRN2 associated with diffuse gliomas. Oligodendrogliomas, anaplastic oligodendrogliomas, astrocytomas and anaplastic astrocytomas were frequently associated with reactive glial cells that also exhibited CRN2. Oligoastrocytomas, anaplastic oligoastrocytomas and glioblastomas appeared to be less frequently associated with a reactive gliosis. However, there was a wide range of the degree of gliosis in

each tumour entity. Therefore, the trend seen in the diagram did not reach significance (Poisson regression analysis, $p = 0.8254$; deviance, 301.812).

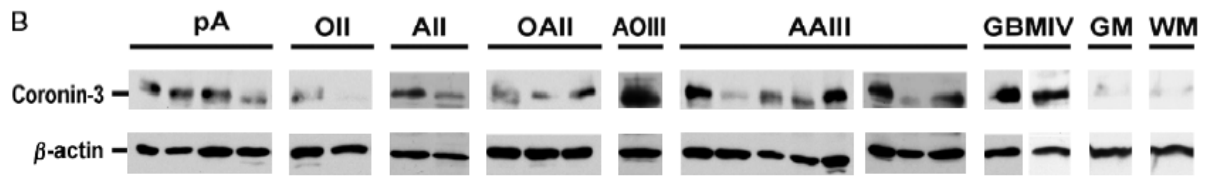


Figure 18, continued. B. Western blot analysis of the different types of diffuse gliomas exhibited weak to moderate CRN2 expression levels in tissue samples of astrocytomas (AII), oligodendrogliomas (OII), oligoastrocytomas (OAII) and anaplastic astrocytomas (AAIII). Two anaplastic astrocytomas (AAIII), the anaplastic oligodendroglioma (AOIII) and the glioblastomas (GBMIV) showed a strong expression of CRN2. Pilocytic astrocytomas (pA), loaded as positive controls, exhibited moderate CRN2 expression levels. Normal human brain tissue of grey (GM) and white matter (WM) did not express more than traces of CRN2; β -actin is given as a loading control.

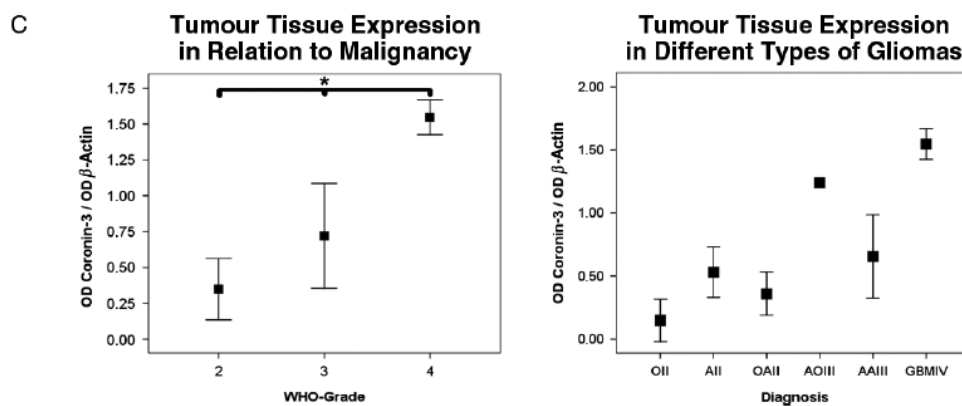


Figure 18, continued. C. CRN2 expression in tumour tissue observed by quantitative western blotting. *Tumour tissue expression in relation to malignancy* showed an increase from benign diffuse gliomas to high-grade glioblastomas (*, Kruskal–Wallis H-test, Trend-test, $p < 0.05$). *Tumour tissue expression in different types of gliomas* exhibited a nearly similar pattern as the immunohistochemical analysis but failed significance because of the possible interference of reactive glial cells in this small sample.

3.3 CRN2 knockdown inhibits cellular functions related to tumour malignancy

U373 and A172 glioblastoma cells, commonly used to study glioma-related cellular functions, express high levels of CRN2. To address the question of whether the expression of CRN2 in gliomas has an impact on tumour cell proliferation, migration, and invasion, we employed lentivirus mediated shRNA-dependent knockdown of CRN2 in U373 and A172 glioblastoma cells, which resulted in a ~95% CRN2 protein reduction (Fig. 19A).

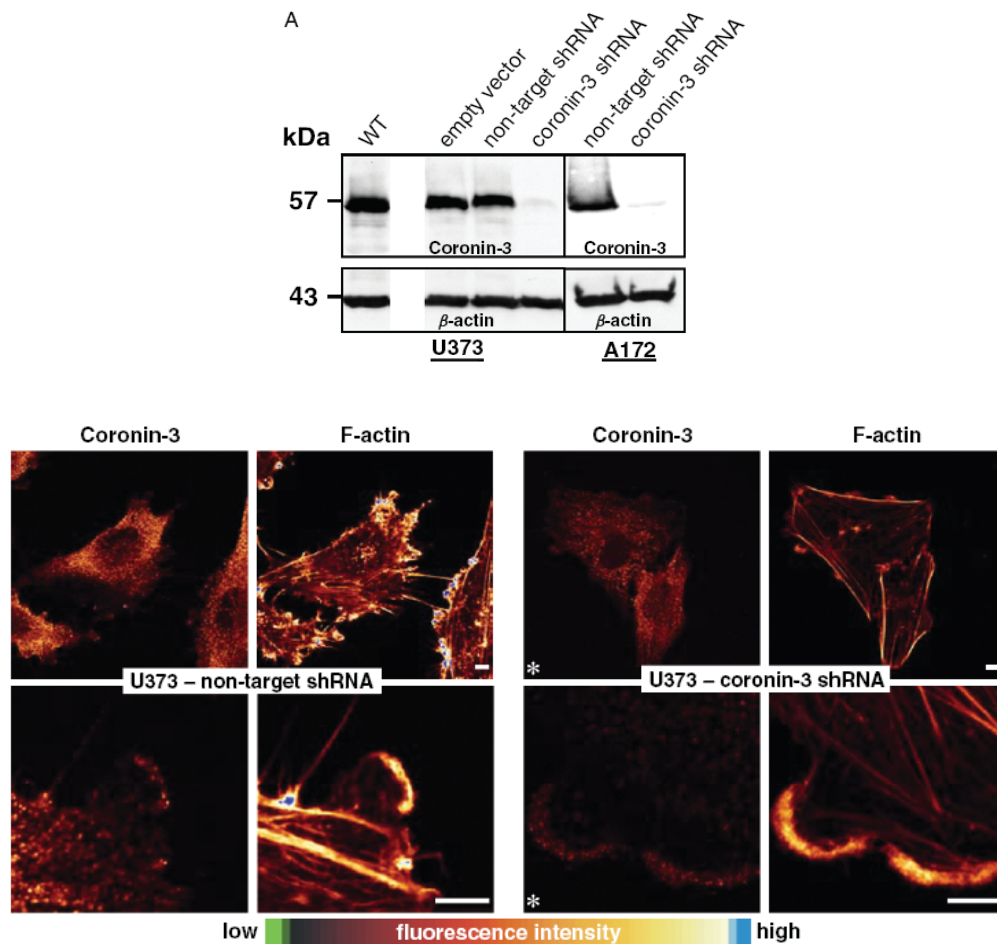


Figure 19. A Effective shRNA-mediated knockdown of CRN2. Western blotting confirms a strong reduction (~95%) of the expression level of CRN2 in transduced U373 and A172 glioblastoma cell lines. Wild-type cells (U373 only), cells transduced with empty vector or a non-target shRNA-cassette (U373 and A172), as well as β -actin staining, are given as controls. Immunofluorescence imaging of U373 glioblastoma cells fixed with 4% paraformaldehyde also indicates an overall decreased expression level of CRN2 in knockdown cells. The F-actin cytoskeleton seems not to be affected in CRN2 knockdown cells. The images showing lamellipodia in higher magnification are not enlarged areas from the images above, but from a different cell. CRN2 was detected by mAb K6-444, F-actin was stained with TRITC-phalloidin. Note the colour-coded fluorescence intensity signals (images with asterisk). Bars, 5 μ m.

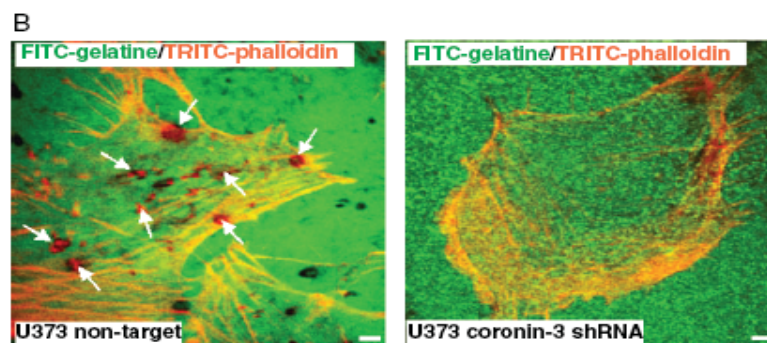


Figure 19, continued. B. CRN2 knockdown inhibits invadopodia formation. Immunofluorescence imaging of invadopodia of a U373 glioblastoma cell. Glioblastoma cells grown on cover slips coated with FITC-gelatin

were fixed with 4% paraformaldehyde and stained with TRITC-phalloidin. One representative cell each is shown for knockdown and non-target control cells. Invadopodia at the ventral surface of the cell are defined by the presence of F-actin and absence of the matrix FITC-signal (arrows). Bars, 10 μm

Immunofluorescence images of the CRN2 knockdown cells did not reveal any obvious changes in the F-actin staining, localization of the Arp2/3 complex and the morphology of lamellipodia. These structures appeared as in normal and non-target controls, although the CRN2-specific signal intensity (images with asterisk; note the colour code, yellow pixels versus dark red pixels) was reduced in virtually all knockdown cells (Fig 19A and data not shown). However, there were still low amounts of CRN2 in the knockdown cells, which exhibited a similar distribution as in non-target glioblastoma cells (Fig 19A). The signal intensity of cortical F-actin staining varied in both non-target and knockdown cells, and the F-actin content remained unchanged in the CRN2 knockdown glioblastoma cells (data not shown).

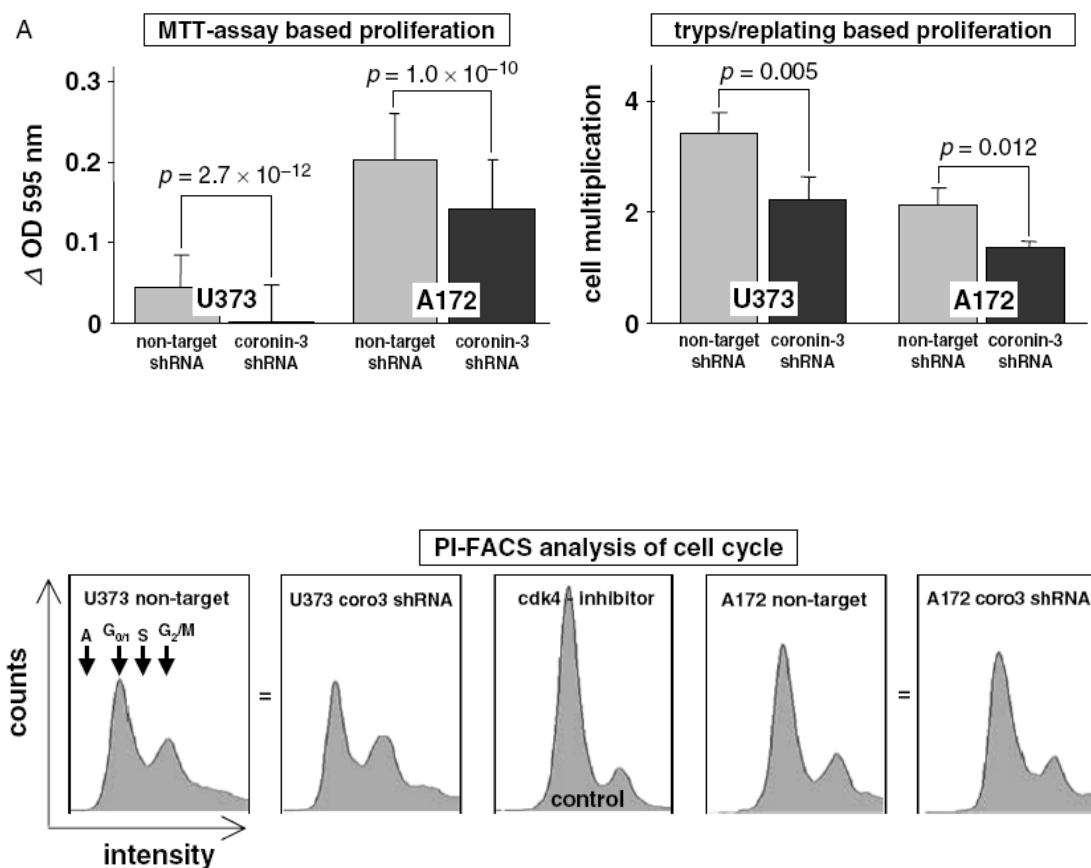


Figure 20. Knockdown of CRN2 inhibits cellular functions related to malignancy. A. CRN2 knockdown inhibits cell proliferation, but not cell cycle state. *MTT-assay based proliferation* rates of U373 and A172 glioblastoma cells lacking CRN2 expression are compared to control cells; 100 independent experiments in 96-well format each, Student's *t*-test; U373, ΔOD_{595} 0.001 versus 0.045, $p = 2.7 \times 10^{-12}$; A172, ΔOD_{595} 0.014 versus

0.20, $p = 1.0 \times 10^{-10}$. Trypsination/replating based proliferation rates of U373 and A172 glioblastoma cells lacking CRN2 expression are compared to control cells; a certain number of cells were seeded and counted again after 2 days; four independent experiments each. Student's *t*-test; U373, factor 2.2 versus 3.4, $p = 0.005$; A172, factor 1.4 versus 2.1, $p = 0.012$. PI-FACS analysis of cell cycle state of U373 and A172 CRN2 knockdown cells. Fixed cells were stained with propidium iodide and 10,000 single cells from three independent experiments were analysed by fluorescence-activated cell sorting (PI-FACS). The histograms demonstrate the fractions of cells in G0/1, G2/M and S phase; A, apoptosis. For control, cells treated for 16 h with a cdk4-inhibitor (Calbiochem, 219476) are given.

In contrast, multiple malignancy-related cellular functions were inhibited. Glioblastoma cells with reduced CRN2 levels exhibited an inhibition of the cell proliferation rate, as determined by two different assays, cell viability measurements (U373, -98% , $p < 10^{-11}$; A172, -30% , $p = 10^{-10}$) as well as trypsination/replating experiments (U373, -35% , $p = 0.005$; A172, -33% , $p = 0.012$) (Fig 20A). An analysis of the cell cycle state by PI-FACS did not indicate an inhibition of the cell cycle (Fig 20A). Monitoring single CRN2 knockdown glioblastoma cells, we determined a reduction of their ability to migrate compared to non-target shRNA control cells (U373, -62% , $p < 10^{-6}$; A172, -54% , $p < 10^{-8}$) (Fig 20B).

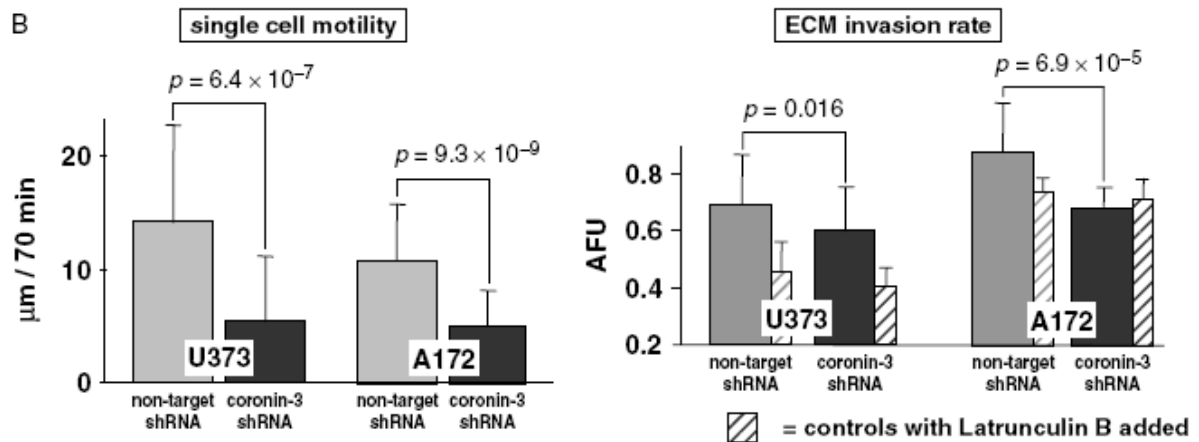


Figure 20, continued. B. CRN2 knockdown inhibits cell migration and invasion. The *single cell motility* chart indicates the values from a total of 40 cells, each derived from several independent experiments; Student's *t*-test: U373, velocity $5.36 \mu\text{m}/70 \text{ min}$ versus $14.3 \mu\text{m}/70 \text{ min}$, $p = 6.4 \times 10^{-7}$; A172, velocity $5.0 \mu\text{m}/70 \text{ min}$ versus $10.9 \mu\text{m}/70 \text{ min}$, $p = 9.3 \times 10^{-9}$. The *extracellular matrix (ECM) invasion rate* graph shows one representative experiment with mean and standard deviation of 40 and 20 measurements of U373 and A172 glioblastoma cells, respectively; Student's *t*-test: U373, 0.6 AFU versus 0.7 AFU , $p = 0.016$; A172, 0.7 AFU versus 0.9 AFU , $p = 6.9 \times 10^{-5}$. Controls with $15 \mu\text{M}$ latrunculin B added to the cells in order to depolymerize the cellular F-actin demonstrate the maximum reduction of the invasion. Controls lacking the fluorescent dye showed background values of 0.2 AFU . For ECM invasion, see also Fig 19B.

In addition, we tested the ability of CRN2 knockdown glioblastoma cells to degrade and invade extracellular matrix (ECM). ECM invasion of CRN2 knockdown glioblastoma cells also exhibited a reduction (U373, -14%, $p = 0.016$; A172, -22%, $p < 0.0001$) (Fig 17B). To investigate the effects of the CRN2 knockdown on ECM invasion in more detail, we determined the overall activity of matrix metalloproteinases (MMPs). A172 cells lacking CRN2 exhibited a reduced activity of MMPs (-12% , $p < 10^{-10}$), however, no difference was detectable for U373 cells (Fig 20C).

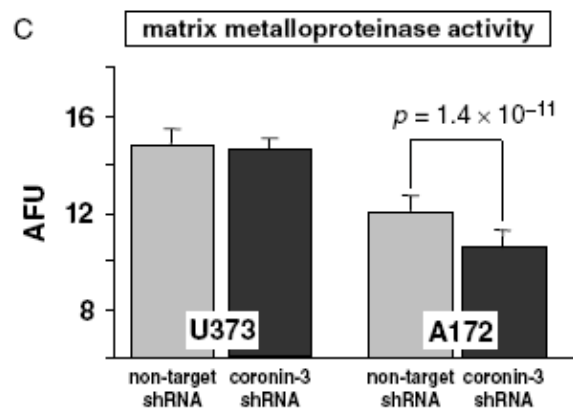


Figure 20, continued. C. CRN2 knockdown inhibits matrix metalloproteinase activity. A172 glioblastoma cells lacking CRN2 exhibit a reduced activity of secreted matrix metalloproteinases (MMP); however, such a difference was not detectable in U373 cells. Thirty measurements from six independent experiments each. Student's *t*-test: U373, 14.4 AFU versus 14.5 AFU, $p = 0.66$; A172, 10.7 AFU versus 12.2 AFU, $p = 1.4 \times 10^{-11}$. Controls lacking the fluorescent substrate showed background values of 7 AFU

We also visualized the formation of invadopodia *in vitro* (Fig 19B). Invadopodia are defined by co-localization of invadopodia markers, ie typical F-actin structures, with the degradation of fluorescently labelled extracellular matrix (Weaver, 2006). U373 non-target cells demonstrated a strong activity of matrix degradation on gelatin matrices, whereas in U373 knockdown cells virtually no invadopodia were detected. For A172 cells, no invadopodia formation was found under our experimental conditions. Only two (gelatin, fibronectin) out of various components of the extracellular matrix have been used in the invadopodium assay, while the matrix metalloproteinase assay detected the overall activity of various, but not all known enzymatic activities. Thus, in both U373 and A172 knockdown, cell matrix degradation activities, although to different degrees, are inhibited upon reduction of CRN2 levels.

4.0 Structural and functional diversity of novel CRN2 isoforms.

4.1 Identification of three CRN2 proteins encoded by two mRNA species

CRN2 usually migrates as a diffuse band of approximately 57 kDa. Immunoblotting of HEK293 and undifferentiated C2F3 cell lysates with the CRN2 specific monoclonal antibody K6-444 (Spoerl et al., 2002) revealed that the diffuse band can be separated into two closely migrating bands of 57/58 kDa (later referred to as CRN2i1/CRN2i2 (coronin-1C isoform 1/isoform 2) (Fig.21A). Moreover, a second slower migrating protein of 60 kDa (later referred to as CRN2i3 (coronin-1C isoform 3) can be detected in murine skeletal muscle and differentiating C2F3 myoblasts as well as in brain and heart tissue (Fig.21A; figure 2B in reference (Spoerl et al., 2002). This protein is the only CRN2 isoform present in mature murine, bovine and human skeletal muscle tissue.

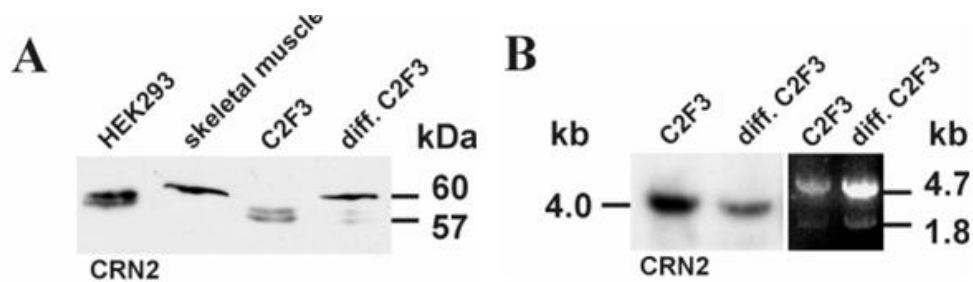


Figure 21. A slower migrating isoform of CRN2 appears during myogenesis. **A**, lysates of HEK293 cells, murine skeletal muscle tissue, C2F3 myoblasts, and C2F3 myotubes (diff.) were analyzed by SDS-PAGE followed by western blotting using mAb K6-444 specific for CRN2 (Spoerl et al., 2002). **B**, 20 μ g of total RNA from C2F3 myoblasts and 50 μ g of total RNA from myotubes (diff.) were subjected to gel electrophoresis under denaturing conditions and analyzed by northern blotting using a full-length CRN2 cDNA as probe; for control, the ethidium bromide stained RNA-gel is shown.

Northern blot analysis from total RNA of different murine organs, ES-cells, and undifferentiated C2F3 myoblasts employing a full-length CRN2 cDNA as a probe resulted in a single band of about 4.0 kb. Highest expression levels were detected in murine ES-cells as well as in thymus, testis, kidney, heart, and brain tissue (data not shown). Lung tissue and undifferentiated C2F3 myoblasts exhibited intermediate signal intensities. Lowest expression levels were detected in mature skeletal muscle and spleen tissue. During the differentiation process of C2F3 myoblasts the amount of CRN2 specific RNA levels decreased markedly (Fig. 21B). The possibility of posttranslational modifications of the CRN2 protein that could lead to differences in the apparent molecular mass was investigated by means of high resolution two-dimensional gel electrophoresis in conjunction with immunoblotting.

Ubiquitinylation and sumoylation (SUMO1-3) could not be detected in protein samples from murine, bovine and human skeletal muscle. Phosphorylations were present in CRN2; however, they did not contribute to the observed difference in the molecular mass (data not shown).

Therefore, 5'-RACE, 5'-RLM-RACE, and RT-PCR protocols were employed and resulted in the identification of additional transcripts. An alternative exon, exon 1b, contains two more start codons that are in frame with the known start codon of CRN2 (Fig. 22) potentially elongating the 'conventional' CRN2 transcript (referred to as isoform 1, CRN2v1, accession no. NM_014325) by addition of either 6 (referred to as isoform 2, CRN2v2, accession no. AM849477) or 53 codons (referred to as isoform 3, CRN2v3, accession no. AM849478). The longer isoform 3 encompasses the sequence of the shorter isoform 2. On the genomic level, the novel exon 1b is located within the previously proposed 30 kb intron 1 present between the 5' untranslated exon, exon 1a, and the first coding exon, exon 2, of the 'conventional' CRN2 sequence. Sequence derived predictions suggest three potential CRN2 protein isoforms (Table.3), with molecular masses of 53 kDa and a pI of 6.7 (CRN2i1, NP_055140), 54 kDa and pI 6.9 (CRN2i2, AM849477), 59 kDa and pI 7.9 (CRN2i3, AM849478), that correspond to the protein bands detected by mAb K6-444.

Isoforms of CRN2 due to different N-terminal extensions

```

MYGPGSQLGKSGNNSWAKERGCSIAQGSLSARLHAPSIGERPLSHMRWKDTMRRVVRQSKFRHVFQ
QAVKNDQCYDDIRVSRVTWDS SFCAVNPRFVAIIIEASGGGAFLVLP LHK TGRIDKSYPTVCGHTGPV
LDIDWC PHNDQVIASGSEDC T VMVWQIPENGLT LSLTEPVVILEGH SKRVGIVAWHPTARNVLLSAGC
DNAII IWNVGTGEALINLDDMHSDMIYNVSWNRNGSLICTASKDKKVRVIDPRKQEI VAEKEKAHEGA
RPMRAIFLADGNVFTTGF SRMSERQLALWNPKNMQEP IALHEMDT SNGVLLPFYDPDTS I IYLCGKGD
SSIRYFEITDESPYVHYLNTFSSKEPQRGMGYMPKRGLDVNKCEIARFFKLHERKCEPIIMTVPRKSD
LFQDDLYPDTAGPEAALEAEWFEGKNADPILISLKHGYIPGKNRDLKVVKNILDSKPTANKKCDLI
SIPKKT TDTASVQNEAKLDEILKEIKSIKDTICNQDERISKLEQQMAKIAA-

```

CRN2i3

CRN2i2

CRN2i1

Table 3. Isoforms of CRN2 due to different N-terminal extensions. Amino acid sequence derived predictions suggest three different proteins with molecular masses (kDa) and pI values of 53/6.7, 54/6.9, and 59/7.9, respectively. New symbols for protein (and mRNA), CRN2i1 (CRN2v1), CRN2i2 (CRN2v2) and CRN2i3 (CRN2v3), according to (Morgan and Fernandez, 2008).

4.2 Evolutionary insight into *CRN2* regulation

Three atypical ESTs initiating from within 3' intron 1 were detected only from human coronin *CRN2*. Comparison of their common 5' segment, up to 282 bp in gb:DC377708, with 39 orthologous mammalian promoters identified a putative alternative exon 1b encoding the N-termini of *CRN2i2* and *CRN2i3* in five catarrhine primates separated by less than 25 million years of evolution (viz. human, chimpanzee, gorilla, orangutan and gibbon). All earlier diverging primates (i.e. macaque, baboon, marmoset, tarsier, lemur and galago) and other mammals (eutherian, metatherian and prototherian) harboured either start codon mutations, frame shift deletions or splice site changes in their genomic sequences that precluded the generation of transcripts encoding *CRN2i3*. Only 3 of 11 primates (macaque, baboon and galago) and 6 of 19 other mammals (tree shrew, dog, horse, alpaca, rabbit and pika) retained the capacity to generate transcripts encoding the shorter *CRN2i2*.

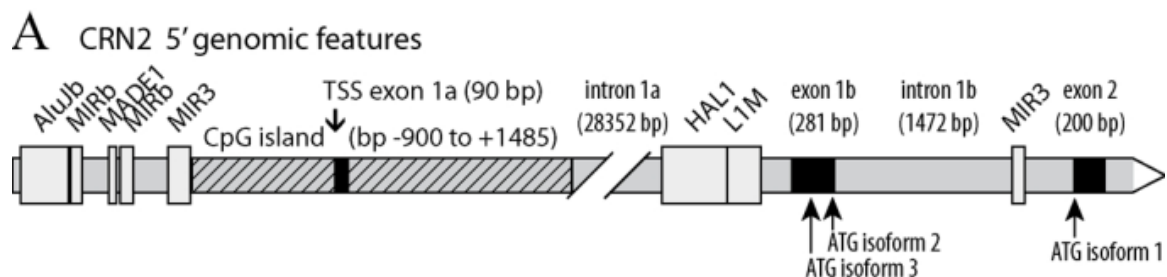


Figure 22. Promoter and exon-intron architecture of 5' *CRN2*. A, the current reference assembly for *CRN2* (NC_000012.10) was characterized for repetitive elements, CpG composition, transcription start site(s) in dbTSS and known exon splice sites.

A single promoter with a primary transcription start site (TSS) was detected in *CRN2* exon 1a (Fig.22A). Sequence conservation of the core promoter among mammals established the functional importance of this region and highlighted several sequence motifs relevant to both general and specific transcriptional regulation. A profile hidden Markov model (pHMM) logo of the aligned sequences (Fig.22B) illustrates the manner by which “phylogenetic footprinting” can localize evolutionary functional constraint through column height (i.e. probability of occurrence) and nucleotide frequencies. Myogenic regulatory factors such as MyoD, Myf5, MRF4 and myogenin are known to control muscle-specific gene expression by forming hetero-dimers with E-proteins that bind E-box motifs (e.g. CACCTG) with candidate sites located in the *CRN2* promoter region. Evolutionary analyses using the VISTA browser and rVISTA (Loots et al., 2002) identified other conserved, functionally relevant regulatory elements, including double representation of a prominent and strategically located motif

UF1H3beta_Q6. This DNA element (TGCGGGGGAGGGGC or CGCGGGGGCGGGGC) contains internal subsites for NGFIC (EGF4), Klf4 and Sp1 (common to many core promoters defined by CpG islands) with conspicuous G-rich stretches. This may bear directly on MyoD regulation of CRN2 transcription as recent evidence identifies guanine-rich quadruplex structures of regulatory sequences as key binding elements for homodimeric MyoD (Yafe et al., 2008).

B CRN2 promoter region

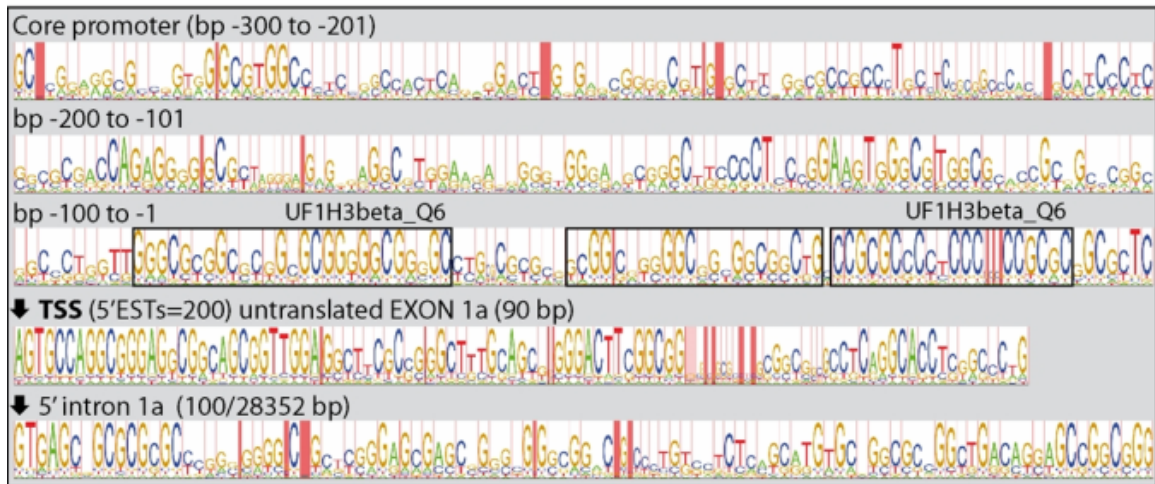


Figure 22, continued. B, promoter sequences from -300 to +100 bp for CRN2 were aligned, converted to an HMM model and visualized as a sequence logo representing 12 mammalian species (i.e. human, orangutan, marmoset, macaque, cow, pig, vampire bat, guinea pig, mouse, rat, dog and opossum). The transcription start site (TSS) was designated by genomic mapping of external database CAGE, EST and full-length cDNA tags. Conserved motifs in the core promoter were characterized by phylogenetic footprinting programs, which identified the doubly represented element UF1H3beta_Q6.

The region between the upstream promoter and coding exon 2 was also subjected to comparative genomic analysis to investigate the origin of an alternative transcription start site near the 3' end on intron 1 (Fig.22C). The genomic sequence capability was restricted to modern primates and the most 5' of three human ESTs came to within 36 bp of a well-conserved CAG motif, possibly reflecting the true end of intron 1a and a novel splice site demarcating alternative exon 1b of 291-317 bp in these primates.

C CRN2 alternatively spliced region

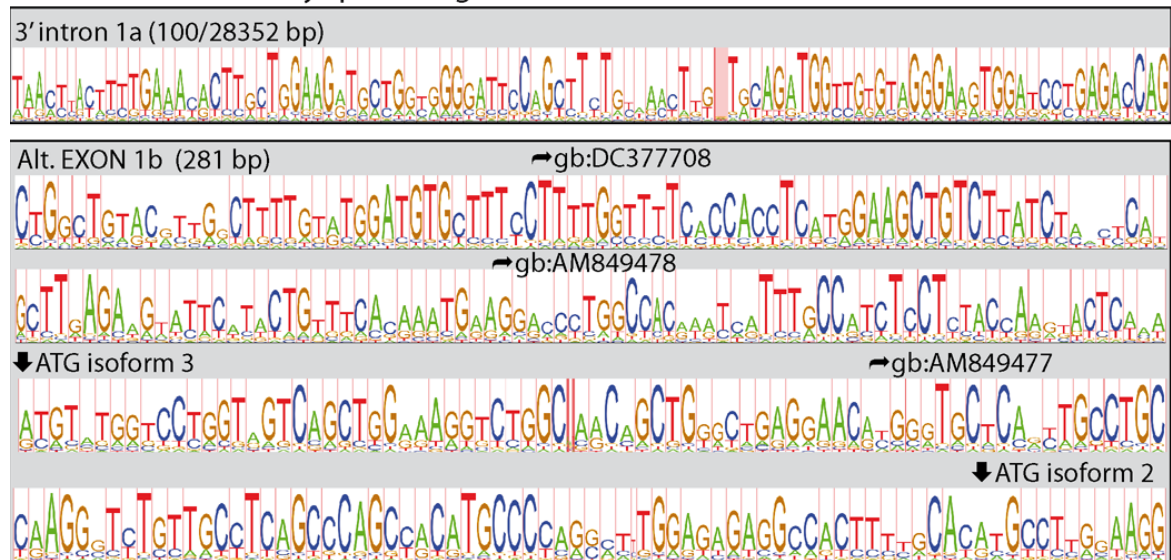


Figure 22, continued. C, the alternatively spliced region is shown as a genomic DNA sequence logo derived from 11 primates capable of generating transcripts for both isoforms 2 and 3 (human, chimp, orangutan, gibbon), isoform 2 only (macaque, baboon, galago, tree shrew) or neither (marmoset, lemur, tarsier). Three human ESTs encoded by exon 1b giving rise to protein isoforms 2 and 3 are preceded by a putative, alternative intron 1a splice site.

4.3 CRN2i3 is part of the myogenic differentiation program

While the ubiquitous CRN2i1/2 (“diffuse” band) appears to be expressed constitutively, expression of the largest isoform CRN2i3 is specifically up-regulated during myogenic differentiation. In contrast to undifferentiated C2F3 myoblasts, differentiated C2F3 myotubes (eight days of differentiation) display mostly CRN2i3, with only a trace of isoforms 1 and 2 (Fig. 21A). We monitored the switch from the faster to the slower migrating isoforms by a time course experiment of differentiating C2F3 cells. At day 0, before induction of differentiation, CRN2i1 and 2 were detected in the C2F3 myoblasts. Low amounts of CRN2i3 were observed after three days of differentiation, with a wide and diffusely migrating band corresponding to CRN2i1 and 2 below a thin band of CRN2i3 (Fig.23A). Detection of annexin A7 was used as control, since the large isoform of annexin A7 (51 kDa) is a marker of late (*in vitro*) myogenesis and also appeared at day three (Clemen et al., 1999). CRN2i3 was exclusively found in mature skeletal muscle (see below). To validate the specificity of CRN2i3 in the myogenic differentiation program, we converted NIH3T3 fibroblasts, which only express the CRN2i1 and 2, into myogenic cells by ectopic expression of MyoD (Clemen et al., 1999). Converted cells initiated expression of CRN2i3 (Fig.23B). Similarly, MyoD

expression in C2F3 cells grown under non-differentiating conditions led to an expression of CRN2i3.

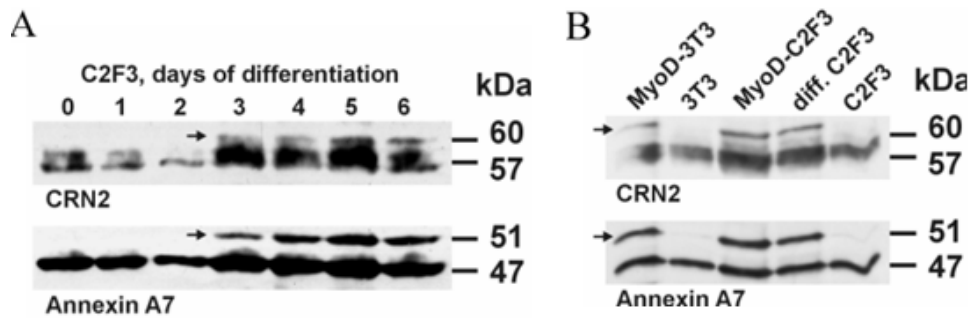


Figure 23. **A.** Time course of differentiation of C2F3 myoblasts. Cells were harvested at the indicated time points (day after initiation of differentiation) and analyzed by immunoblotting using mAb K6-444 and mAb 203-217 specific for annexin A7 as a control of myogenic differentiation. **B.** myogenic conversion of NIH3T3 fibroblasts using a retroviral vector encoding human MyoD. CRN2 from hMyoD-transduced and untransduced NIH3T3 and hMyoD-transduced, differentiated and undifferentiated C2F3 myoblasts is shown. Cells were harvested four days after transduction or after five days of differentiation, and analyzed by SDS-PAGE followed by western blotting using the CRN2 and annexin A7 specific antibodies.

4.4 Different oligomerization state of the CRN2 isoforms

Sucrose gradient fractionation of lysates of differentiated C2F3 myotubes demonstrates a co-distribution of the three CRN2 isoforms (Fig.24). They were present in fractions of low density (fractions 4-9) that contained part of the membrane-associated cortical F-actin as well as Golgi membranes (β -COP staining).

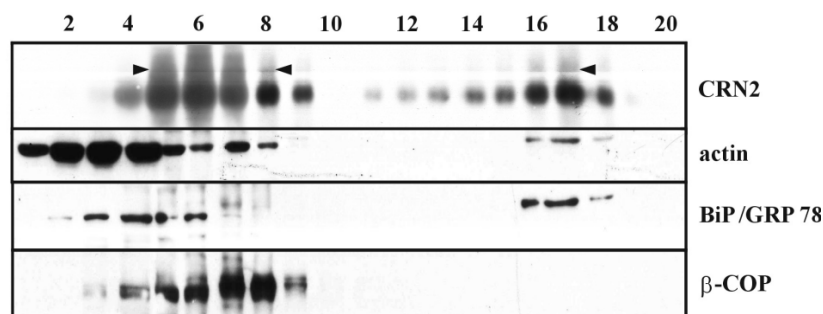


Figure 24. Identical subcellular localization of CRN2 isoforms. **A.** Fractionation of cell lysates from differentiated C2F3 myotubes by sucrose gradient centrifugation. Fractions were collected and analyzed by SDS-PAGE followed by western blotting using the antibodies K6-444 (CRN2), mAb AC 40 (β -actin; Sigma), anti-BiP/GRP 78 (Transduction Laboratories), and maD (β -COP (Pepperkok et al., 1993)). Arrow heads indicate the position of the slower migrating isoform 3.

A second pool of CRN2 was detected in fractions 15-18 that contain heavy membranes like ER-membranes indicated by the presence of BiP/GRP78. CRN2 (isoform 1) like other short coronin proteins forms homo-trimers. Oligomerization is mediated by the C-terminal coiled coil domain (Kammerer et al., 2005; McArdle and Hofmann, 2008; Rybakin and Clemen, 2005) Gel filtration analysis of soluble fractions derived from murine kidney and skeletal muscle tissue indicates that CRN2i1/2 of kidney is mainly present in fractions corresponding to a molecular mass of 180 kDa, indicating the presence of at least a part of CRN2 in a trimeric state. In contrast, CRN2i3 derived from skeletal muscle is present mostly in fractions of approx. 60 kDa, corresponding to a monomer (Fig. 25).

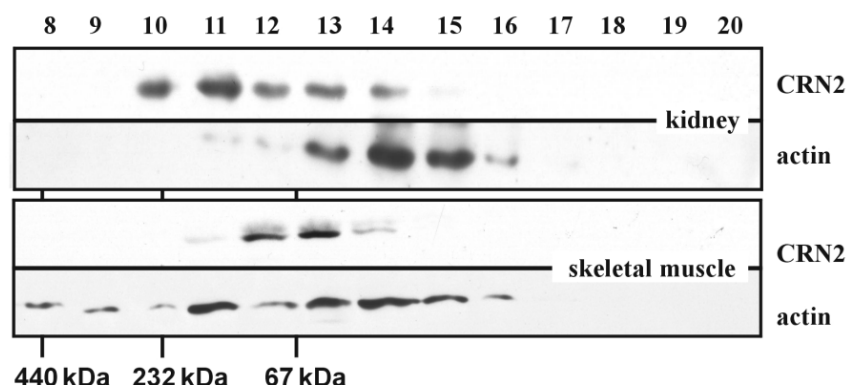


Figure 25. Gel filtration analysis of cytoskeletal protein extracts (100,000 g supernatant) of murine kidney and skeletal muscle tissue using a Superdex G200 column. Fractions were collected and analyzed by SDS-PAGE followed by western blotting using mAb K6-444, mAb AC 40, and mAb 5C5 (sarcomeric-actin; Sigma). The molecular mass is given.

4.5 Structural models of CRN2 isoforms

Following the typical topology of WD40 repeat proteins, in which the first β -strand of a blade is provided by the last β -strand of the preceding WD40-repeat (Hudson and Cooley, 2008; Smith, 2008). The N-terminal β -strand formed by residues 17-22 in CRN4 provides the first β -strand of the last propeller blade of the protein (Fig.25). Therefore, we suggest that in CRN2i3, which harbors an N-terminal 53 amino acid extension, residues 69-74 map onto this motif of CRN4, thus aligning residues 66-402 of CRN2i3 with the seven-bladed β propeller fold (Fig. 25).

Using PSIPRED (McGuffin et al., 2000) the additional amino acid sequence in CRN2i2 (aa 1-6) and CRN2i3 (aa 1-53) was predicted to consist of one (isoform 2) or three (isoform 3) β -strands (Fig.25). It is highly unlikely that the additional peptide will form an eighth blade within the β -propeller. We rather suggest that the additional β -strands either form an

independent domain or they interact with accessible secondary structure elements of the 'core' protein, for example by annealing to existing β -strands.

N-TERMINUS		CRN2i3		CRN2i2 CRN2i1		
CRN4					MSR QVVRSSK FRH	13
CRN2i3	MYGPGSQLGKSGN NSNAKER GCST ACQGS LTSA RLH APSTGRP LSHMRW KDTMR RVRVRSK FRH					65
pred	CCCCCCCCCCCCCCCCCCCC EEEE CCCCC EEEE CCCCCCCCCC EEEEE CCCC EEEEEEE CCE					
7-BLADED BETA-PROPELLER						
STRAND		--1--	-2--	-3--	-4--	
CRN4				VFG	QPAKAD QCYEDVRVS	31
CRN2i3				VFG	QAVKND QCYDDIRVS	83
pred				CCC	CCCCC CCCCCEEEE	
CRN4	QTTWD SGFCAVN FK		FMALIC EASGGG AFLVLP LGKTGRVD	KNV	PLVC	78
CRN2i3	RVTWD SSFCAVN FR		FVALII EASGGG AFLVLP LHKTGRID	KSY	PTVC	130
pred	ECCCC CEEEEEC CC		CCCCEE ECCCC EEEEE CCCCCCCC	CCE	EEEE	
CRN4	GHTAP VLDIAWC PHNDN		VIASGS EDC TVMVWE IPDGGGLVLP	REPV	VTLE	126
CRN2i3	GHTGP VLDIDWC PHNDQ		VIASGS EDC TVMVWQ IPENGLTSL	TEPV	VILE	180
pred	ECCCC EEEEEEC CCCC		EEEEEC CCC EEEEE ECCCCCCCC CCEE	EEEE		
CRN4	GHTKR VGIWAMH PTAQN		VLLSAG CDN VILVWD VGTG	AAV	LTGFPD	173
CRN2i3	GHSKR VGIWAMH PTARN		VLLSAG CDN AIIIVN VGTG	EAL	INLDD-	224
pred	CCCC EEEEEEC CCCC		EEEEEE CCC EEEEE CCCC	CEE	EEEEC	
CRN4	VHPDT IYSVDWS RDGA		LICTSC RDK RVRVIE PRKG	TVV	AEKDR	216
CRN2i3	MHSDM IYNVSWN RNGS		LICTAS KDK KVRVID PRKQ	EIV	AEKEK	267
pred	CCCC EEEEEEC CCCC		EEEEEC CCC EEEEE CCCC	CEE	EEEEC	
CRN4	PHEGTR PVHAVEV SEG		KILTTG FSRMSER QVALMD TKHLE	EPL	SLQELD	265
CRN2i3	AHEGAR PMRAIFL ADG		NVFTTG FSRMSER QLALMN PKMQ	EPI	ALHEMD	316
pred	CCCC EEEEEEC CCC		CEEEEC CCCCC EEEEE CCCC	CEE	EEEEC	
CRN4	TSSG VLLPFDD PDTN		IYVLOG KGDS SIRYFE ITSEAPP	LHYL	SMF	310
CRN2i3	TSNG VLLPFYD PDS		IYVLOG KGDS SIRYFE ITDESPY	VHYL	NT-	360
pred	CCC EEEEEEC CCCC		EEEEEE CCCC	EEEEEE CCCCCE	EEEE	CC
CRN4	SSKES QRGMGYM PKRGLVNVKCEIA RYKRLH ER		KCEPIA MT			351
CRN2i3	FSSKEP QRGMGYM PKRGLVNVKCEIA RFFKRLH ER		KCEPII MT			402
pred	CCCCC EEEEEEC CCCCCEECCCC CEEEEE EC		CCCEEE EE			
C-TERMINAL EXTENSION						
CRN4	VPRKS DLFQEDL YPPTAGFPDPAIT AEWL GGRDAG PLLIS LKDGYPVPKSREL RVN R--GLDS---ARRRATPEPSTPSSDT--V					430
CRN2i3	VPRKS DLFQDDL YPDTAGPEAALE AEEWF EGNAD PLLIS LKHGYIPGKNRDL KVV KKNILDSKPTANKKCDLISI PKMTDTASV					486
pred	ECCCC EEEEEEE CCCCCCCCCC HHHHH CCCCC EEEEE CCCCCCCCCCCC EEE CCCCCCCCCCCCCCCCCCCCCCCCCC					
COILED-COIL						
CRN4	SRLEED VRNLNAI ----- VQKLQER LDRLEET VQAK---					461
CRN2i3	QNEAKL DEILKEI KSIKDT ICNQDER ISKLEQQ -MAKIAA					527
pred	CCCHHH HHHHHHH HHHHHH HHHCHH HHHHHH HHHHCC					

Figure 25. Structure-based sequence alignment of CRN2 with CRN4. The CRN4 amino acid sequence is sectioned according to the fold observed in the crystal structure (Appleton et al., 2006). The amino acid sequences of all three isoforms of CRN2 are aligned with CRN4 using amino acid sequence similarity and predicted secondary structure elements. The secondary structure of CRN2 was predicted using PsiPred (Bryson et al., 2005) and is annotated in the lines shown as 'pred' (H: helix, E: strand, C: coil). The first amino acids of CRN2i1, CRN2i2 and CRN2i3 are indicated. The motifs printed in bold are similar to the heptad repeat motifs found in coiled coils. Potential phosphorylation sites in the N-terminal region of CRN2 are underlined.

Based on the three-dimensional structure of CRN2, in which the N- and C-termini of the coronin β propeller are in spatial vicinity (Fig.26; aa 7-400 of CRN2i1 are visualized), the additional secondary structure elements at the N-terminus may interact with a β -strand in the C-terminal extension or with residues of the coiled coil domain, and thus interfere with oligomerization.



Figure 26. Homology model of CRN2 β propeller and C-terminal extension domains. The homology model of CRN2 (isoform 1; aa 7-400) was generated as reported earlier (Rosentreter et al., 2007). The N-terminal region is colored blue, the WD40 repeat domain (β propeller domain) is shown in aqua, and the C-terminal extension domain is shown in brown. Additional amino acids of isoforms 2 and 3 are fused to the N-terminal region and, in the case of isoform 3, can possibly extend to interact with the C-terminal extension domain and/or the coiled coil domain.

4.6 GFP-fusion proteins of CRN2 isoforms localize to F-actin structures

The three isoforms of CRN2 were expressed as GFP-fusion proteins and their distribution was studied in HEK293 cells and in undifferentiated C2F3 myoblasts and differentiated C2F3 myotubes. Expression of the fusion proteins was confirmed by western blotting. C2F3 myotubes expressing CRN2i1 or CRN2i2 additionally displayed the endogenous CRN2i3 (data not shown). In general, all isoforms localized in a diffuse and punctuated manner in the cytosol (Fig.27 A-C, arrows), at the leading edges of lamellipodia and filopodia (double-arrows), at the submembranous area (arrowheads), and to F-actin fibers (double-arrowheads). In C2F3 myotubes the GFP-fusion proteins mainly localized to F-actin fibers. CRN2 was highly enriched in F-actin rich areas, with high signal intensities of CRN2 matching high signal intensities of F-actin. Significant differences of the CRN2 isoforms with regard to F-actin association or contribution to cellular function could not be observed as assessed by differential centrifugation and cell motility assays (data not shown).

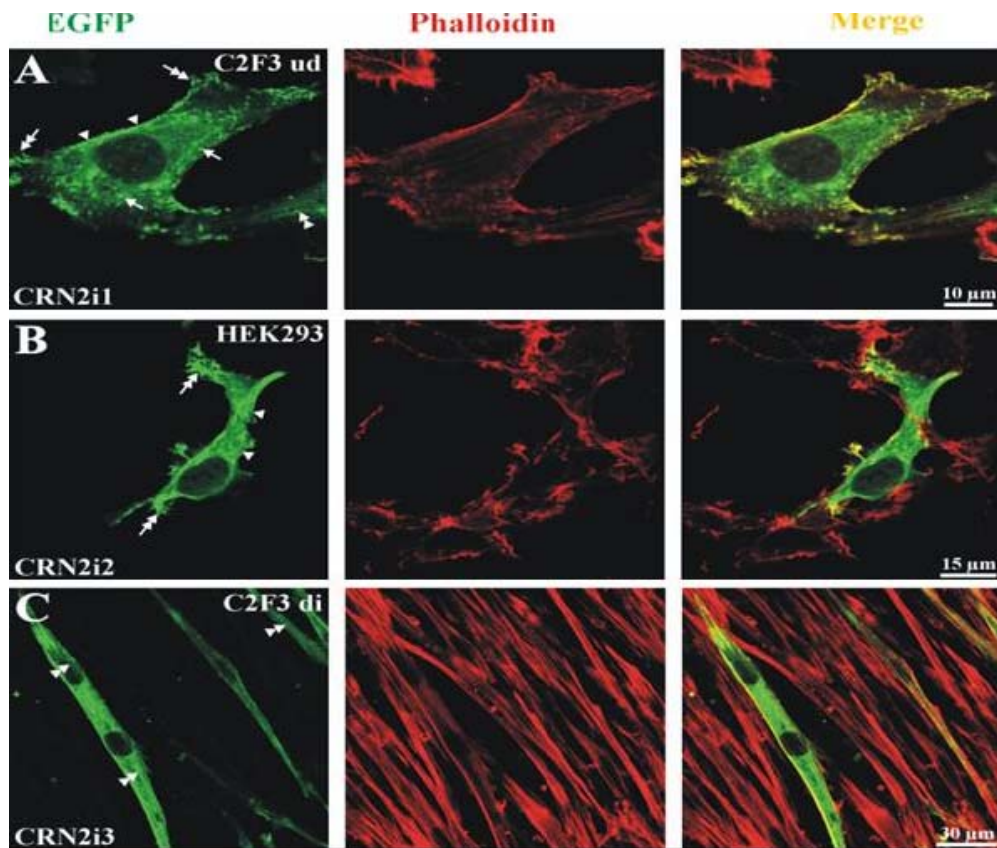


Figure 27. Subcellular localization of CRN2 isoforms expressed as GFP-fusion proteins. **A**, undifferentiated C2F3 myoblasts expressing EGFP-CRN2i1; **B**, HEK293 cells expressing EGFP-CRN2i2, **C**, differentiated C2F3 myotubes expressing EGFP-CRN2i3. Cells were fixed with formaldehyde. Green- fluorescence signal of EGFP-fused CRN2 isoforms, red- F-actin staining with TRITC-phalloidin. Arrowhead, submembranous localization; double-arrow, lamellipodial and filopodial enrichments of CRN2; arrow, dot-like structures at the bottom of the cell; double-arrowhead, localization of CRN2 to actin fibers.

4.7 CRN2 is a novel component of podosomes

Immunoblotting of podosome-enriched cell fractions from primary human macrophages indicated expression and potential podosomal localization of CRN2i1/2 (Fig.28A). Immunofluorescence images using mAb K6-444 confirmed endogenous CRN2 as a novel component of podosomes (Fig.28B). A comparable distribution of CRN2 proteins was seen in macrophages transfected with constructs encoding isoforms 1, 2, and 3 fused to GFP (Fig. 28C; only CRN2i1 is shown). Every podosome displayed an enrichment of CRN2 within the F-actin-rich core structure (arrows). In addition, CRN2 co-localized to submembranous F-actin structures of macrophages (Fig.28D, arrowheads).

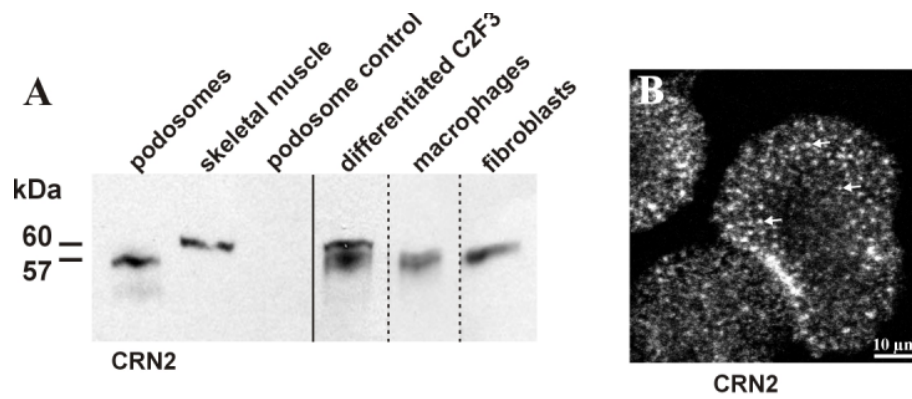


Figure 28. CRN2 is a component of podosomes. **A**, fractions of human primary macrophages enriched in podosomes, bovine skeletal muscle tissue, control fractions devoid of podosomes (Gringel et al., 2006), C2F3 myotubes, macrophages, and 10T1/2 fibroblasts were analyzed by SDS-PAGE followed by western blotting using mAb K6-444 specific for CRN2. **B**, confocal images demonstrate an enrichment of endogenous CRN2 at podosomes of primary human macrophages, fixed with formaldehyde and stained with mAb K6-444.

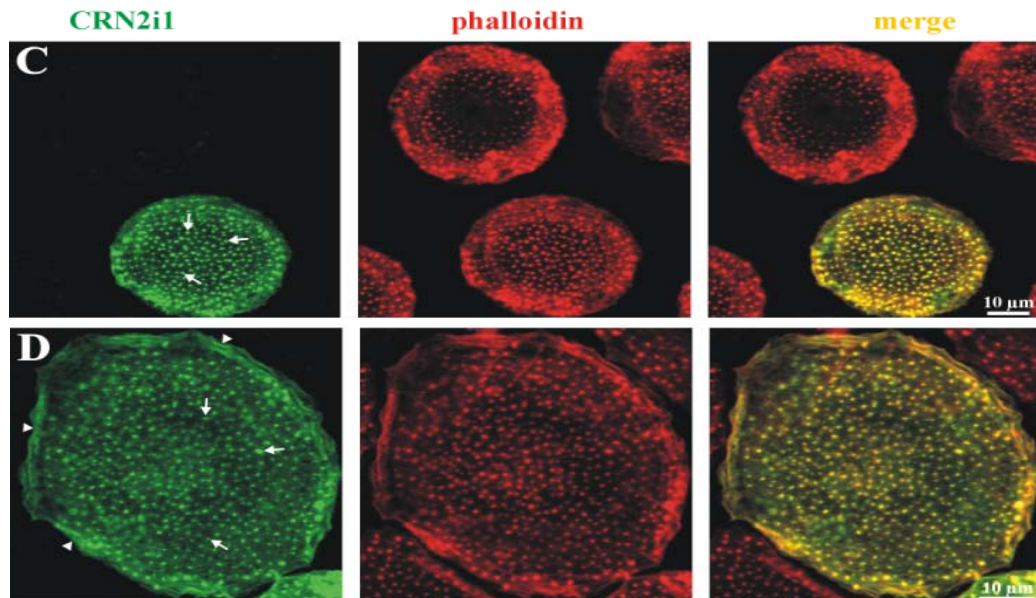


Figure 28 continued C, Primary human macrophages transfected with EGFP-fused CRN2i1. **D**, Enlarged view of a GFP-CRN2i1 positive human primary macrophage. Arrow, localization of CRN2 in podosomes; arrowhead, submembranous enrichment of CRN2.

To address the question whether CRN2 is essential for the formation of podosomes a pool of CRN2-specific siRNAs was transfected into primary human macrophages. In contrast to cells transfected with a control (scrambled) siRNA, a significant reduction of the CRN2 protein started three days after transfection (Fig.29). Immunofluorescence images of macrophages still expressing (day 1 after transfection) and completely lacking endogenous CRN2 (day four after transfection) demonstrate normal podosomes (data not shown). CRN2 knockdown neither did influence number, size, and distribution nor fluorescence intensity of podosomes.

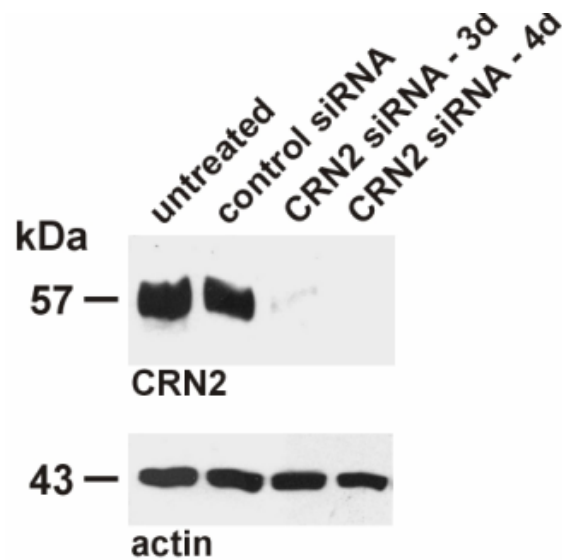


Figure 29. CRN2 knockdown human in macrophages. Effective siRNA-mediated knockdown of CRN2 in human macrophages. Western blotting confirms a strong reduction in the expression level, three days after transfection, and no CRN2 is detectable at four days. β -actin staining used as control.

4.8 CRN2i3 is a structural component of neuromuscular junctions and myofibrils

Based on our observation that mature skeletal muscle fibers exclusively express CRN2i3, transverse sections of human skeletal muscle were immunolabelled with mAb K6-444. In general, the antibody showed a relatively uniform distribution throughout the muscle fibres (data not shown). However, in a subset of muscle fibers, subsarcolemmal enrichments of CRN2 were visible. Co-staining with FITC-labelled α -bungarotoxin demonstrated that these areas correspond to the postsynaptic area and the junctional sarcoplasm of motor end-plates (Fig.30, arrow). Longitudinal optic sections of single human muscle fibers labelled with CRN2 mAb revealed a striated CRN2 staining pattern. Co-stainings with an antibody against the M-band component myomesin (Fig.31A) and an antibody against actin (Fig.31B) showed that CRN2i3 is a component of the thin-filament of myofibrils (Fig.31, 32).

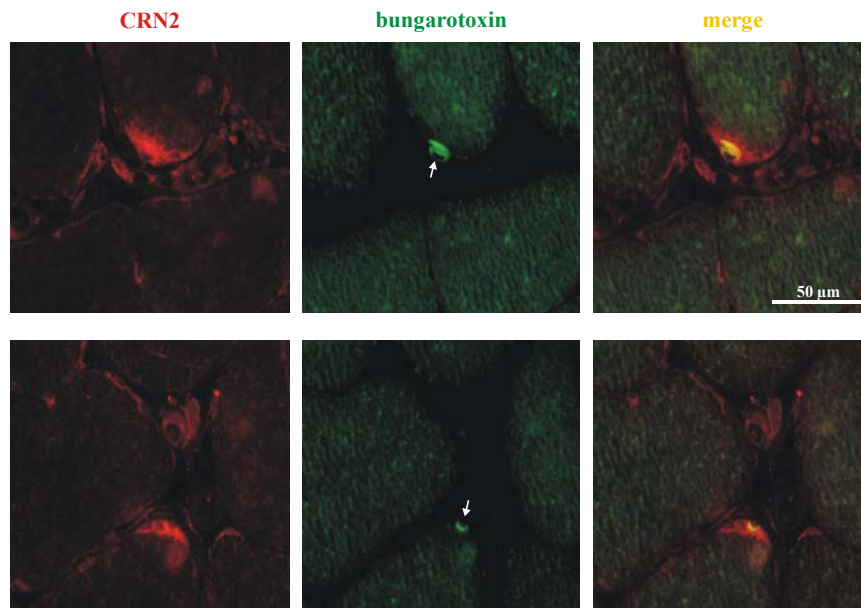


Figure 30. CRN2i3 co-localizes with the motor end plate. Immunostaining for endogenous CRN2 in transversal cryosections of mature human skeletal muscle frequently indicates subsarcolemmal enrichments. Double stainings with FITC-labelled α -bungarotoxin indicate a co-localization of CRN2 at postsynaptic area and the junctional sarcoplasm of the motor end plate (arrow). Note that the intensity of CRN2-staining as well as background levels in both channels differ from normal staining procedures by the lack of fixation to preserve α -bungarotoxin reactivity.

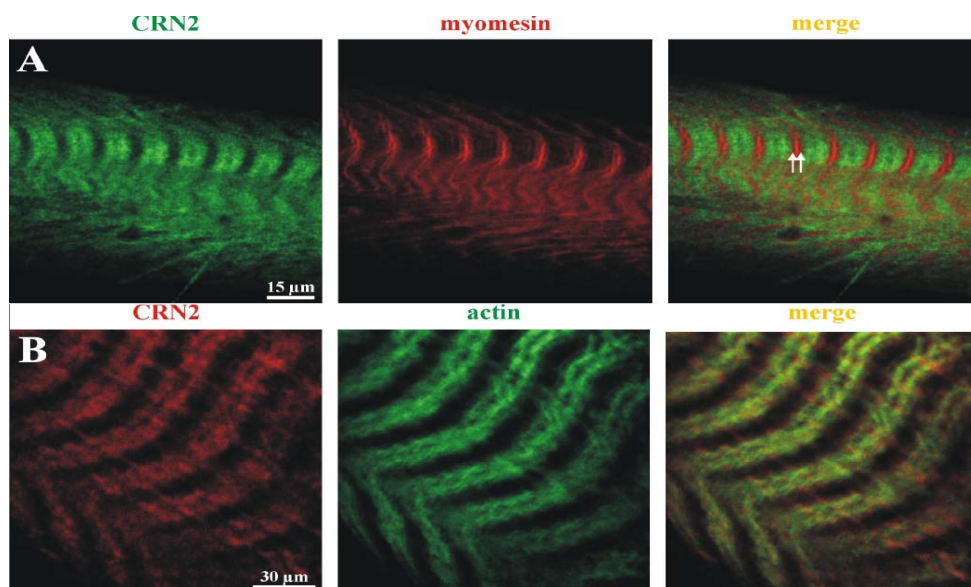


Figure 31. CRN2i3 targets to thin filaments of myofibrils. Human myofibers were isolated, double-labelled, and images were taken by confocal microscopy. A, co-staining with myomesin antibody indicates a gap (arrows) between CRN2 and the M-band. B, co-staining with actin antibody demonstrates a specific co-localization of CRN2 with sarcomeric actin.

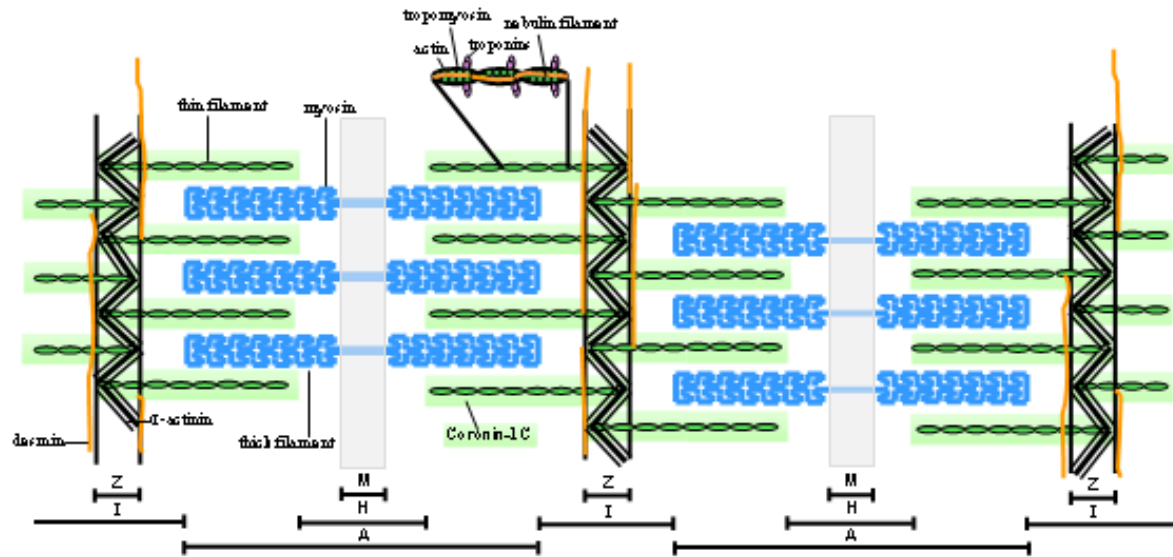


Figure 32. Cartoon represents CRN2i3 localization at the sarcomeric actin filaments. Here a longitudinal section of muscle fibre is shown. Components of sarcomeric unit, such as thick filament composed of myosin (highlighted in blue color) and thin filaments primary composed of actin filaments (highlighted in dark green color) are displayed. The components of each thin filament subunit which comprise of actin, topomyosins, topoinins, nebulin filaments are shown. The co-localization of CRN2i3 to the specific regions of F-actin of the thin filament of a sarcomere is shown in light green color. CRN2i3 seem to be involved in bundling and crosslinking of these sarcomeric actin filaments. Other regions of sarcomere like Z-band (in the form a zip zag triple lines composed of α -actinin) M-band (transparent region) are also shown.

5.0 Influence of phosphorylation on structure and function of CRN2

5.1 Posttranslational modifications of CRN2

In order to evaluate the potential of posttranslational modifications on structure and function of CRN2, the complete amino acid sequence of CRN2 was subjected to *in silico* analyses. A number of posttranslational modifications were predicted in the CRN2 protein as shown in (Fig 33). One of the residues of particular interest was Ser463 of the coiled coil domain, which is a predicted phosphorylation site. Structural modelling indicates that phosphorylation of Ser463 residue of CRN2 will result in disruption of the CRN2 trimer (Hofmann and Clemen, unpublished).

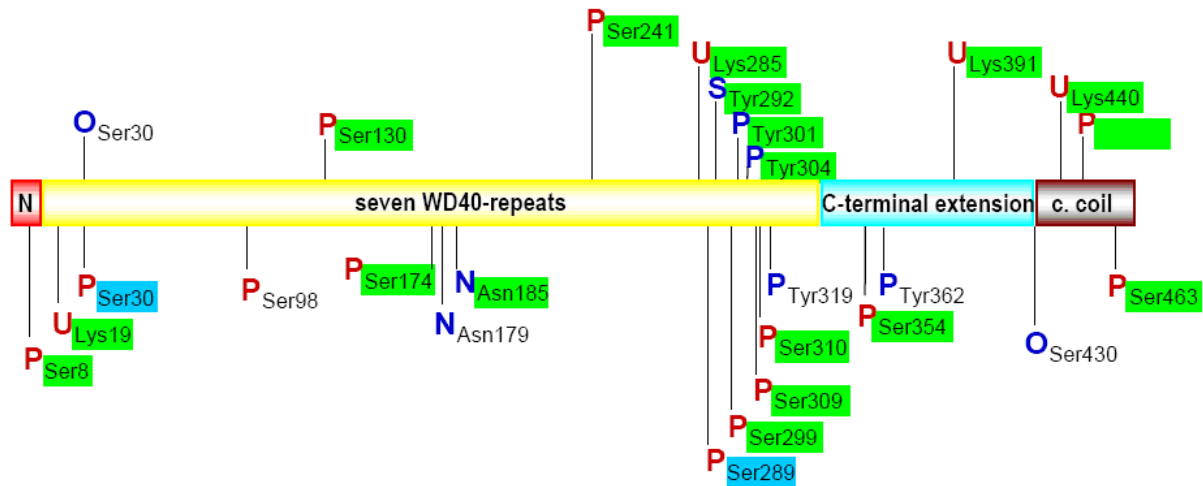


Figure 33. Predicted posttranslational modifications of CRN2. Post-translational modifications of the CRN2 protein predicted with high probability scores; **N**, N-glycosylation; **O**, O-β-GlcNAc addition; **P**, tyrosine phosphorylation; **P**, serine phosphorylation; **S**, sulfation; **U**, sumoylation. Surface exposed residues are highlighted in light green, surface accessible residues in light blue.

5.2 CRN2 interacts with actin cytoskeleton regulator CK2α kinase

Further *in silico* analyses indicated that CRN2 residue Ser463 is part of a potential CK2α binding motif. CK2 is a pleiotropic, constitutively active, heterotetrameric protein with two α and two β units (Allende and Allende, 1995; Guerra et al., 1999). It is well characterized as one of the actin cytoskeleton regulators. It phosphorylates VCA domain of WASP, which in turn enhances the interaction of VCA domain with the Arp2/3 complex and thereby increases Arp2/3 mediated actin polymerization (Canton and Litchfield, 2006). To examine the putative interaction of CK2α and CRN2, we conducted pulldown assays using recombinant GST–

CK2 α together with His6-CRN2 wild-type or S463D mutant peptides (aa 300-474) as well as together with GFP-CRN2 wild-type or S463D mutant (full-length CRN2). GST-CK2 α firmly interacted with both wild-type as well as phosphomimetic CRN2 peptides without any notable difference in binding (Fig 34A). Comparatively, in case of full-length CRN2 the GFP-CRN2 wild-type interaction was much stronger than the S463D mutant. (Fig 34B).

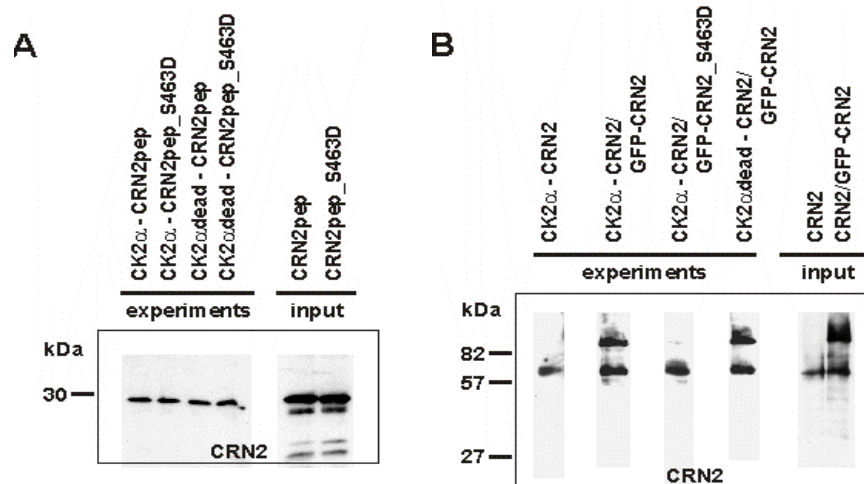


Figure 34. CRN2 interacts with CK2 α . **A**, pulldown assay employing full length CK2 α and C-terminal peptides of CRN2. Cell lysates for input: *E. coli* expressing His6-tagged wild-type CRN2_aa300-474 and mutant CRN2_300-474_S463D (30 kDa). Recombinant proteins bound to glutathione-coated beads: GST-CK2 α , GST-CK2 α dead, GST; and blank beads. **B**, pulldown assay employing full length CK2 α and full length CRN2. Cell lysates for input: HEK293 cells, which express endogenous CRN2 (57 kDa), stably transfected with constructs coding for GFP-CRN2, GFP-CRN2_S463D (82 kDa), and GFP (27 kDa). Recombinant proteins bound to glutathione-coated beads: GST-CK2 α , GST-CK2 α dead, GST; and blank beads. After incubation with the cell lysates, beads were washed and mixed with SDS sample buffer. CRN2 was visualized by western blotting using mAb K6-444.

5.3 *In vivo* phosphorylation of CRN2

Two-dimensional gel electrophoresis in conjunction with immunoblotting revealed several distinct spots of CRN2 in the murine brain and heart, but only a single or two spots were detectable in case of murine as well as human skeletal muscle. Treatment of the protein samples with alkaline phosphatase resulted in a shift of all spots observed to a more alkaline pI (Fig. 35A and data not shown). To confirm a phosphorylation we used a mixture of native and dephosphorylated samples resulting in two spots of the same relative positions (Fig. 35A, bottom panel). The apparent difference between spots of phosphorylated and dephosphorylated CRN2 is 0.5 pH degrees and in theory corresponds well to a loss of three phosphate residues.

We further tried to screen CRN2 for other predicted posttranslational modifications by high-resolution two-dimensional gel electrophoresis combined with mass spectrometry, but a direct analysis failed due to limited protein expression levels. However, high-resolution two-dimensional gel electrophoresis of samples of human skeletal muscle tissue in conjunction with immunoblotting demonstrated that none of the signal spots obtained for ubiquitin or SUMO1-3 could be merged to the signals of CRN2 (data not shown).

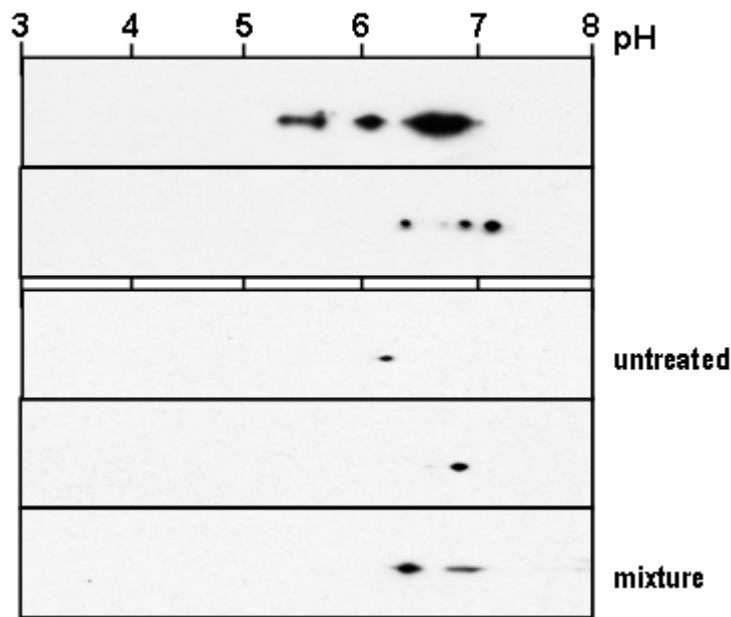


Figure 35. Presence of a phosphorylated pool of CRN2. Lysates of murine brain and skeletal muscle tissue were separated by 2D-gel electrophoresis. CRN2 was visualized by western blotting using mAb K6-444. The upper panel presents the untreated, the lower panel the sample of CRN2 which was dephosphorylated *in vitro*, respectively. As a control, the third panel of murine skeletal muscle additionally shows a mixture of both, the untreated and *in vitro* dephosphorylated samples, resulting in two separated CRN2 spots.

5.4 *In vitro* phosphorylation of CRN2 by CK2 α kinase

The stable interaction between CK2 α kinase and CRN2 further lead to reason, whether these interactions result in favourable phosphorylation of CRN2. To address this, His-tagged wild-type and S463D and S463A mutant CRN2 peptides (aa 300-474) from *E.coli* as well as GST-tagged CRN2 full-length proteins from SF9 cells were used. The purified CRN2 proteins were incubated with GST-CK2 α kinase or a kinase dead control. Reactions were analysed by SDS-PAGE followed by autoradiography. CK2 α kinase steadily phosphorylated the CRN2 wild-type peptide, but such signals were undetected with phosphomutant CRN2 S463A and S463D peptides (Fig 35A). Similar results, however with weaker signal intensity, were obtained from

the full-length CRN2 proteins (Fig 36B). Protein samples loading control are shown with representative coomassie gels (Fig 36).

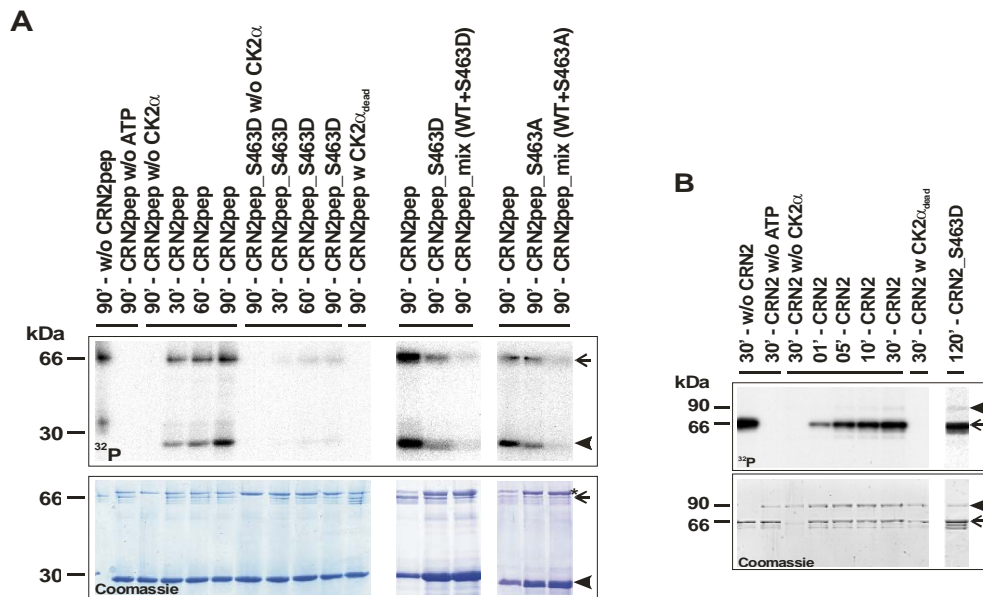


Figure 36. CRN2 is a target of CK2α. **A**, *In vitro* kinase assay employing full length recombinant GST-CK2α (66 kDa, arrow) and His6-tagged C-terminal peptides of CRN2 (30 kDa, arrowhead). Time course (30, 60, 90 minutes) of α ³²ATP incorporation into wild-type CRN2_aa300-474, and mutant S463D and S463A peptides. Controls where the CRN2 peptide, α ³²ATP, or CK2α were omitted, and use of a kinase-dead CK2α are indicated. Upper panel, ³²P, autoradiogram of phosphorylation of CRN2 and auto-phosphorylation of CK2α. Lower panel, the corresponding Coomassie brilliant blue stained gel. Asterisk, recombinant CRN2 peptides contaminated by an E. coli chaperone (PMF identification was done). Note that the phosphorylation levels of the mutant peptides after 90 min are strongly reduced and that the mutant peptides inhibit the activity of CK2α (mix). **B**, *In vitro* kinase assay employing full length recombinant GST-CK2α (66 kDa, arrow) and GST-His6-tagged full length CRN2 (90 kDa, arrowhead). Time course (1, 5, 10, 30, 120 minutes) of α ³²ATP incorporation into wild-type and S463D-mutant CRN2. Controls where CRN2, α ³²ATP, or CK2α were omitted, and use of a kinase-dead CK2α are indicated. Upper panel ³²P, autoradiogram of phosphorylation of CRN2 and auto-phosphorylation of CK2α. Lower panel, the corresponding Coomassie brilliant blue stained gel. Note that after longer incubation time similar phosphorylation levels of wild-type and mutant full length CRN2 are visible.

5.5 Phosphorylation of Ser463 regulates oligomerisation of CRN2

Wild-type as well as phosphomimetic S463D and non-phosphorylatable S463A mutant CRN2 peptides (aa 300-474aa) were subjected to gel filtration experiments followed by SDS-PAGE and western blotting. We observed a notable change in the oligomerisation state of CRN2 S463D. The two wild-type and S463A peptides formed trimers (81kDa), whereas phosphomimetic CRN2 S463D eluted as a dimer (Fig.37). These observations well agree with our results from *in silico* modelling studies, in which phosphorylation of Ser463 were predicted to lead to a dimeric coiled coil domain. However, changes of the oligomerization

state could neither be observed in the GFP- nor GST-tagged full-length CRN2 S463D phosphomimetic mutant (data not shown).

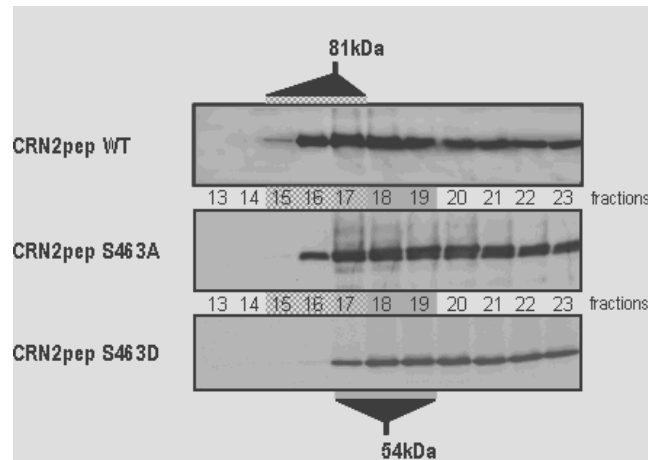


Figure 37. S463D phosphomimetic mutation of CRN2 abolishes trimerization. A. Gel filtration analysis of purified recombinant wild-type as well as S463A and S463D mutants of C-terminal CRN2 peptides mimicking non-phosphorylated and phosphorylated states respectively using a Superdex G75 column (monomers: 22 kDa calculated, 27 kDa apparent molecular weight). As predicted from structural data analysis phosphorylation mutant S463D clearly indicates the formation of dimers instead of trimers. All fractions were collected and analyzed by SDS-PAGE followed by western blotting using antibody K6-444.

5.6 Phosphomimetic S463D mutant CRN2 inhibits actin polymerisation

Previously, we have demonstrated that CRN2 interacts with the Arp2/3 complex (Rosentreter et al., 2007). This led us to further dissect the role of CRN2 on Arp2/3-mediated actin polymerization. We engaged both wild-type and phosphomimetic S463D CRN2 peptides (aa 300-474) in an Arp2/3 mediated actin polymerization assay. Actin polymerization in presence of Arp2/3 complex and its activator N-WASP-VCA domain significantly reduced after addition of CRN2. CRN2 was added in two different concentrations, 1x (0.8 μ M) and 2x (1.6 μ M), which showed a dose-dependent inhibitory effect. Moreover, compared to wild-type CRN2, phosphomimetic S463D CRN2 executed a significantly higher inhibitory effect on Arp2/3-mediated actin polymerisation (Fig.38).

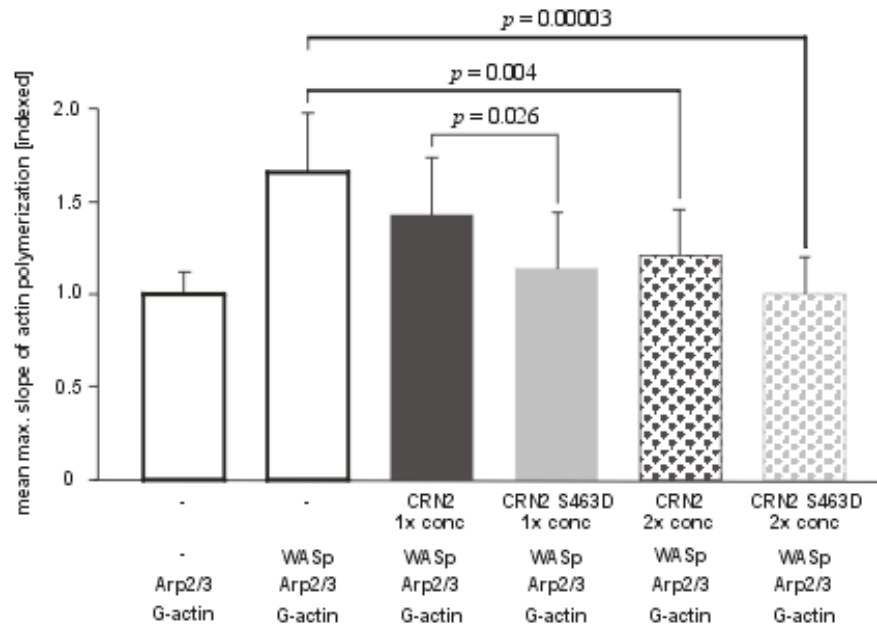


Figure 38. CRN2 wild-type and S463D mutant peptides exhibit different inhibitory effects on Arp2/3 mediated actin polymerisation. Bar graph represents the mean maximal slope of actin polymerization calculated from 50 independent experiments normalized to G-actin/Arp2/3 (first bar = 1.0). Concentrations of CRN2-1x (0.8 μ M) and 2x (1.6 μ M). Control reactions with and without WASP-VCA domain protein are shown. p values indicate statistically significant inhibitions of the Arp2/3 mediated actin polymerisation in the presence of CRN2.

5.7 Phosphomimetic S463D mutant of CRN2 suppresses migration

To determine the biological implication of CRN2 phosphorylation, confluent monolayers of HEK293 cells stably expressing GFP-CRN2 wild-type as well as S463A and S463D mutants were used for *in vitro* wound healing assays. Wound closure was monitored over a period of 7hrs. A statistically considerable reduced velocity in wound closure was measured in case of CRN2 S463D phosphomimetic mutant (22.9 μ m/h versus 28.9 μ m/h and 27.6 μ m/h for wild-type and S463A, respectively) (Fig 39).

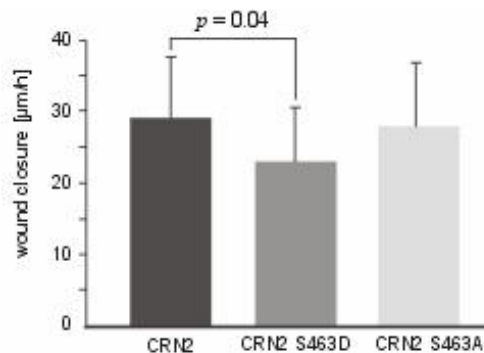


Figure 39. CRN2 S463D mutation inhibits wound closure *in vitro*. See text for details; number of experiments: 60; Student's t-test $p < 0.05$ is significant.

5.8 Phosphomimetic S463D mutant CRN2 hinders formation of cellular protrusions

HEK293 cells stably expressing GFP-CRN2 wild-type as well as S463D and S463A mutants were further used to investigate the formation of cellular protrusions. Cells were monitored for formation of cellular protrusions over a period of 30mins. In comparison to HEK293 cells expressing wild-type CRN2 or the S463A mutant, cells with the CRN2 S463D phosphomimetic mutant demonstrated a significantly hindered formation of cellular protrusions by producing only half the number of cell protrusions (Fig 40 A, B).

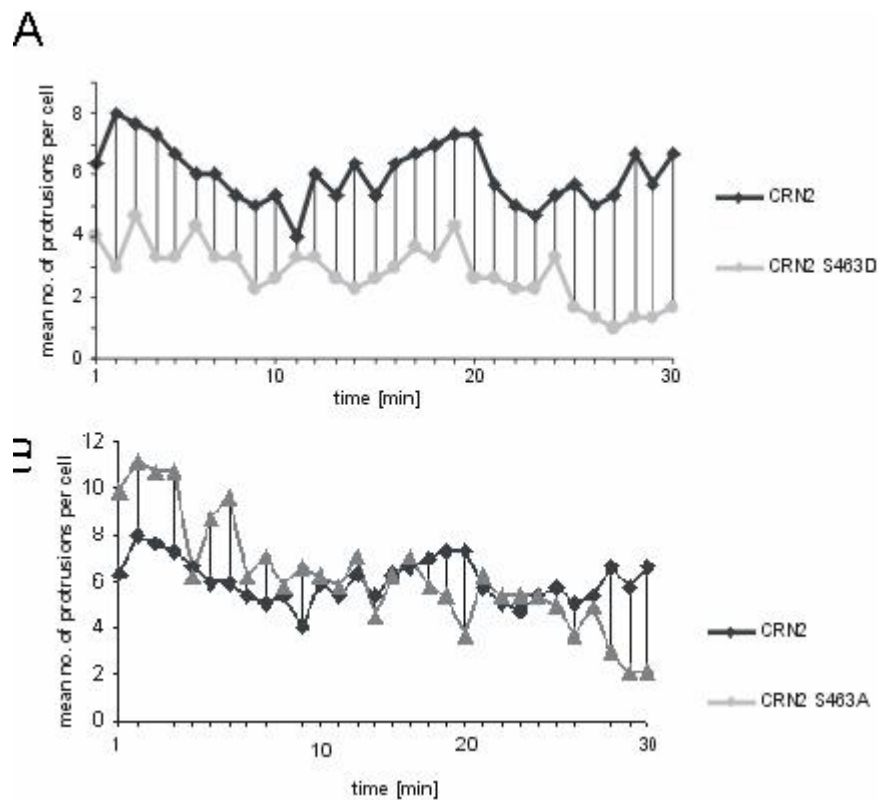


Figure 40. CRN2 S463D mutation suppresses the formation of cellular extensions. A, CRN2 versus CRN2-S463D: mean no. of cellular protrusions 6.0 / 2.8, standard deviation 2.1 / 2.2, number of measurements 90 / 90, Student's t-test $p = 4 \times 10^{-19}$, statistically significant difference. **B,** CRN2 versus CRN2-S463A: mean no. of cellular protrusions 4.9 / 5.0, standard deviation 1.5 / 1.9 number of measurements 90 / 90, Student's t-test $p = 0.73$, no statistically significant difference.

III. Discussion

6.0 Role of CRN2 in cellular processes

Until now biochemical or biological properties of only few coronin proteins have been characterized in detail within different species (for review see (Clemen et al., 2008). We previously identified CRN2 as an actin filament crosslinking and bundling protein in vitro (Spoerl et al., 2002) and described its expression and distribution pattern in the developing murine brain (Hasse et al., 2005). In these studies, we address biological functions of CRN2 in mammalian cells.

6.1 Structural properties of CRN2

Until a crystal structure of CRN4 became available (Appleton et al., 2006), CRN2 was thought to consist of a N-terminal domain (aa 1–71) with a coronin-specific signature motif (aa 1–11), a core region containing five predicted WD40-repeats (aa 72–299), and a C-terminal domain (aa 300–474) with a very C-terminal-coiled coil motif (aa 444–474) (Ref. Rosentreter). Based on the X-ray structure of CRN4, our structural homology model of CRN2 indicates that CRN2 also forms a seven-bladed WD40-repeat beta-propeller. The two additional WD40-repeats do not have the canonical WD motif, but this is also observed in other WD40 propellers. The structural attributes, stabilizing intramolecular interactions of domains, and functional implications described for CRN4 can be assigned to CRN2 too. In specific, surface areas of CRN4 that in silico interact with F-actin, can as well be assigned to CRN2. F-actin binding of CRN4 was mapped to a short stretch of positively charged amino acids (aa 400–416, KSRELRVNRGLDSARRR) within the C terminus preceding the coiled coil. This stretch of positively charged amino acids is conserved in CRN2 (aa 398–419, KNRDLKVVKKNILDSKPTANKK).

6.2 CRN2 regulates F-actin dependent processes

We analyzed the role of CRN2 in various F-actin dependent cellular processes. In wound healing assays the exclusive presence or lack of the five central WD40-repeats strongly inhibited wound closure. These effects and the fact that CRN2 localizes to the cellular cortex prompted us to broaden our investigation with more emphasis on cell proliferation, cytokinesis and cell activity. Based on our data we may define different types of effects induced by the expression of the CRN2 peptides. CRN2 peptides containing WD-repeats and lacking F-actin binding sites (CRN2WD, CRN2 Δ NC) generally resulted in major inhibitory influence on wound healing and cellular protrusions. They most likely act indirectly by

dominant negative effects, as these ectopically expressed WD-repeats could compete for binding partners of the endogenous CRN2. CRN2 peptides comprising the F-actin binding domains but lacking the central WD-repeats (CRN2NC, CRN2NGC) most likely act directly on F-actin by their intrinsic F-actin bundling and crosslinking activity. Their effects could arise by that they act without a specific regulation via putative binding partners of the WD-propeller platform. Slight changes in cellular functions are obtained when full-length CRN2 (NWDC) is overexpressed, although these cells demonstrated an increased number of small filopodia-like extensions. Effective knock down of CRN2 by RNAi finally showed a strong inhibition of cellular migration, but lacked a significant change in the overall structure of the F-actin cytoskeleton.

This complex situation may be resolved by studies on interactions of CRN2 with other proteins. These interactions may vary locally at distinct cellular compartments to specifically regulate the formation and maintenance of different types of actin filaments. To date, there is no evidence that CRN2 acts independent of F-actin or that CRN2 is involved in vesicle trafficking as described for CRN7 and other long coronins (Rybakin and Clemen, 2005). In the light of growing reports on coronin protein interactions, two major mechanisms appear that involve the Arp2/3 complex and cofilin. In this context, it is noteworthy that we were able to co-immunoprecipitate cofilin and p34 in complex with CRN2. Yeast CRN11 was found to directly associate with the Arp2/3 complex, most likely via the Arc35 subunit, and exhibits an inhibitory function on the actin nucleation activity of the Arp2/3 complex (Humphries et al., 2002; Rodal et al., 2005). The Arc35 binding motif is located in the coiled coil region of yeast CRN11. Consistent with this observation C-terminally truncated murine CRN4 did not bind to the Arp2/3 complex (Appleton et al., 2006). Likewise, mammalian CRN1 was shown to bind to the p34 subunit of the Arp2/3 complex ((Kalil and Dent, 2005; Kammerer et al., 2005; Pollard and Borisy, 2003). CRN1 interaction with Arp2/3 complex was demonstrated to be regulated by protein kinase C (PKC) mediated phosphorylation (Cai et al., 2005). Likewise, an inhibitory function of CRN2 on the Arp2/3 complex would provide an explanation for some of our functional results. Indeed, we could show that CRN2 inhibits actin polymerization *in vitro* (see below).

Cofilins emerge as key regulators of axonal growth cone dynamics. The central region of the growth cone contains a F-actin meshwork as well as F-actin bundles playing a central role in motility (Kalil and Dent, 2005; Kammerer et al., 2005; Pollard and Borisy, 2003). The severing activity of cofilins is regulated by LIM kinases, slingshot phosphatases, and their upstream effectors (Gungabissoon and Bamberg, 2003). Moreover, cofilin can act

synergistically with the Arp2/3 complex to amplify local actin polymerization in lamellipods (DesMarais et al., 2005; DesMarais et al., 2004). Although not investigated yet, CRN2 could play a regulatory role in this cofilin-dependent F-actin turnover process as well. Yeast CRN11 interacts and synergizes with cofilin and accelerates the actin turnover via its WD40-repeat domain (Gandhi and Goode, 2008b). Mammalian CRN1 was shown to direct Slingshot phosphatase (SSH1L) to lamellipodia, where this (SSH1L) were shown to regulate cofilin activity via effective dephosphorylation (Cai et al., 2007b). Moreover (Briher et al., 2006) proposed an experimentally based model of interactions between CRN4, cofilin, and Aip1. All three proteins synergistically led to a disassembly of F-actin structures. In this model CRN4 bound to F-actin promotes cofilin and subsequently Aip1-binding to the actin filament triggers its fast disassembly.

6.3 Influence of phosphorylation on structure and function of CRN2

Conventional short coronins like CRN2 are found to possess a fourfold repeat of the characteristic coiled coil hepta-peptide sequence at their C-terminal extension. This coiled coil domain is predicted to be actively involved in homo-trimers (McArdle and Hofmann, 2008). Contribution of this salient coiled coil domain towards the regulation of these proteins functions has been topic of speculation in recent years. Therefore we investigated this domain by *in silico* analysis and examined for posttranslational modification sites. This drew our attention to serine 463 residue found in this domain, whose phosphorylation might influence the oligomerisation state. This was confirmed by gel filtration studies using C-terminal CRN2 peptides. We were able to observe only dimers being eluted in case of the S463D phosphomimetic peptides, instead of trimers with wild-type and S463A peptide.

CK2 is an ubiquitously expressed serine/threonine protein kinase found in all mammalian tissues (Issinger, 1993). CK2 is reported to play a role in the regulation of cellular morphology which includes cell polarity and the cytoskeleton across a variety of biological systems that expands from unicellular organisms to higher eukaryotes (Canton and Litchfield, 2006). From *in silico* analysis we predicted CK2 kinase phosphorylation at three residues, Ser463, Ser174, and Ser98 that are currently investigated. Here, we demonstrated a CK2 α kinase interaction with CRN2. Further, *in vitro* phosphorylation studies confirmed a phosphorylation by CK2 α kinase. Actually, we study the CK2 α dependent phosphorylation of CRN2 and possible changes in its interaction with the Arp2/3 complex and with cofilin *in vivo* employing 2D gel electrophoresis and co-immunoprecipitation studies with and without specific CK2 inhibitors (data not shown).

In this respect, at least three major functions are constituted by the coiled coil domains of short coronins. Apart from interaction with F-actin and homo-oligomerisation, they also interact with Arp2/3 complex (Gandhi and Goode, 2008a). CRN2 interaction with Arp2/3 complex was already reported (see Fig.12). In CRN2, serine 463 at the coiled coil domain was predicted to be a conserved acidic motif which was similar to those found in Arp2/3-activating proteins of the SCAR/WASP family (McArdle and Hofmann, 2008). CK2 kinases are shown to phosphorylate various proteins involved in actin polymerisation like WASP and MAPs (Canton and Litchfield, 2006). In specific CK2 kinase phosphorylation of VCA domain of WASP protein is reported to enhance activation of Arp2/3 complex resulting in increased actin polymerisation (Cory et al., 2003; Mullins et al., 1998). Similarly, the exact mechanism or significance of CK2 phosphorylation of CRN2 on Arp2/3 interaction currently is investigated and we may find a contribution to the regulation of CRN2 activity in actin dynamics.

At the cellular level the activity of CRN2 wild-type as well as CRN2 S463D phosphomimetic and S463A non-phosphorylatable mutant were studied with respect to a couple of cell based assays, like wound healing and single cell protrusion, and in vitro Arp2/3 mediated actin polymerisation assay. Our first results show that phosphomutant CRN2 S463D suppressed cell migration and formation of cellular protrusions compared to wild-type and S463A, which were similar to CRN1 activity (Cai et al., 2005). Coronins are reported to be molecular inhibitors of Arp2/3 by stabilising an inactive and closed form of this complex (Rodal et al., 2005), however at the cellular level this turns out to be an activating process for Arp2/3-dependent processes like cell migration (McArdle and Hofmann, 2008). Further, our in vitro Arp2/3 mediated actin polymerisation studies using CRN2 peptides showed an enhanced inhibitory effect of S463D mutant compared to CRN2 wild-type. Our further studies aim to reveal the exact effect of CRN2 phosphorylation on Arp2/3 mediated actin polymerisation.

6.4 Structural and functional diversity of novel CRN2 isoforms

We identified two novel isoforms of CRN2, named CRN2i2 and CRN2i3. They do not arise from post-translationally modified 'conventional' CRN2i1, but they are encoded by a common, alternatively spliced transcript. A novel alternative exon, exon 1b, which contains two more start codons, replaces an untranslated exon, now termed exon 1a, preceding the normal start codon present in exon 2 of the CRN2 gene. Accordingly, two transcripts differing at their 5' end code for three protein isoforms of CRN2 that vary in their N-terminal length. Expression of the largest CRN2 protein, CRN2i3, can be specifically induced by MyoD, while the other two smaller isoforms are repressed. Thus, CRN2i3 is expressed as part of the

myogenic differentiation program and is the only CRN2 isoform present in mature skeletal muscle tissue. The possibility that MyoD homo-dimers could bind directly to guanine-rich core promoter elements in CRN2 (Yafe et al., 2008) might explain how it alters, directly or indirectly, the transcription start site specificity within the unique CRN2 promoter. The prospect that the novel protein isoforms 2 and 3 may originate from alternative processing of a single primary transcript requires validation by the eventual isolation of a composite, elongated transcript encoded by both exons 1a and 1b.

The mechanism by which myogenic regulatory factors operate on a single promoter to enhance transcript diversity by alternative processing of the primary transcript is known to involve RNA binding proteins such as MBNL and CELF, which have been genetically linked to several neuromuscular disorders (Yuan et al., 2007). The possibility should therefore be considered that such alternative splicing regulators play an accessory role downstream of MyoD to (de)stabilize or reconfigure a primary transcript comprising exons 1a, 1b and flanking introns (i.e. containing splicing factor binding motifs) resulting in the excision of different segments and the formation of distinctly processed CRN2 transcripts during myogenic differentiation in primates.

The elongated N-terminus in CRN2i3 changed the oligomerization state of the protein. While CRN2 derived from kidney tissue (isoforms 1 and 2) forms trimers, CRN2i3 from skeletal muscle tissue eluted as a monomer from gel filtration experiments. Within the three-dimensional structure, the N- and C-terminal ends of the coronin β propeller are in spatial vicinity (Fig.26). From this, two scenarios for an interaction can be envisioned; (i) an interaction of the additional secondary structure elements in the elongated N-terminus of CRN2i3 with the β -strand formed by residues 438-442 in the C-terminal extension causes conformational changes and prevents the following helical domain from engaging in a coiled coil; (ii) amino acid residues 1-47 from the additional N-terminal peptide directly interact with residues 489-527 in the coiled coil domain and thus prevent formation of a coiled coil. It remains to be seen how an interaction suggested in (ii) may be structurally achieved.

The current model depicting coronin function shows a dual regulation in the F-actin turnover (Gandhi and Goode, 2008a). 'Coronin' recruits the Arp2/3-complex to the barbed end and protects growing actin-filaments from depolymerisation, but promotes cofilin-dependent actin sequestration at the pointed end of actin filaments. Additionally, CRN2 (Hasse et al., 2005; Spoerl et al., 2002).CRN4 (Galkin et al., 2008) and further coronins (Xavier et al., 2008) have been shown to bundle and crosslink F-actin *in vitro*. It is tempting to speculate that the oligomerization state of coronin proteins turns out as a mechanism controlling actin-related

cellular functions (see above). Intriguingly, both hepta-peptide motifs in the N-terminal domain of CRN2i3 contain additional predicted phosphorylation sites, where posttranslational modifications might assist in regulation of the CRN2 activities.

Confocal microscopy analysis of endogenous CRN2 and of GFP-fusion proteins in various cells as well as differential centrifugation assays indicated a similar subcellular localization of the CRN2 isoforms. The GFP-fusion proteins associated with F-actin structures at cellular extensions and cytosolic F-actin fibers. We further used substrate-attached human primary macrophages that constitutively form well-defined podosomes (Linder et al., 1999) and could demonstrate that at least two CRN2 isoforms are a novel components of the F-actin-rich core structure of podosomes. While CRN2 does not seem to be essential for the formation of podosomes, it may affect their lifetime, internal actin turnover or function such as in matrix degradation. The finding, that CRN2 is essential for formation and function of invadopodia (see below), but not for the formation of podosomes, points to a different regulation of these complex invasion-mediating structures.

Analyses of normal human skeletal muscle tissue showed a localization of CRN2i3 within the thin filament region of the sarcomere. Identification of novel components of the sarcomere is not uncommon. For example, myomesin-3 (Schoenauer et al., 2008), CAP-2 (Peche et al., 2007) and leiomodlin (Chereau et al., 2008) have been described recently. The physiological role of CRN2 within the thin filament structure is currently unclear. CRN2i3 may play a role either structurally, in the organization of the sarcomere via stabilization of the sarcomeric F-actin bundles, or functionally, e.g. in force development. CRN2i3 further co-localized with the postsynaptic area and the junctional sarcoplasm of motor end-plates. Actin is also a known component of this structure (Hall et al., 1981) which is characterized by folds of the sarcolemma and clustered ligand-gated Na⁺/K⁺-channels (Guth, 1983);(Ogata, 1988). The actin cytoskeleton directly or indirectly seems to be involved in the formation and stabilization of the motor endplate (Hall et al., 1981; (Berthier and Blaineau, 1997) and (Blaineau, 1997; (Dobbins et al., 2006) however, the details are unknown. CRN2i3 represents as a novel candidate possibly involved in the formation of this part of the neuromuscular junction. ADF/cofilin and related proteins have been identified as binding partners of coronin proteins (Rosentreter et al., 2007);(Gandhi and Goode, 2008b) together regulating the sequestration of actin monomers. In skeletal muscle cofilin-2 is thought to be involved in muscle function and regeneration (Thirion et al., 2001). Mutations of cofilin-2 lead to rare congenital nemaline myopathy (OMIM 601443) characterized by severe proximal muscle

weakness and the presence of nemaline rod bodies (Emery, 1999). The latter finding provides a possible pathophysiological link between cofilin-2 mutations and CRN2i3.

7.0 Expression of CRN2 in diffuse gliomas is related to malignancy

The relationship between CRN2 expression and malignancy was only seen in diffuse gliomas. Other tumours, including the pilocytic astrocytoma, either expressed or did not express CRN2, irrespective of their malignancy. However, in these particular tumour entities the presence or absence of CRN2 appears to be a characteristic feature. For example, all pilocytic astrocytomas analysed in this study expressed CRN2. On the other hand, medulloblastomas and neuroblastomas never showed CRN2 in immunoreactive cells.

Interactions between CRN2 and F-actin described above further strengthen the vitality of the CRN2–F-actin system, together contributing to the malignancy of diffuse gliomas. Since the expression level of CRN2 in diffuse gliomas clearly correlated with the degree of malignancy, we focused on this specific group of tumours to further investigate, whether the function of CRN2 in glial cells is related to its effects in diffuse gliomas. The hypothesis that CRN2 expression in glial cells is related to migration is supported by our observation, wherein CRN2 was found to be highly expressed in reactive astrocytes and microglial cells that had been triggered by circumscriptive tumour, infarct and traumatic lesions. Moreover, our previous studies of CRN2 expression in migratory progenitor cells in the developing mouse brain define a critical function of CRN2 in cell migration (Hasse et al., 2005).

Further to envisage the role of CRN2 in glioma cells, we efficiently silenced CRN2 expression through lentivirally delivered shRNA-cassette expression vectors in these cell lines and analysed various malignancy associated cellular activities. These experiments validated our immunohistochemistry results and strongly supported our hypothesis that CRN2 expression in diffuse gliomas is responsible for cell migration and invasion of healthy tissue. Silencing CRN2 expression in glioblastoma cell lines significantly reduced cell proliferation rates; however, analysis of the number of cells in the G0/1, S or G2/M phases of the cell cycle showed no difference. This indicates that there is neither an inhibition of the cell cycle nor a difference in the tumour cell growth fraction, but a difference in the duplication time, possibly due to a role of CRN2 in the formation of the cytokinetic actin ring (Glutzer, 2005). This view is supported by the previously reported role of CRN2 in cytokinesis (Rosentreter et al., 2007). The knockdown of CRN2 expression also reduced cell migration, the formation of invadopodia and invasion into the extracellular matrix. The degree of migration and invasion into healthy tissue is a critical parameter which defines malignancy in diffuse gliomas and moreover, a critical factor that limits the success of surgery (Kleihues and Cavenee, 2000).

Invasion assays showed a prominent reduction in case of A172 glioblastoma CRN2 knockdown cells. In addition these cells also showed a reduced secretion of matrix metalloproteinases (MMPs), while U373 CRN2 knockdown cells failed to invade a 3D-gelatin matrix. In particular, secretion of MMP-2 (gelatinase A) has been shown to play a central role in glioma invasion (Binder and Berger, 2002; Lefranc et al., 2005; Rao, 2003). A role of CRN2 in secretion of epinephrine has been previously found in PC-12 cells (Rosentreter et al., 2007).

CRN2 knockdown in the glioblastoma cell lines did not show identical patterns in the reduced capacity of matrix metalloproteinase activity and invadopodia formation. This strengthens the hypothesis that CRN2 has different effects in different tumours, including different glioblastomas. On the other hand, CRN2 is stably expressed in glioblastomas and in two types of glioblastoma cell lines studied, CRN2 knockdown led to an inhibition of cell proliferation, migration and invasion, suggesting a general role of CRN2 in the malignant phenotype of glioblastomas. We aim to conduct further studies using transgenic mouse models to explain the exact function CRN2 exerts towards local actin dynamics, which in turn will define the role of CRN2 in the development of gliomas.

IV. Materials and Methods

1.0 Kits and Reagents

NucleoSpin Extract 2 in 1	Macherey-Nagel
Quick Change Site-Directed Mutagenesis kit	Stratagene
pGEM-Teasy Vector kit	Promega
Pure Yield Plasmid System	Promega
Actin Polymerisation Biochem Kit	Cytoskeleton
Nucleobond AX 100 and 500	Macherey & Nagel
NucleoSpin Plus	Macherey & Nagel
1 kb DNA-marker	Gibco-BRL
High molecular weight protein marker	Amersham Biosciences
Prestained protein marker	Bio-Rad
Protein marker for gel filtration	Amersham Biosciences
Drystrip gel pI 3-10, 7 cm	Amersham Biosciences
IPG buffer	Amersham Biosciences
IPGphor isoelectric focusing units	Amersham Biosciences
Lipofectamine 2000	Sigma
Cellfactine	Sigma
CytoSelect 96-well Cell Invasion Assay kit	CELL BIOLABS
QMTT Cell Viability Assay kit	BioCat
SensoLyte 520 Generic MMP assay kit	Mobitec

1.2 Enzymes, antibodies, radioactive probes, antibiotics, inhibitors

1.2.1 Enzymes for molecular biology

Calf Intestinal Alkaline Phosphatase (CIP)	Boehringer
Klenow fragment	Boehringer
Lysozyme	Sigma
Proteinase K	Sigma
T4 DNA ligase	Boehringer
<i>Taq</i> -polymerase	Boehringer
Pfu DNA Polymerase	Promega
AcTEV Protease	Invitrogen

1.2.2 Inhibitors

Complete mini protease inhibitor cocktail	Roche
PMSF (phenylmethylsulfonylfluoride)	Sigma-Aldrich
Ellagic acid	Calbiochem
DMAT	Calbiochem

1.2.3 Antibodies**1.2.3.1 Primary antibodies**

Mouse anti-GFP-antibody mAb K3-184-2	Noegel et al., 2004
Mouse-anti-annexin 7-antibody mAB 203-217	Clemen et al., 2000
Mouse-anti- β -actin-antibody	Sigma-Aldrich
Goat-anti-GST-antibody	Amersham Biosciences
Mouse-anti-CRN2 antibody K6-444-4	Spoerl et al. 2002
Mouse monoclonal anti-GFP mAb K3-167-2	Noegel et al., 2004
Rabbit anti-Phosphoserine	ZYMED laboratories
Rabbit Anti-p34-Arc/ARPC2	upstate
Rabbit Anti-Cofilin	Sigma

1.2.3.2 Secondary antibodies

Goat-anti-mouse-IgG, peroxidase-conjugated	Sigma-Aldrich
Goat-anti-rabbit-IgG, peroxidase-conjugated	Sigma-Aldrich
Goat-anti-mouse-IgG, Cy3-conjugated	Sigma-Aldrich
Rabbit-anti-mouse-IgG, Alexa 488-conjugated	Sigma-Aldrich
Rabbit-anti-mouse-IgG, Alexa 586-conjugated	Sigma-Aldrich
Goat-anti-rabbit-IgG, FITC-conjugated	Sigma-Aldrich
TRITC-labelled Phalloidine	Sigma-Aldrich

1.2.4 Antibiotics

Ampicillin	Sigma
Kanamycin	Sigma
Tetracycline	Sigma
Gentamicin	Sigma
G418	Sigma

1.2.5 Radiolabelled nucleotide

α -³²P -deoxyadenosine triphosphate, (10 μ Ci/ μ l) Amersham

1.3 Reagents

acrylamide (Protogel: 30: 0.8 AA/Bis-AA)	National Diagnostics
agarose (electrophoresis grade)	Life Technologies
acetone	Riedel-de-Haen
APS (Ammoniumperoxodisulfate)	Fluka
Bacto-Agar, Bacto-Tryptone	Difco
Benzamidine	Sigma-Aldrich
Bromophenol blue (Na-salt)	Serva
BSA (bovine serum albumin)	Sigma-Aldrich
Chloroform	Riedel-de-Haen
Calcium chloride	Sigma-Aldrich
Coomassie-brilliant-blue R250	Serva
p-coumaric acid	Fluka
DMSO (Dimethyl sulfoxide)	Merck
DTT (1,4-dithiothreitol)	Gerbu
EDTA (Ethylenediaminetetraacetic acid)	Merck
EGTA [ethylene-glycol-bis(2-aminoethylether)- N,N,N',N'-tetraacetic acid]	Sigma-Aldrich
Acetic acid	Riedel-de-Haen
Ethanol	Riedel-de-Haen
Ethidium bromide	Sigma-Aldrich
FCS (fetal calf serum)	Sigma-Aldrich
Formamide	Merck
Formaldehyde	Sigma-Aldrich
Glucose	Sigma-Aldrich
Glycine	Degussa
Glycerol	Oxoid
IPTG (isopropyl β -D-thiogalactopyranoside)	Sigma-Aldrich
isopropanol	Merck
HEPES [(N-2-hydroxyethyl)piperazine-N'- (2-ethansulfonic acid)]	Sigma-Aldrich

β -mercaptoethanol	Sigma-Aldrich
Methanol	Riedel-de-Haen
Mineral oil	Amersham Biosciences
MOPS (g-[Morpholino] propanesulfonic acid	Gerbu
Ni-NTA agarose	Qiagen
Nucleosidtriphosphate	Roche
Nonidet-P40 (Nonylphenyl-polyethylenglycerine)	Fluka
Paraformaldehyde	Sigma-Aldrich
PIPES (1,4-piperazindiethansulfonic acid)	Sigma-Aldrich
Ponceau S-concentrate	Sigma-Aldrich
Protein-A-sepharose	LifeTechnologies
Phalloidin TRITC-conjugated	Sigma-Aldrich
SDS (sodium dodecylsulfate)	Serva
Sucrose	Fluka
Sodium azide	Merck
TEMED (tetramethylethylenediamine)	Merck
Tris (hydroxymethyl) aminomethane	Sigma-Aldrich
Triton-X-100 (t-octylphenoxypolyethoxyethanol)	Merck
Tween 20 (Polyoxyethylensorbitanmonolaurate)	Sigma-Aldrich
X-gal (5-bromo-4-chloro-3-indolyl- β -galactopyranoside)	Roth
Yeast extract	Oxoid

1.4 Plasmids

pEGFP-C1	Clontech
pcDNA3.1/myc-His	Invitrogen
pQE-30	Qiagen
pVSV-G	BioCat
pPACKH1-GAG	BioCat
pPACKH1-REV	BioCat
pLKO.1 -puro empty vector only	Open Biosystems
pLKO.1- puro non-target-shRNA	Sigma
pLKO.1-puro-GFP	Sigma

1.4.1 Oligonucleotides

Coro3mutS98DF	5' GGTCATTGCCAGCGGTTTCAGAGG 3'
Coro3mutS98DRev	5' CCTCTGAACCGTCGGCAATGACC 3'
Coro3mutS174DF	5' GACGATATGCATGACGACATGATTTACAATGTGAGCTGG 3'
Coro3mutS174DRev	5' CCAGCTCACATTGTAAATCATGTCGTCATGCATATCGTCC3'
Coro3mutS463DF	5' GCAATCAAGATGAGCGTATTTCCAAGTTAGAACAGCAGATGGC3'
Coro3mutS463DRev	5' GCCATCTGCTGTTCTAACTTGCAATACGCTCATCTTGATTGC 3'
Coro3mutS463AF	5' CAATCAAGATGAGCGTATTGCCAAGTTAGAACAGCAGATGGC3'
Coro3mutS463ARev	5' GCCATCTGCTGTTCTAACTTGCAATACGCTCATCTTGATTGC 3'
Coro3 shRNA	5'CGTCCACTACCTCAACACATT 3' (TRCNOOOOO62777)

1.5 Bacterial host strains

<i>E. coli</i> XL1 blue	Bullock et al., 1987
<i>E. coli</i> JM 109	Yanisch-Perron et al., 1985
<i>E. coli</i> DH5 α	Hanahan, 1983
<i>E. coli</i> M15	Qiagen
<i>E. coli</i> BL21	Studier and Moffatt, 1986

1.6 Insect cell lines

<i>Sf-9 cells</i>	Invitrogen
<i>Sf</i> -High five cells	Invitrogen

1.7 Mammalian cell lines

HEK293	Graham et al., 1977
TN	BioCat
Cos7	Gluzman, 1981
U372	(Thal et al., 2008)
A172	(Thal et al., 2008)

1.8 Media and buffers

All media and buffers were prepared with deionised water, filtered through an ion-exchange unit (Membra Pure). The media and buffers were sterilized by autoclaving at 120°C and antibiotics were added to the media after cooling to approx. 50°C. For making agar plates, a semi-automatic plate-pouring machine (Technomat) was used.

1.8.1 Media for *E. coli* culture

LB medium, pH 7.4	(Sambrook, (1989))
SOC medium, pH 7.0	(Sambrook, (1989))

1.8.2 Media for Mammalian cell culture

DMEM (4,500 mg/l glucose)	Sigma-Aldrich
DMEM (1,000 mg/l glucose)	Sigma-Aldrich

1.8.3 Media for Insect Cell Culture

SF-900 III SFM	GIBCO
Express FIVE SFM	GIBCO

1.9 Instruments and Equipments

All the instruments that were used in this thesis work were from Department Facilities.

1.10 Immunoblotting and antibodies

For Western blot analysis samples were prepared according to standard procedures (Laemmli, 1970) (Towbin et al., 1979). Detection of CRN2 was done with mAb K6-444 (Smith et al., 1999), β -actin was detected by mAb AC 40 (Sigma).

1.11 Mammalian cell culture

HEK293 human embryonic kidney cells (ATCC: CRL-1573), HaCaT human keratinocytes (Boukamp et al., 1988), U373, A172, Cos7 and C2F3 were grown in Dulbecco's modified Eagle's medium (DMEM, 4.5 g/l glucose, Sigma) supplemented with 10% fetal calf serum (Biochrom), 1 mM sodium pyruvate (Sigma), 2 mM L-glutamine (Sigma), 100 units/ml penicillin G, and 100 μ g/ml streptomycin (Invitrogen). In case of NIH3T3 murine fibroblasts (ATCC: CRL-1658) DMEM with 1 g/l glucose was used. PC-12 cells (ATCC: CRL-1721) were cultured in suspension in RPMI 1640 medium with 25mM HEPES pH 7.4, supplemented with 10% horse serum, 5% FCS, 4 mM L-glutamine, 100 U/ml penicillin G and 100 μ g/ml streptomycin. All cells were grown at 37 °C with 5% CO₂.

Electroporation of HEK293 and PC-12 cells was done by electroporation ((Rosentreter et al., 2007) stably transfected HEK293 cell clones were selected in culture medium containing 1200 μ g/ml geneticin (G418; Invitrogen). To stably express CRN2 in HaCaT cells they were retrovirally transduced according to (Clemen et al., 1999).

1.12 2D-gel electrophoresis

Two-dimensional gel electrophoresis in conjunction with immunoblotting was performed according to (Clemen et al., 2005). Incubation with primary antibody was followed by incubation with goat anti-mouse IgG coupled to horseradish peroxidase (Sigma); visualisation was done by enhanced chemiluminescence and exposure to x-ray films (Kodak).

CRN2 was detected with mAb K6-444 (Spoerl et al., 2002) mAb 203-217 specifically recognized annexin A7 (Selbert et al., 1995). β -COP was detected using mAb maD ((Pepperkok et al., 1993), sarcomeric actin was recognized by mAb 5C5 (Sigma), and anti-BiP/GRP78 was from Transduction Laboratories. Furthermore a rabbit polyclonal antibody against myomesin (1:200; a gift from Peter van der Ven, Bonn), a rabbit polyclonal antibody against desmin (1:200; 2203PDE; Euro-Diagnostica), a sheep polyclonal antibody against the skeletal muscle ryanodine receptor (RyR1; 1:100; 70372(27); Upstate Biotechnology; developed by Kevin P. Campbell), and a monoclonal antibody against actin (1:100; AC40; Sigma) were used.

1.13 Statistical methods

Statistical analysis was performed using ANOVA or Student's t-test, as appropriate. The exact probability values and the significance of an analysis as well as the number of independent experiments and repeated measurements are indicated.

Most of the specific experimental procedures described in the following paragraphs have been included in preliminary publications prepared from this thesis work, as listed at the end of the Introduction section. Therefore, where possible, descriptions of the experimental procedures have been shortened. Moreover, the experimental procedures are categorized according to the separate parts presented within the Results section.

2.0 Role of CRN2 in cellular processes

2.1 Generation of EGFP-fusion constructs of CRN2 domains

Plasmids EGFP-CRN2NWDC (human, full-length, aa 1-474; NM_014325), EGFP-CRN2 Δ CC (aa 1-444), and EGFP-CRN2 Δ NC (aa 72-404) are described in Spoerl et al. (Spoerl et al., 2002). pEGFP-CRN2WD (aa 72-299), pEGFP-CRN2NC (aa 1-71 fused to aa 300-474), and pEGFP-CRN2NGC (aa 1-71 fused to aa 300-474 via a 5-glycine loop), which code for truncated EGFP-CRN2 fusion proteins as well as the retroviral vector GFP-hCRN2-BMN were generated according to (Rosentreter et al., 2007).

2.2 Subcellular fractionation

Differential centrifugation was done according to (Fox, 1985; Lehtonen et al., 2002; Spoerl et al., 2002; Tohyama et al., 1994). For F-actin depolymerization, confluent HaCaT or HEK293 cell monolayers were incubated in normal cell culture medium containing 5 μ M latrunculin B (30 min; Sigma) Ref: Rosentreter. Sample volumes of the Triton X-100-soluble fraction, the 10,000 g pellet (highly crosslinked actin filaments), the pellet of 100,000 g (free or loosely crosslinked actin filaments associated with membranes), and the supernatant of 100,000 g (cytosolic fraction) (Fox, 1985; Lehtonen et al., 2002; Spoerl et al., 2002; Tohyama et al., 1994) were normalized to the original number of cells used.

2.3 RNAi silencing

To reduce the amount of CRN2 protein in murine NIH3T3 fibroblasts a siRNA SMARTpool directed against murine CRN2 was obtained from Dharmacon (CORO1C, Cat # M-007778-00-50), which had been derived from the sequence NM_011779. The siRNA pool contains four different siRNA complexes. Transfection of the siRNA duplexes was done according to Rosentreter et al, 200x.

2.4 Immunofluorescence, confocal microscopy, and live cell imaging

To visualize endogenous CRN2 and F-actin, HaCaT cells were either first fixed in 4 °C cold 4% paraformaldehyde for 20 min followed by permeabilization with 0.5% Triton X-100 in PBS or first permeabilized and then fixed. HEK293 cells were fixed and then permeabilized. Immunostaining was performed according to (Spoerl et al., 2002). Secondary IgG were goat anti-mouse coupled to Alexa 488 or Cy3 (Molecular Probes and Sigma). F-actin was labelled by incubation for 60 min with 200 ng/ml TRITC- or FITC-phalloidin (Sigma), nuclei were visualized by incubation for 60 min with 100 ng/ml DAPI (Sigma), both together with the secondary antibody. Appropriate control experiments were performed. Images were recorded with a Leica DM IRBE microscope and TCS SP confocal laser scanning technology with TCSNT software. Image processing was done with Adobe PhotoShop. For cell migration and cell activity assays live cell imaging was performed using the Leica DM IRE 2 microscope and Leica DFC 350 FX camera with Leica FW 4000 software. In all these experiments cells were grown at 37 °C with 5% CO₂.

2.5 In vitro wound healing, proliferation, cytokinesis, and cell activity assays

For in vitro wound healing a confluent layer of stably transfected HEK293 cells or of siRNA-treated NIH3T3 cells was scratched with a 27-gauge needle. The culture medium was

changed to remove detached cells or debris. Closure of the wound was followed by recording an image every 10 min with the equipment described above. For calculation of the velocity of the wound healing the distance of the wound borders at 1 h and 11 h after scratching were determined in at least three positions. Three (HEK293) or four (NIH3T3) independent experiments were performed. To measure the proliferation rate, stably transfected HEK293 cells were seeded at 106 cells/10-cm culture dish. After 3 days the cells from three independent experiments were trypsinized and counted again. To reveal defects in the cytokinesis, stably transfected HEK293 cells were seeded at 105 cells/10-cm culture dish and the relative amounts of multinuclear cells were determined by fluorescent microscopy after 3 days of cultivation from two independent experiments. To visualize the activity of stably transfected HEK293 cells, they were seeded at low concentrations. 12 h later the GFP fluorescence signal of single cells was recorded for 30 min with a Leica DM IRE 2 microscope and a Leica DFC 350 FX camera with Leica FW 4000 software. For each population the number of forming and retracting protrusions of single cells were determined. Similarly, the dynamics of GFP–CRN2 and RFP–actin were recorded by confocal microscopy (Leica DM IRBE microscope and TCS SP confocal laser scanning technology) in double-transfected HEK293 cells. Every 10 s a 3-fold averaged image of single-cellular protrusions was taken.

2.6 Co-immunoprecipitation

1.5×10^8 HEK293 cells stably transfected with EGFP–CRN2 were treated for 30 min with 5 μ M latrunculin B (Sigma) in order to prevent unspecific co-precipitation of proteins bound to F-actin, washed twice with PBS, resuspended in 6 ml immunoprecipitation (IP) buffer (0.33 \times PBS pH 7.4, 2 mM benzamidine, 4mM DTT, 2mM EDTA, 0.5 mM PMSF, 0.5% Triton X-100 (added after sonication)), sonicated, and microscopically examined to confirm complete cell lysis. The resulting lysate was centrifuged at 2000 \times g for 3 min at 4 °C and precleared prior to immunoprecipitation with equilibrated Protein G sepharose beads for 30 min. 3ml of pre-cleared supernatant were incubated with 500 μ l of anti- GFP mAb (K3-184 or K3-167; (NH₄)₂SO₄-concentrated hybridoma supernatant; (Noegel et al., 2004)) 7 μ l Triton X-100 and 70 μ l protein G sepharose beads at 4 °C for 1.5 h. The beads were washed four times with 1 ml IP buffer, incubated with 2 \times SDS–sample buffer for 5 min at 95 °C, and analyzed by immunoblotting using antibodies specifically recognizing CRN2, p34-Arc (rabbit polyclonal Ab, Upstate), and cofilin (rabbit polyclonal Ab, Sigma). For control, the experiment was carried out with cell lysate or with anti-GFP-mAb only. Immunoblotting with anti-

BiP/GRP78 (Transduction Laboratories) and anti- β -actin (Sigma) was used for control to test for the specificity of immunoprecipitation. The experiment was done several times.

3.0. Expression of CRN2 in diffuse gliomas is related to malignancy

3.1 Neuropathology

We have studied 69 biopsy and five autopsy cases by means of immunohistochemistry, and 24 additional cases by immunoblotting, for the expression of CRN2. For details refer to (Thal et al., 2008)

3.2 Visualization of invadopodia

Invadopodia of U373 and A172 glioblastoma cells were visualized according to (Chen W-T, 1994; Osiak AE, 2005). U373 cells, which form wide-stretched cellular extensions, and A172 cells were seeded at low density and grown for 24 h on cover slips that had a 3D coat of FITC-labelled fibronectin or FITC-labelled gelatin. Invadopodia are actin-rich finger-like protrusions under the ventral surface of a cell that localize matrix-degrading activity, extend into the extracellular matrix, and are recognizable by co-localization of invadopodia markers with the degradation of fluorescently labelled extracellular matrix (Weaver, 2006).

3.3 Lentiviral transduction of shRNA vectors

Small hairpin RNAs (shRNAs) were used to stably and specifically reduce the expression of CRN2 in human glioblastoma cells. shRNA-oligo cgtccactacctcaacacatt (TRCN0000062777) cloned into pLKO.1-puro (BioCat/SBI/Open Biosystems) led to a 95% reduction in the expression level of CRN2 (CRN2). Each shRNA plasmid was co-transfected into 293TN cells, together with the three lentiviral packaging plasmids, pVSV-G, pPACKH1-GAG and pPACKH1-REV (BioCat/SBI: LV500A-1). The resulting lentiviruses were used to infect the target glioblastoma cells (approximately 95% transduction efficiency), which were subsequently enriched/selected to 99.9% transduction efficiency within 7 days by addition of 0.75 μ g/ml puromycin to the growth medium. Control cells expressed pLKO.1-puro empty vector only ('mock'; Open Biosystems, RHS4078), a pLKO.1-puro-non-target-shRNA construct ('scrambled'; Sigma, SHC002), or positive control pLKO.1-puro-GFP (Sigma, SHC003). Transfections of 293TN (60 mm plates) and transductions of target cells (three infections of the same 60 mm target cell plate for each shRNA, with viral supernatant collected after 24, 48 and 72 h) were done according to the manufacturer's protocol (SBI) and Ref: Thal et al., 2008. Transduction efficiency was determined from the fluorescent GFP-positive control.

3.4 Determinations of Cell based assays.

Here Cell based assays include cell proliferation rate, cell cycle state, cell motility, cell invasion, matrix metalloproteinase activity and cellular F-actin content. To measure cell proliferation rates, seeding/trypsination as well as colorimetric cell viability assays (QMTT Cell Viability Assay; BioCat Z5030007-BC; (T.Mosmann, 1983) were used. To determine the cell cycle distribution, standard propidium iodide fluorescence-activated cell sorting (PI-FACS) analyses were performed. Cell motility was determined, employing live cell imaging. To determine cell invasion rates, CytoSelect 96-well Cell Invasion Assays (BioCat CBA-112-CB), based on the principle of a Boyden Chamber with basement membrane-coated inserts, were employed. SensoLyte 520 Generic MMP assays (Mobictec: 71158AS) were used to determine the overall activity of matrix metalloproteinases. The F-actin content of glioblastoma cells was determined according to Cunningham (Cunningham, 1995). The knockdown of CRN2 was verified by immunoblotting of samples of cells from each experiment.

4.0 Structural and functional diversity of novel CRN2 isoforms

4.1 Immunofluorescence and immunohistochemistry

Immunofluorescence imaging of cultured cell lines was performed according to (Thal et al., 2008). Isolation of human myofibers was performed by manual separation of fresh muscle biopsies in “relaxation solution” (Vielhaber et al., 2000). Further details see (Xavier-C.P, 2008) submitted for publication.

4.2 Mammalian cell culture

Human peripheral blood monocytes were isolated and differentiated into macrophages as described previously (Linder et al., 1999). For myogenic conversion of NIH3T3 fibroblasts a retrovirus derived from plasmid BMN-hMyoD-IRES-GFP (transfected into Φ NX-E cells) containing a cassette coding for human MyoD was used (Clemen et al., 1999). Highly efficient transfection of primary human macrophages with a CRN2 specific siRNA-pool (Dharmacon siGENOME siRNA # M-017331-00) was performed according to (Rosentreter et al., 2007) using a Microporator device (Peqlab). In vitro wound healing was performed as described earlier (Rosentreter et al., 2007).

4.3 RNA purification, northern blotting, 5'-RACE, 5'-RLM-RACE, and RT-PCR

RNA-samples: Total RNA from cells was extracted using the RNeasy Mini kit (Qiagen); total RNA from murine tissues was prepared using a TRIzol (Invitrogen) protocol ((Chomczynski and Sacchi, 1987); total RNA from samples of human skeletal muscle biopsies was prepared with RNA-Magic (Bio-Budget) following the manufacturer's protocol. In addition, a pool of RNA from adult human skeletal muscle was obtained from Clontech.

Northern blotting: 30 µg of total RNA from murine ES-cells, undifferentiated C2F3 myoblasts, differentiated C2F3 myotubes, and various murine organs were analyzed by northern blotting using full-length murine CRN2 (accession no. AF143957) and β-actin cDNAs as probes. 5'-RACE: Standard 5'-RACE was performed on various samples of total RNA extracted from human skeletal muscle tissue. Reactions were carried out according to the manufacturer's protocol (Roche, 5'/3' RACE Kit 2nd Generation, #03353621001). The PCR products were cloned into pGEMTeasy vector (Promega) and sequenced.

5'-RLM-RACE: RLM (RNA-Ligase Mediated)-RACE allows the amplification of cDNA only from full-length capped mRNA and determines the real 5-prime end of an mRNA. 5'-RLM-RACE was performed on various samples of total RNA extracted from human skeletal muscle tissue and reactions were carried out according to the manufacturer's protocol (Ambion, FirstChoice RLM-RACE Kit, #1700). Reverse transcription using random decamers was carried out at 49°C. PCR products from various primer pairs ((Xavier-C.P, 2008) were cloned into pGEMTeasy or purified and sequenced directly.

RT-PCRs: cDNA from human skeletal muscle total RNA was obtained using p(dN6)-oligomers and M-MLV reverse transcriptase (Promega) at 37°C for 1 h. PCRs were performed according to Xavier et al. to confirm or expand the sequences of the different CRN2 clones identified by RACE. Fragments obtained were cloned into pGEMTeasy and sequenced or the PCR-products were purified and sequenced directly using a 377 ABI DNA-sequencer (Applied Biosystems).

4.4 Differential centrifugation, subcellular fractionation, and gel filtration

Differential centrifugation was done according to (Spoerl et al., 2002), isopycnic separation on a discontinuous sucrose gradient according to (Clemen et al., 1999). For gel filtration analysis 100 mg of murine skeletal muscle or kidney tissue were lysed in 20 mM HEPES, pH 7.2, 1 mM EDTA, protease inhibitor cocktail, and sonicated. The lysate was centrifuged for 30 min at 10,000 g, followed by centrifugation of the supernatant at 100,000 g for 1 h. The latter supernatant was adjusted to 0.6 M KCl, incubated for 1 h at 4°C, and re-centrifuged at

100,000 g for 1 h. KCl minimizes interactions between CRN2 and other proteins as well as interactions between actin and myosin (Berryman et al., 1995). The supernatants were adjusted to 1 µg/µl protein, and 50 µl were separated on a Superdex G200 gel filtration column using the SMART system (Amersham Biosciences).

4.5 Plasmids for expression of CRN2 isoforms

To express human EGFP-CRN2i1 ('conventional' CRN2 isoform 1, accession no. NM_014325) in C2F3 myoblasts, an AgeI/BamHI EGFP-CRN2i1-837bp3'UTR cassette was retrieved from EGFP-CRN2i1 (Spoerl et al., 2002), blunt ended and cloned into the BamHI/NotI backbone of pBMN-Z (Nolan, Stanford University). Retroviruses derived from the resulting plasmid EGFP-CRN2i1-BMN transfected into ΦNX-E cells were used to infect C2F3 target cells according to (Clemen et al., 1999). For expression of EGFP-CRN2i1 in HEK293 cells construct EGFP-CRN2i1 (Spoerl et al., 2002), was used; stably expressing cells were obtained after neomycin selection. Primary human macrophages were transfected with EGFP-CRN2i1 using a microporator device (PeqLab; Erlangen, Germany) according to the manufacturer's instructions.

In vitro mutagenesis was employed to generate plasmids coding for the two additional isoforms. Plasmids EGFP-CRN2i1-BMN and EGFP-CRN2i1 were used as templates. See Ref. Xavier et al., submitted for publication for details. All CRN2 expression constructs were verified by restriction enzyme digest and sequencing.

4.6 Bioinformatic analysis

Genomic sequence data for CRN2 from 11 primates and 28 other mammals were retrieved from NCBI (<http://www.ncbi.nlm.nih.gov>) and Ensembl (http://www.ensembl.org/Homo_sapiens/geneview?gene=ENSG00000110880). Regions encompassing the 5' promoter up to exon 2 were assembled, aligned by CLUSTALW and scrutinized bioinformatically for promoter features, transcription start sites, coding regions, exon splice sites, regulatory elements, and further analyses as described in Xavier et al., submitted for publication..

5.0 Influence of Phosphorylation on Structure and function of CRN2

5.1 Expression of wild-type and mutant CRN2 coiled coil peptides.

Construct pQE30 harbouring CRN2 wild-type peptide (aa 300-474) was used as a template. Using primers CRN2mutS463DFor and Rev, CRN2mutS463AFor and Rev and the Quick Change Site-Directed Mutagenesis kit, CRN2 S463D (aspartate), S463A (alanin) were

obtained. Corresponding recombinant proteins were expressed and purified according to (Spoerl et al., 2002).

5.2 *In vitro* wound healing and single protrusion assay

Constructs pEGFP-CRN2 (Spoerl et al., 2002), and mutants pEGFP-CRN2-S463D and pEGFP-CRN2-S463A (obtained as described above) were transfected into HEK293 cells and used in wound healing and single cell protrusion assays according to (Rosentreter et al., 2007).

5.3 *In vitro* phosphorylation assay

The assay was performed in a phosphorylation buffer that composed 10mM MgCl₂, 50mM MOPS pH7.0, 150mM NaCl and α -³²P-dATP, (10 μ Ci/ μ l, Amersham). CRN2 wild-type (aa 300-474) (2.5 μ g), S463D (4.0 μ g), and S463A (4.0 μ g) peptides as well as CRN2 wild-type full-length (0.4 μ g) and S463D (0.5 μ g) proteins were added to the phosphorylation buffer without α -³²P-dATP. The reaction was initiated with CK2 α (0.12 μ g) and CK2 α dead (0.4 μ g) with final addition of radioactive dATP. Reaction volume was adjusted to a total of 100 μ l. The reaction mixtures were incubated for 1, 5, 10, 30, 60, and 90 mins at 30⁰C. In order to terminate the reaction; each sample was placed on ice and 60mM EDTA and 1x SDS sample buffer were added to each. All the samples were analysed by SDS-PAGE followed by autoradiography. (Skjerpen et al., 2002)

5.4 *Actin polymerization assays*

Actin polymerization assays were performed using a pyrene actin assay kit (Cytoskeleton) in which the rate of pyrene-labelled G-actin conversion into F-actin is monitored. The pyrene conjugated G-actin stock was depolymerized (as per the manufacturer's instruction) and spun at 100,000g for 1 h at 4 °C to minimize oligomers that may have formed during storage before use in the assay. The general actin buffer, Pyrene labelled G-actin and polymerisation buffer (Actin Polymerization Biochem Kit, Cytoskeleton) were incubated at RT for 15mins. GST-VCA domain (final concentration of 18.9 nM) and Arp2/3 complex (final concentration of 37 nM) were incubated either in the presence or absence of CRN2 wild-type peptide (aa 300-474) or S463D mutant (final concentrations 1x, 0.8 μ M, and 2x, 1.6 μ M) with actin for 1min before the addition of polymerisation buffer.

Fluorescence was read immediately after the addition of polymerisation buffer using a Fluorescence system (Photon technology international –PTI system) set on kinetic mode to read every 1 min for the duration of the assay. PTI system was adjusted to wavelengths as

follows: Excitation, 350 nM; emission, 407 nM; and sensitivity, maximum. The assay was conducted in black-walled clear-two side windows cuvettes. Mean value of the maximum slope of each polymerisation curve was measured (Serrels et al., 2007) and used for statistical analyses.

5.5 Co-immunoprecipitation

HEK293 cells stably transfected with EGFP-CRN2 were treated for 24hrs min with CK2 inhibitors DMAT (1.4 μ M) and ellagic acid 0.4 μ M (Calbiochem), and controls with equivalent amounts of DMSO, washed twice with PBS, resuspended in 6 ml immunoprecipitation (IP) buffer (20mM HEPES pH 7.0, 100mM KCl, 0.5% NP-40, 1mM EDTA, 50mM PMSF, 10 μ g/ml 1,10-phenanthroline, 10 μ g/ml aprotinin, 10 μ g/ml leupeptin, 10mM sodium fluoride and 2mM Sodium orthovanadate), sonicated, and the lysates were cleared at 13,000xg for 5mins and incubated for 1-2hrs with 500 μ l of concentrated anti-GFP mAb K3-167 (Noegel et al., 2004). Beads were washed extensively with IP buffer before pre-blocking with 5% BSA and further incubated overnight with GFP antibody. The immune complexes were collected and washed 5 times with IP buffer, separated by SDS PAGE and transferred to Nylon membrane, and further analyzed by immunoblotting using antibodies specifically recognizing CRN2, phosphorylated CRN2 (phosphoserine antibody, Zymed laboratories), p34-Arc (rabbit polyclonal Ab, Upstate), and cofilin (rabbit polyclonal Ab, Sigma).

5.6 CRN2 pull down experiments

For pulldown assays, GST-CK2 or CK2-dead fusion proteins were purified from bacteria. The GST fusion proteins were supplemented with 100 μ l of equilibrated glutathione beads and incubated under constant rotation for 2hrs at 4⁰C. After washing 4-5 times with washing buffer (4.3mM NaH₂PO₄, 1.47mM KH₂PO₄, 1.37mM NaCl, 2.7mM KCl) aliquots of the beads, now carrying the GST-CK2 fusion proteins, were incubated together with extracts from equal numbers of HEK293 cells (1.5 x 10⁸) either expressing GFP-CRN2 wild-type, GFP-CRN2-S463D, or only the endogenous CRN2 protein. Alternatively, the aliquots were incubated with lysates of bacterial cells expressing His-CRN2-wild-type or His-CRN2-S463D C-terminal peptides. Incubation was done for 2hrs at 4⁰C to pull down respective proteins. Cell extracts were prepared by lysing HEK293 cells in lysis buffer A (10mM HEPES pH7.9, 10mM KCl, 0.1mM EDTA, 1mM DTT, 0.5mM PMSF, 0.5% NP40) and M15 bacterial cells in lysis buffer B (10mM DTT, 0.5mM PMSF, 2mM Benzamidin, 10 μ g/ml Aprotinin and leupeptin, 200mM NaCl, 5% Glycerine, 100 μ /ml lysozyme and 0.5% NP40), incubation for

30mins at 4⁰C, sonication, and the supernatant was collected by centrifugation for 5mins at 13,000rpm. Protein bound beads were washed 10 times with washing buffer (4.3mM NaH₂PO₄, 1.47mM KH₂PO₄, 1.37mM NaCl, 2.7mM KCl with 5% glycerine and 30mM NaCl) and analysed by SDS-PAGE and immunoblotting. Control experiments were performed with GST or GFP alone.

IV. Bibliography

- Allende JE, Allende CC.** Protein kinases. 4. Protein kinase CK2: an enzyme with multiple substrates and a puzzling regulation. *Faseb J* 1995; 9: 313-23.
- Ammar DA, Nguyen PN, Forte JG.** Functionally distinct pools of actin in secretory cells. *Am J Physiol Cell Physiol* 2001; 281: C407-17.
- Anes E, Kuhnel MP, Bos E, Moniz-Pereira J, Habermann A, Griffiths G.** Selected lipids activate phagosome actin assembly and maturation resulting in killing of pathogenic mycobacteria. *Nat Cell Biol* 2003; 5: 793-802.
- Appleton BA, Wu P, Wiesmann C.** The crystal structure of murine coronin-1: A regulator of actin cytoskeletal dynamics in lymphocytes. *Structure* 2006; 14: 87-96.
- Berthier C, Blaineau S.** Supramolecular organization of the subsarcolemmal cytoskeleton of adult skeletal muscle fibers. A review. *Biol Cell* 1997; 89: 413-34.
- Binder DK, Berger MS.** Proteases and the biology of glioma invasion. *J Neuro oncol* 2002; 56: 149-58.
- Boukamp P, Petrussevska RT, Breitkreutz D, Hornung J, Markham A, Fusenig NE.** Normal keratinization in a spontaneously immortalized aneuploid human keratinocyte cell line. *J Cell Biol* 1988; 106: 761-71.
- Brieher WM, Kueh HY, Ballif BA, Mitchison TJ.** Rapid actin monomer-insensitive depolymerization of Listeria actin comet tails by cofilin, coronin, and Aip1. *J Cell Biol* 2006; 175: 315-24.
- Bryson K, McGuffin LJ, Marsden RL, Ward JJ, Sodhi JS, Jones DT.** Protein structure prediction servers at University College London. *Nucl. Acids Res.* 2005; 33: W36-W38.
- Cai L, Holoweckyj N, Schaller MD, Bear JE.** Phosphorylation of coronin 1B by protein kinase C regulates interaction with Arp2/3 and cell motility. *J Biol Chem* 2005; 280: 31913-23.
- Cai L, Makhov AM, Bear JE.** F-actin binding is essential for coronin 1B function in vivo. *J Cell Sci* 2007a; 120: 1779-90.
- Cai L, Marshall TW, Uetrecht AC, Schafer DA, Bear JE.** Coronin 1B coordinates Arp2/3 complex and cofilin activities at the leading edge. *Cell* 2007b; 128: 915-29.
- Canton DA, Litchfield DW.** The shape of things to come: an emerging role for protein kinase CK2 in the regulation of cell morphology and the cytoskeleton. *Cell Signal* 2006; 18: 267-75.
- Chen W-T YY, Nakahara H.** An in vitro cell invasion assay:determination of cell surface proteolytic activity that degrades extracellular matrix. *J Tissue Culture Methods* 1994: 177-181.

- Chereau D, Boczkowska M, Skwarek-Maruszewska A, Fujiwara I, Hayes DB, Rebowski G, et al.** Leiomodin is an actin filament nucleator in muscle cells. *Science* 2008; 320: 239-43.
- Chomczynski P, Sacchi N.** Single-step method of RNA isolation by acid guanidinium thiocyanate-phenol-chloroform extraction. *Anal Biochem* 1987; 162: 156-159.
- Clemen CS, Eichinger L, Rybakin V.** The Coronin Family of Proteins. Vol 48: Landes Bioscience & Springer, 2008. <http://www.eurekah.com/chapter/3785>
- Clemen CS, Fischer D, Roth U, Simon S, Vicart P, Kato K, et al.** Hsp27-2D-gel electrophoresis is a diagnostic tool to differentiate primary desminopathies from myofibrillar myopathies. *FEBS Lett* 2005; 579: 3777-82.
- Clemen CS, Hofmann A, Zamparelli C, Noegel AA.** Expression and localisation of annexin VII (synexin) isoforms in differentiating myoblasts. *J Muscle Res Cell Motil* 1999; 20: 669-79.
- Cooper JA, Wear MA, Weaver AM.** Arp2/3 complex: advances on the inner workings of a molecular machine. *Cell* 2001; 107: 703-5.
- Cory GO, Cramer R, Blanchoin L, Ridley AJ.** Phosphorylation of the WASP-VCA domain increases its affinity for the Arp2/3 complex and enhances actin polymerization by WASP. *Mol Cell* 2003; 11: 1229-39.
- Cunningham C.** Actin polymerization and intracellular solvent flow in cell surface blebbing. *J Cell Biol* 1995: 1589–1599.
- Cvrckova F, Rivero F, Bavluka B.** Evolutionarily conserved modules in actin nucleation: lessons from Dictyostelium discoideum and plants. Review article. *Protoplasma* 2004; 224: 15-31.
- de Hostos EL.** The coronin family of actin-associated proteins. *Trends Cell Biol* 1999; 9: 345-50.
- de Hostos EL, Bradtke B, Lottspeich F, Guggenheim R, Gerisch G.** Coronin, an actin binding protein of Dictyostelium discoideum localized to cell surface projections, has sequence similarities to G protein beta subunits. *Embo J* 1991; 10: 4097-104.
- DesMarais V, Ghosh M, Eddy R, Condeelis J.** Cofilin takes the lead. *J Cell Sci* 2005; 118: 19-26.
- DesMarais V, Macaluso F, Condeelis J, Bailly M.** Synergistic interaction between the Arp2/3 complex and cofilin drives stimulated lamellipod extension. *J Cell Sci* 2004; 117: 3499-510.
- Di Giovanni S, De Biase A, Yakovlev A, Finn T, Beers J, Hoffman EP, et al.** In vivo and in vitro characterization of novel neuronal plasticity factors identified following spinal cord injury. *J Biol Chem* 2005; 280: 2084-91.

- Dobbins GC, Zhang B, Xiong WC, Mei L.** The role of the cytoskeleton in neuromuscular junction formation. *J Mol Neurosci* 2006; 30: 115-8.
- Emery AEH.** Neuromuscular disorders: Clinical and Molecular Genetics. New York: Wiley, 1999.
- Ferrari G, Langen H, Naito M, Pieters J.** A coat protein on phagosomes involved in the intracellular survival of mycobacteria. *Cell* 1999; 97: 435-47.
- Foger N, Rangell L, Danilenko DM, Chan AC.** Requirement for coronin 1 in T lymphocyte trafficking and cellular homeostasis. *Science* 2006; 313: 839-42.
- Fox JE.** Linkage of a membrane skeleton to integral membrane glycoproteins in human platelets. Identification of one of the glycoproteins as glycoprotein Ib. *J Clin Invest* 1985; 76: 1673-83.
- Galkin VE, Orlova A, Briehner W, Kueh HY, Mitchison TJ, Egelman EH.** Coronin-1A stabilizes F-actin by bridging adjacent actin protomers and stapling opposite strands of the actin filament. *J Mol Biol* 2008; 376: 607-13.
- Gandhi M, Goode BL.** Coronin: The Double-Edged Sword of Actin Dynamics. In: Clemen CS, Eichinger L and Rybakina V, editors. *The Coronin Family of Proteins*. Vol 48: Landes Bioscience & Springer, 2008a. <http://www.eurekah.com/chapter/3812>
- Gandhi M, Goode BL.** Coronin: the double-edged sword of actin dynamics. *Subcell Biochem* 2008b; 48: 72-87.
- Gatfield J, Albrecht I, Zanolari B, Steinmetz MO, Pieters J.** Association of the leukocyte plasma membrane with the actin cytoskeleton through coiled coil-mediated trimeric coronin 1 molecules. *Mol Biol Cell* 2005; 16: 2786-98.
- Glotzer M.** The molecular requirements for cytokinesis. *Science* 2005; 307: 1735-9. Goley ED, Welch MD. The ARP2/3 complex: an actin nucleator comes of age. *Nat Rev Mol Cell Biol* 2006; 7: 713-26.
- Goode BL, Wong JJ, Butty AC, Peter M, McCormack AL, Yates JR, et al.** Coronin promotes the rapid assembly and cross-linking of actin filaments and may link the actin and microtubule cytoskeletons in yeast. *J Cell Biol* 1999; 144: 83-98.
- Gournier H, Goley ED, Niederstrasser H, Trinh T, Welch MD.** Reconstitution of human Arp2/3 complex reveals critical roles of individual subunits in complex structure and activity. *Mol Cell* 2001; 8: 1041-52.
- Gringel A, Walz D, Rosenberger G, Minden A, Kutsche K, Kopp P, et al.** PAK4 and alphaPIX determine podosome size and number in macrophages through localized actin regulation. *J Cell Physiol* 2006; 209: 568-79.
- Guerra B, Boldyreff B, Sarno S, Cesaro L, Issinger OG, Pinna LA.** CK2: a protein kinase in need of control. *Pharmacol Ther* 1999; 82: 303-13.

- Gungabissoon RA, Bamburg JR.** Regulation of growth cone actin dynamics by ADF/cofilin. *J Histochem Cytochem* 2003; 51: 411-20.
- Guth L.** An overview of motor unit structure and function. *Arch Phys Med Rehabil* 1983; 64: 408-11.
- Hall ZW, Lubit BW, Schwartz JH.** Cytoplasmic actin in postsynaptic structures at the neuromuscular junction. *J Cell Biol* 1981; 90: 789-92.
- Hasse A, Rosentreter A, Spoerl Z, Stumpf M, Noegel AA, Clemen CS.** Coronin 3 and its role in murine brain morphogenesis. *Eur J Neurosci* 2005; 21: 1155-68.
- Hudson AM, Cooley L.** Phylogenetic, Structural and Functional Relationships between WD- and Kelch-Repeat Proteins. In: Clemen CS, Eichinger L and Rybakina V, editors. *The Coronin Family of Proteins*. Vol 48: Landes Bioscience & Springer, 2008. <http://www.eurekah.com/chapter/3791>
- Humphries CL, Balcer HI, D'Agostino JL, Winsor B, Drubin DG, Barnes G, et al.** Direct regulation of Arp2/3 complex activity and function by the actin binding protein coronin. *J Cell Biol* 2002; 159: 993-1004.
- Issinger OG.** Casein kinases: pleiotropic mediators of cellular regulation. *Pharmacol Ther* 1993; 59: 1-30.
- Itoh S, Suzuki K, Nishihata J, Iwasa M, Oku T, Nakajin S, et al.** The role of protein kinase C in the transient association of p57, a coronin family actin-binding protein, with phagosomes. *Biol Pharm Bull* 2002; 25: 837-44.
- Kalil K, Dent EW.** Touch and go: guidance cues signal to the growth cone cytoskeleton. *Curr Opin Neurobiol* 2005; 15: 521-6.
- Kammerer RA, Kostrewa D, Progius P, Honnappa S, Avila D, Lustig A, et al.** A conserved trimerization motif controls the topology of short coiled coils. *PNAS* 2005; 102: 13891-6.
- Kleihues P, Cavenee WK.** *Pathology and Genetics of Tumours of the Nervous System*. Lyon: IARC Press, 2000.
- Laemmli UK.** Cleavage of structural proteins during the assembly of the head of bacteriophage T4. *Nature* 1970; 227: 680-5.
- Lefranc F, Brotchi J, Kiss R.** Possible future issues in the treatment of glioblastomas: special emphasis on cell migration and the resistance of migrating glioblastoma cells to apoptosis. *J Clin Oncol* 2005; 23: 2411-22.
- Lehtonen S, Zhao F, Lehtonen E.** CD2-associated protein directly interacts with the actin cytoskeleton. *Am J Physiol Renal Physiol* 2002; 283: F734-43.
- Linder S, Nelson D, Weiss M, Aepfelbacher M.** Wiskott-Aldrich syndrome protein regulates podosomes in primary human macrophages. *Proc Natl Acad Sci U S A* 1999; 96: 9648-53.

- Loots GG, Ovcharenko I, Pachter L, Dubchak I, Rubin EM.** rVista for comparative sequence-based discovery of functional transcription factor binding sites. *Genome Res* 2002; 12: 832-9.
- Machesky LM, Reeves E, Wientjes F, Mattheyse FJ, Grogan A, Totty NF, et al.** Mammalian actin-related protein 2/3 complex localizes to regions of lamellipodial protrusion and is composed of evolutionarily conserved proteins. *Biochem J* 1997; 328 (Pt 1): 105-12.
- McArdle B, Hofmann A. Coronin Structure and Implications.** In: Clemen CS, Eichinger L and Rybakin V, editors. *The Coronin Family of Proteins*. Vol 48: Landes Bioscience & Springer, 2008. <http://www.eurekah.com/chapter/3821>
- McGuffin LJ, Bryson K, Jones DT.** The PSIPRED protein structure prediction server. *Bioinformatics* 2000; 16: 404-5.
- Morgan RO, Fernandez MP.** Molecular Phylogeny and Evolution of the Coronin Gene Family. In: Clemen CS, Eichinger L and Rybakin V, editors. *The Coronin Family of Proteins*. Vol 48: Landes Bioscience & Springer, 2008. <http://www.eurekah.com/chapter/3820>
- Mullins RD, Heuser JA, Pollard TD.** The interaction of Arp2/3 complex with actin: nucleation, high affinity pointed end capping, and formation of branching networks of filaments. *Proc Natl Acad Sci U S A* 1998; 95: 6181-6.
- Nabi IR.** The polarization of the motile cell. *J Cell Sci* 1999; 112 (Pt 12): 1803-11.
- Noegel AA, Blau-Wasser R, Sultana H, Muller R, Israel L, Schleicher M, et al.** The cyclase-associated protein CAP as regulator of cell polarity and cAMP signaling in *Dictyostelium*. *Mol Biol Cell* 2004; 15: 934-45.
- Ogata T.** Structure of motor endplates in the different fiber types of vertebrate skeletal muscles. *Arch Histol Cytol* 1988; 51: 385-424.
- Oku T, Itoh S, Ishii R, Suzuki K, Nauseef WM, Toyoshima S, et al.** Homotypic dimerization of the actin-binding protein p57/coronin-1 mediated by a leucine zipper motif in the C-terminal region. *Biochem J* 2005; 387: 325-31.
- Osiak AE ZG, Linder S.** Subconfluent endothelial cells form podosomes downstream of cytokine and RhoGTPase signaling. *Exp Cell Res* 2005: 342-353.
- Pantaloni D, Le Clainche C, Carlier MF.** Mechanism of actin-based motility. *Science* 2001; 292: 1502-6.
- Peche V, Shekar S, Leichter M, Korte H, Schroder R, Schleicher M, et al.** CAP2, cyclase-associated protein 2, is a dual compartment protein. *Cell Mol Life Sci* 2007; 64: 2702-15.

- Pepperkok R, Scheel J, Horstmann H, Hauri HP, Griffiths G, Kreis TE.** Beta-COP is essential for biosynthetic membrane transport from the endoplasmic reticulum to the Golgi complex in vivo. *Cell* 1993; 74: 71-82.
- Pollard TD, Beltzner CC.** Structure and function of the Arp2/3 complex. *Curr Opin Struct Biol* 2002; 12: 768-74.
- Pollard TD, Borisy GG.** Cellular motility driven by assembly and disassembly of actin filaments. *Cell* 2003; 112: 453-65.
- Ponti A, Matov A, Adams M, Gupton S, Waterman-Storer CM, Danuser G.** Periodic patterns of actin turnover in lamellipodia and lamellae of migrating epithelial cells analyzed by quantitative Fluorescent Speckle Microscopy. *Biophys J* 2005; 89: 3456-69.
- Rao JS.** Molecular mechanisms of glioma invasiveness: the role of proteases. *Nat Rev Cancer* 2003; 3: 489-501.
- Roadcap DW, Clemen CS, Bear JE.** The Role of Mammalian Coronins in Development and Disease. In: Clemen CS, Eichinger L and Rybakin V, editors. *The Coronin Family of Proteins*. Vol 48: Landes Bioscience & Springer, 2008. <http://www.eurekah.com/chapter/3798>
- Rodal AA, Sokolova O, Robins DB, Daugherty KM, Hippenmeyer S, Riezman H, et al.** Conformational changes in the Arp2/3 complex leading to actin nucleation. *Nat Struct Mol Biol* 2005; 12: 26-31.
- Rosentreter A, Hofmann A, Xavier CP, Stumpf M, Noegel AA, Clemen CS.** Coronin 3 involvement in F-actin-dependent processes at the cell cortex. *Exp Cell Res* 2007; 313: 878-95.
- Rybakin V, Clemen CS.** Coronin proteins as multifunctional regulators of the cytoskeleton and membrane trafficking. *Bioessays* 2005; 27: 625-32.
- Rybakin V, Stumpf M, Schulze A, Majoul IV, Noegel AA, Hasse A.** Coronin 7, the mammalian POD-1 homologue, localizes to the Golgi apparatus. *FEBS Lett* 2004; 573: 161-7.
- Sali A, Blundell TL.** Comparative protein modelling by satisfaction of spatial restraints. *J Mol Biol* 1993; 234: 779-815.
- Sambrook J, Fritsch, E.F., Maniatis, T.** *Molecular cloning. A laboratory manual.*, Cold Spring Harbour Laboratory, Cold Spring, NY, (1989).
- Schoenauer R, Lange S, Hirschy A, Ehler E, Perriard JC, Agarkova I.** Myomesin 3, a novel structural component of the M-band in striated muscle. *J Mol Biol* 2008; 376: 338-51.
- Selbert S, Fischer P, Pongratz D, Stewart M, Noegel AA.** Expression and localization of annexin VII (synexin) in muscle cells. *J Cell Sci* 1995; 108 (Pt 1): 85-95.

- Serrels B, Serrels A, Brunton VG, Holt M, McLean GW, Gray CH, et al.** Focal adhesion kinase controls actin assembly via a FERM-mediated interaction with the Arp2/3 complex. *Nat Cell Biol* 2007; 9: 1046-56.
- Skjerpen CS, Nilsen T, Wesche J, Olsnes S.** Binding of FGF-1 variants to protein kinase CK2 correlates with mitogenicity. *Embo J* 2002; 21: 4058-69.
- Smith TF.** Diversity of WD-Repeat Proteins. In: Clemen CS, Eichinger L and Rybakina V, editors. *The Coronin Family of Proteins*. Vol 48: Landes Bioscience & Springer, 2008. <http://www.eurekah.com/chapter/3787>
- Smith TF, Gaitatzes C, Saxena K, Neer EJ.** The WD repeat: a common architecture for diverse functions. *Trends Biochem Sci* 1999; 24: 181-5.
- Spoerl Z, Stumpf M, Noegel AA, Hasse A.** Oligomerization, F-actin interaction, and membrane association of the ubiquitous mammalian coronin 3 are mediated by its carboxyl terminus. *J Biol Chem* 2002; 277: 48858-67.
- Stradal TE, Scita G.** Protein complexes regulating Arp2/3-mediated actin assembly. *Curr Opin Cell Biol* 2006; 18: 4-10.
- Sutherland JD, Witke W.** Molecular genetic approaches to understanding the actin cytoskeleton. *Curr Opin Cell Biol* 1999; 11: 142-51.
- T.Mosmann.** Rapid colorimetric assay for cellular growth and survival: application to proliferation and cytotoxicity assays. *Immunol Methods* 1983: 55-63.
- Thal D, Xavier CP, Rosentreter A, Linder S, Friedrichs B, Waha A, et al.** Expression of coronin-3 (coronin-1C) in diffuse gliomas is related to malignancy. *J Pathol* 2008; 214: 415-24.
- Thirion C, Stucka R, Mendel B, Gruhler A, Jaksch M, Nowak KJ, et al.** Characterization of human muscle type cofilin (CFL2) in normal and regenerating muscle. *Eur J Biochem* 2001; 268: 3473-82.
- Tohyama Y, Yanagi S, Sada K, Yamamura H.** Translocation of p72syk to the cytoskeleton in thrombin-stimulated platelets. *J Biol Chem* 1994; 269: 32796-9.
- Towbin H, Staehelin T, Gordon J.** Electrophoretic transfer of proteins from polyacrylamide gels to nitrocellulose sheets: procedure and some applications. *Proc Natl Acad Sci U S A* 1979; 76: 4350-4.
- Utrecht AC, Bear JE.** Coronins: the return of the crown. *Trends Cell Biol* 2006; 16: 421-6.
- Vergne I, Chua J, Singh SB, Deretic V.** Cell biology of mycobacterium tuberculosis phagosome. *Annu Rev Cell Dev Biol* 2004; 20: 367-94.
- Vielhaber S, Kunz D, Winkler K, Wiedemann FR, Kirches E, Feistner H, et al.** Mitochondrial DNA abnormalities in skeletal muscle of patients with sporadic amyotrophic lateral sclerosis. *Brain* 2000; 123 (Pt 7): 1339-48.

- W.L. DeLano.** The PyMOL Molecular Graphics System. (<http://www.pymol.org>). 2002.
- Weaver AM.** Invadopodia: specialized cell structures for cancer invasion. *Clin Exp Metastasis* 2006; 23: 97-105.
- Xavier-C.P RA, Reimann.J, Cornfine.S,Linder.S, Vliet.V.V, Hofmann.A, Morgan.R.O, Fernandez.M.P, Stumpf.S, Müller.R, Jungbauer.T, Schröder.R, Noegel.A.A,Clemen.C.S.** Structural and functional diversity of novel coronin-1C (CRN2) isoforms. submitted manuscript 2008.
- Xavier C-P, Eichinger L, Fernandez MP, Morgan RO, Clemen CS.** Evolutionary and Functional Diversity of Coronin Proteins. In: Clemen CS, Eichinger L and Rybakin V, editors. *The Coronin Family of Proteins*. Vol 48: Landes Bioscience & Springer, 2008. <http://www.eurekah.com/chapter/3808>
- Yafe A, Shklover J, Weisman-Shomer P, Bengal E, Fry M.** Differential binding of quadruplex structures of muscle-specific genes regulatory sequences by MyoD, MRF4 and myogenin. *Nucleic Acids Res* 2008; 36: 3916-25.
- Yuan Y, Compton SA, Sobczak K, Stenberg MG, Thornton CA, Griffith JD, et al.** Muscleblind-like 1 interacts with RNA hairpins in splicing target and pathogenic RNAs. *Nucleic Acids Res* 2007; 35: 5474-86.

VI. Appendix

1. Abbreviations

APS	ammonium persulphate
ATP	adenosintriphosphate
Bp	base pair(s)
BSA	bovine serum albumin
cAM	cyclic adenosine monophosphate
cDNA	complementary DNA
<i>C. elegans</i>	<i>Caenorhabditis elegans</i>
CIAP	calf intertinal alkaline phosphatase
dNTP	deoxyribonucleotide triphosphate
CRN2	Coronin 1C, Coronin 3
DMSO	dimethylsulphoxide
DNA	deoxyribonucleic acid
DNase	deoxyribonuclease
ds DNA	double strand DNA
DTT	1,4- dithiothreitol
ECL	enhanced chemiluminescence
<i>E. coli</i>	<i>Escherichia coli</i>
EDTA	ethylenediaminetetraacetic acid
EGTA	ethyleneglycol-bis(2-amino-ethylene) N,N,N,N-tetraacetic acid
FCS	fetal calf serum
FL	Full length
G418	geneticin
EGFP	enhanced green fluorescent protein
GST	glutathione S-transferase
HEPES	N-(2-hydroxyethyl)piperazine-N'-2-ethanesulphonic acid
HRP	horse radish peroxidase
IgG	immunoglobulin G
IPTG	iso-propylthio-galactopyranoside
Kb	kilobase pairs
kDa	kilodalton
MES	morpholinoethansulphonic acid
β -ME	beta-mercaptoethanol
MOPS	Morpholinopropanesulphonic acid
MW	molecular weight
NP-40	nonylphenylpolyethyleneglycol
OD	optical density
PAGE	polyacrylamide gel electrophoresis
PBS	phosphate buffer solution
PBG	phosphate buffer with fish gelatine
PIPES	piperazine-N,N'-bis(2-ethanesulphonic acid)
PMSF	phenylmethylsulphonylfluoride
RNA	ribonucleic acid
RNase	ribonuclease
Rpm	rotations per minute
SDS	sodium dodecyl sulphate

ss DNA	single strand DNA
TE	Tris-EDTA
TEMED	N,N,N',N'-tetramethyl-ethylenediamine
Tris	Tris-(hydroxymethyl)aminomethane
TRITC	tetramethylrhodamine isothiocyanate
Triton X-100	t-Octylphenoxy polyethoxyethanol
Tween	20 polyoxyethylensorbitanmonolaurate
UV	ultraviolet
vol.	volume
v/v	volume by volume
w/v	weight by volume
X-gal	5-bromo-4-chloro-3-indolyl-D-galactopyranoside

Summary

Coronins are in general versatile actin filament-crosslinking and bundling proteins. In human, seven subfamilies of coronins are identified. One of these proteins found ubiquitously expressed in human tissues is CRN2 (synonyms: coronin-1C, coronin-3). Here, we study in vivo and in vitro F-actin associated properties of CRN2. Using different GFP tagged structural domain proteins and RNAi mediated knock down of CRN2, we studied the role of these domains in various cellular activities like wound healing, formation of protrusions, proliferation, cytokinesis and endocytosis. We found an inhibitory effect of the WD repeat or coiled coil domain of CRN2 in specific to be profound on wound closure and formation of cellular protrusions.

Screening of the CRN2 protein sequence for posttranslational modifications resulted in identification of Ser463 as a putative serine phosphorylation site located in the coiled coil domain. An important cytoskeleton regulator, CK2 α kinase, was found to interact and phosphorylate this residue. The consequence of this phosphorylation is to regulate oligomerization of this domain as evident from gel filtration studies. Further, at the cellular level it induced a significant inhibitory effect on wound closure and cell protrusion as studied using a phosphomimetic S463D mutation. CRN2 like other coronins interacted with the Arp2/3-complex and cofilin. In addition, both wild type and phosphomutant CRN2 executed an inhibitory effect on Arp2/3-mediated actin polymerisation, however, this effect was more pronounced in the case of phosphomutant.

Two novel CRN2 isoforms which differ in their N-terminal length were found to arise from an alternative exon, exon 1a, identified in intron 1. All three isoforms co-localize with and associate with F-actin. Biochemical evidence suggests that, in contrast to the conventional isoform 1 and the longer isoform 2, the largest isoform 3 exists as a monomer. Structural modelling reveals that this difference in the oligomerization state may result from an interaction of the elongated N-terminus of CRN2-isoform 3 with the C-terminal coiled coil. In addition, this isoform, which is expressed during the myogenic differentiation and in mature skeletal muscle tissue, was found as a novel component specifically localizing to sarcomeric F-actin as well as to the motor end plate.

Further we performed a detailed study on the expression pattern of CRN2 in human brain tumours. We found a correlation between the number of CRN2 positive cells and the malignant phenotype in diffuse gliomas. In addition, CRN2 knockdown glioblastoma cells exhibited significantly reduced levels of cell proliferation, motility and invasion into the extracellular matrix. Our findings provide evidence for a contribution of CRN2 in the malignant progression of diffuse gliomas.

Zusammenfassung

Coronine gelten als vielseitige Aktinfilament-vernetzende und -bündelnde Proteine. In menschlichen Zellen wurden sieben Mitglieder der Coronin-Familie identifiziert. Eines dieser Coronine, das ubiquitär exprimiert wird, ist CRN2 (Synonyme: Coronin-1C, Coronin-3). In dieser Arbeit untersuchten wir die mit Aktinfilamenten assoziierten Funktionen von CRN2. Mit verschiedenen GFP-Fusionsproteinen von CRN2-Domänen und einer RNAi-vermittelten Herunterregulation von CRN2 haben wir als Funktionen von CRN2 z.B. die *in vitro* Wundheilung, Ausbildung von Zellfortsätzen, Proliferation, Zellteilung und Endozytose ermittelt. Dabei fanden wir hemmende Effekte verschiedener CRN2-Domänen, insbesondere in der Wundheilung und Ausbildung von Zellfortsätzen.

Eine Analyse der CRN2 Aminosäuresequenz hinsichtlich posttranslationaler Modifikationen zeigte Ser463 in der Coiled coil-Domäne als eine mögliche Phosphorylierungsstelle. Wir konnten hier zeigen, dass die Kinase CK2, ein wesentlicher Regulator des Zytoskeletts, mit Ser463 interagiert und diesen Rest phosphoryliert. Als eine Konsequenz ändert sich der Oligomerisierungsstatus von CRN2, wie mit Gelfiltrationsexperimenten belegt werden konnte. Weiterhin zeigten Experimente mit der phosphomimetischen S463D CRN2-Variante signifikant hemmende Effekte auf die Wundheilung und Ausbildung von Zellfortsätzen. CRN2 interagiert wie andere Coronine mit dem Arp2/3-Komplex und mit Cofilin. Diesbezüglich zeigten Aktinpolymerisations-Versuche einen ausgeprägten hemmenden Effekt von normalem wie auch S463D CRN2, wobei die Mutante eine deutlichere Hemmung aufwies.

Wir haben zwei neue Isoformen des CRN2 beschrieben, die sich in der Länge des N-Terminus unterscheiden und durch Spleißen eines alternativen Exons entstehen. Alle drei Isoformen kolokalisieren und assoziieren mit F-Aktin. Biochemische Untersuchungen zeigten, dass die längste Isoform 3 nicht wie die anderen beiden als Trimer, sondern als Monomer vorliegt. Strukturmodelle ließen hier vermuten, dass der Unterschied im Oligomerisierungsstatus von einer Interaktion des verlängerten N-Terminus mit dem C-Terminus herrührt. Die Isoform 3 wurde während der myogenen Differenzierung exprimiert und ist die alleinige Isoform in reifem Skelettmuskel. Hier haben wir CRN2 als eine neue Komponente des Sarkomers und der motorischen Endplatte beschrieben.

Darüberhinaus haben wir eine detaillierte Studie zur Expression von CRN2 in humanen Hirntumoren durchgeführt. Es zeigte sich eine Korrelation zwischen der Anzahl CRN2-positiver Tumorzellen mit dem malignen Phänotyp Diffuser Gliome. Die Herunterregulation von CRN2 in humanen Glioblastomzellen ergab signifikant verminderte Raten von Proliferation, Motilität und Invasion in die Extrazellulärmatrix. CRN2 könnte ein Faktor für die Ausbreitung oder die schlechte Prognose von Diffusen Gliomen sein.

Curriculum Vitae

- Name** : Charles-Peter Xavier
- Address** : Luxemburger Str, 124-136,
Unicenter, Et-Zi: 06-36,
50939 Cologne, Germany.
- Present address** : His Grace, Petter's Cottage,
No: 319, 4th B Cross, OMBR layout,
Bangalore-560043, India.
E-mail: charlescpx@gmail.com
- Date of birth** : 11.02.1976
- Nationality** : Indian
- School Studies**
- 1983-1993 : St. Aloysius High School, Bangalore, India
1993-1995 : St. Josephs Science & Arts College, Bangalore, India
- University Studies**
- 1995-1998 : Bachelor of Science (Microbiology, Chemistry,
Botany)
Bangalore University, India
- 1998-2000 : Master of Science (Microbiology)
Bangalore University, India
- Doctoral Studies**
- 10.2005-10.2008 : Faculty of Mathematics and Natural Science,
University of Cologne,
Supervisor: Prof. Dr. Angelika A. Noegel,
Institute for Biochemistry I, Medical Faculty,
University of Cologne, 50931 Cologne, Germany

Lebenslauf

- Name** : Charles-Peter Xavier
- Adresse** : Luxemburger Str, 124-136,
Unicenter, Et-Zi:06-36,
50939, Köln, Deutschland.
- Heimatadresse** : His Grace, Petter's Cottage,
No: 319, 4th B Cross, OMBR layout,
Bangalore-560043, India.
E-mail: charlescpx@gmail.com
- Geburtsdatum** : 11.02.1976
- Staatsangehörigkeit** : Indisch
- Schulbildung**
- 1983-1993 : St. Aloysius High School, Bangalore, India
1991-1993 : St. Josephs Science & Arts College, Bangalore, India
- Universität Studium**
- 1995-1998 : Bachelor of Science (Microbiology, Chemistry,
Botany)
Bangalore University, Indien
- 1998-2000 : Master of Science (Microbiology)
Bangalore University, Indien
- Promotions Studium**
- 10.2005- 10.2008 : Mathematisch-Naturwissenschaftliche Fakultät,
Universität zu Köln,
Betreuerin: Prof. Dr. Angelika A. Noegel,
Institut für Biochemie I, Medizinische Fakultät,
Universität zu Köln, 50931 Köln, Deutschland